Alzheimer's Disease Electrophysiology

Diagnosis, Pathophysiology, Monitoring

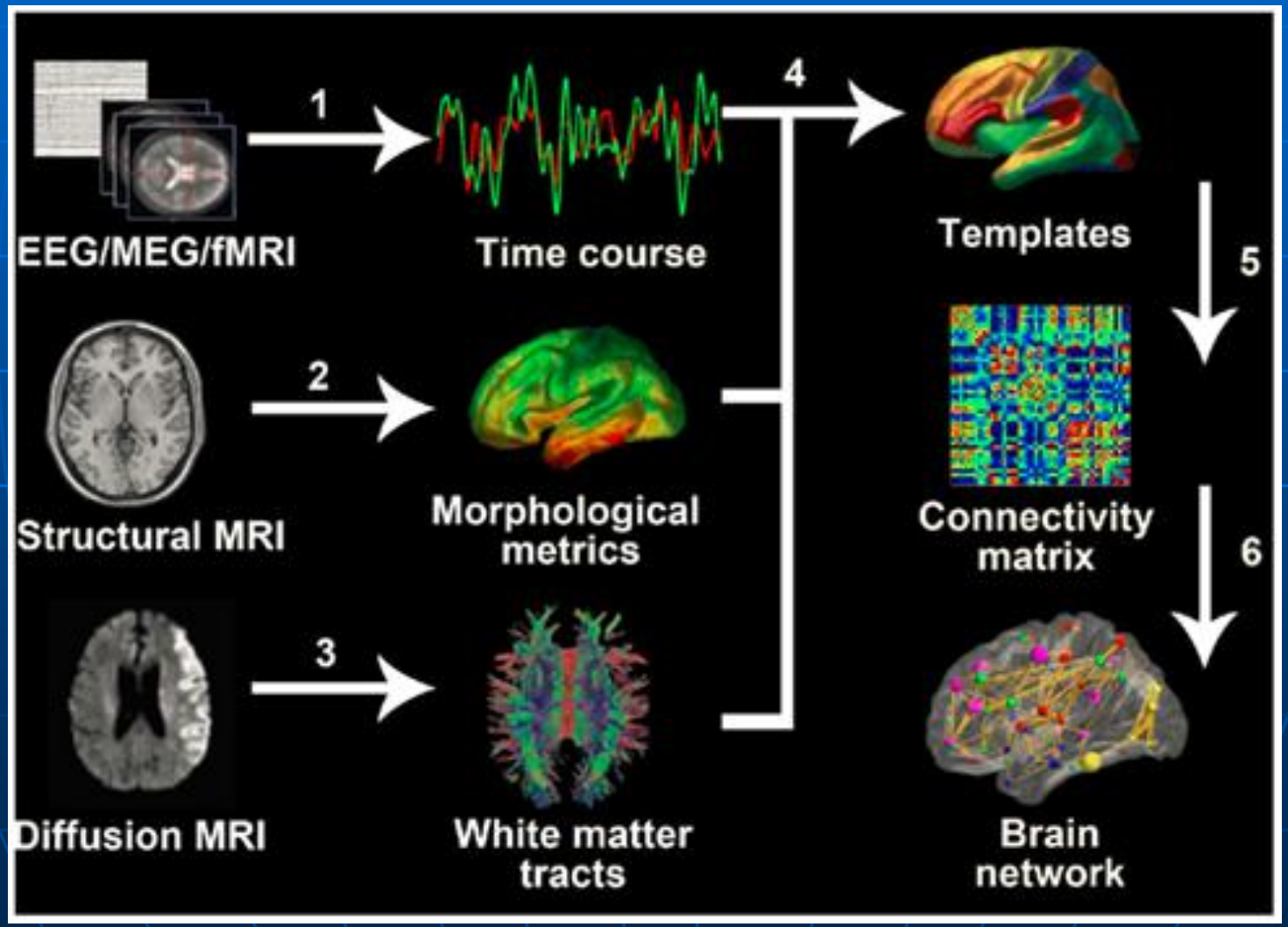

Repairing Rhythms in Alzheimer's Models

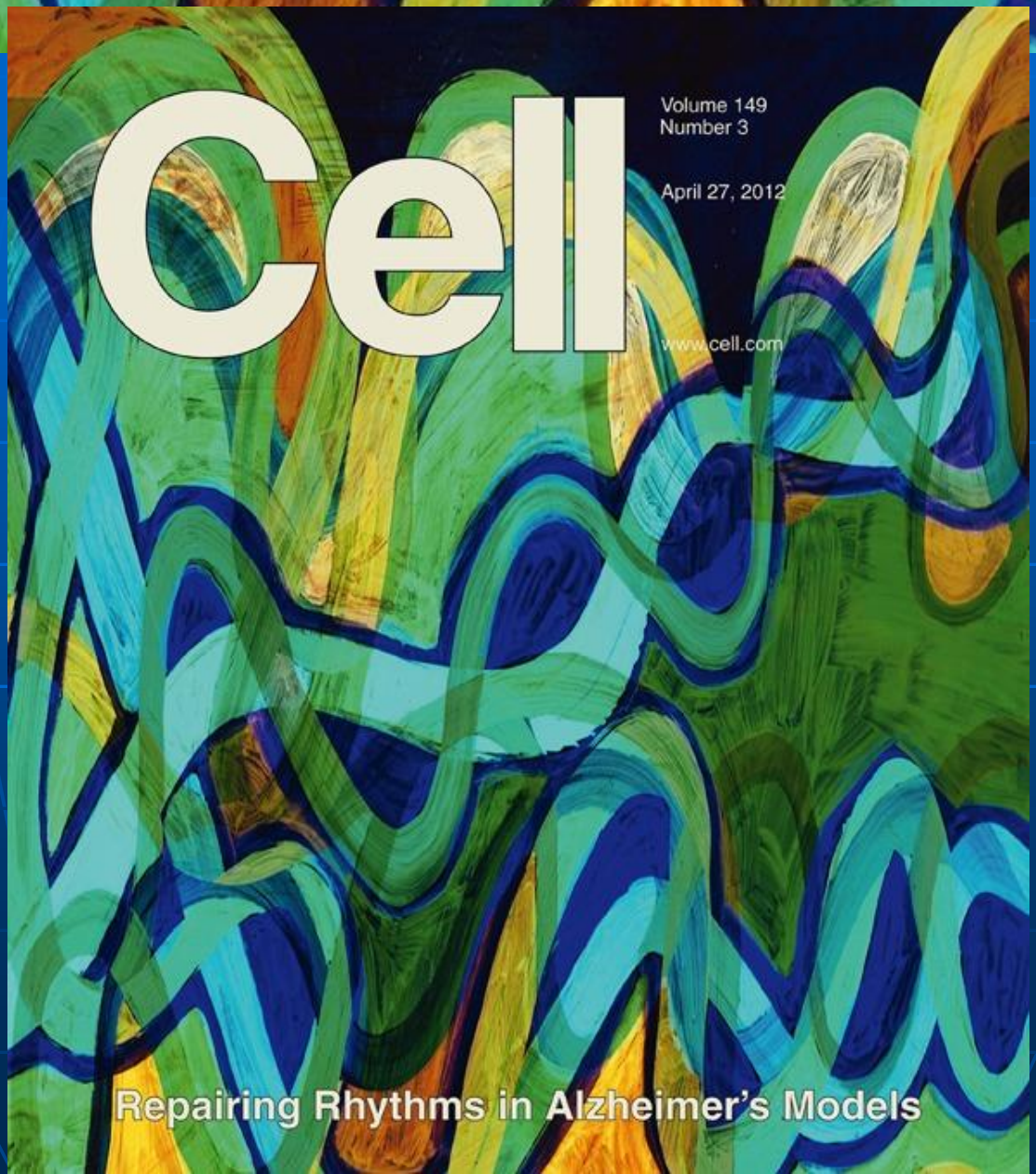

How is EEG generated ?

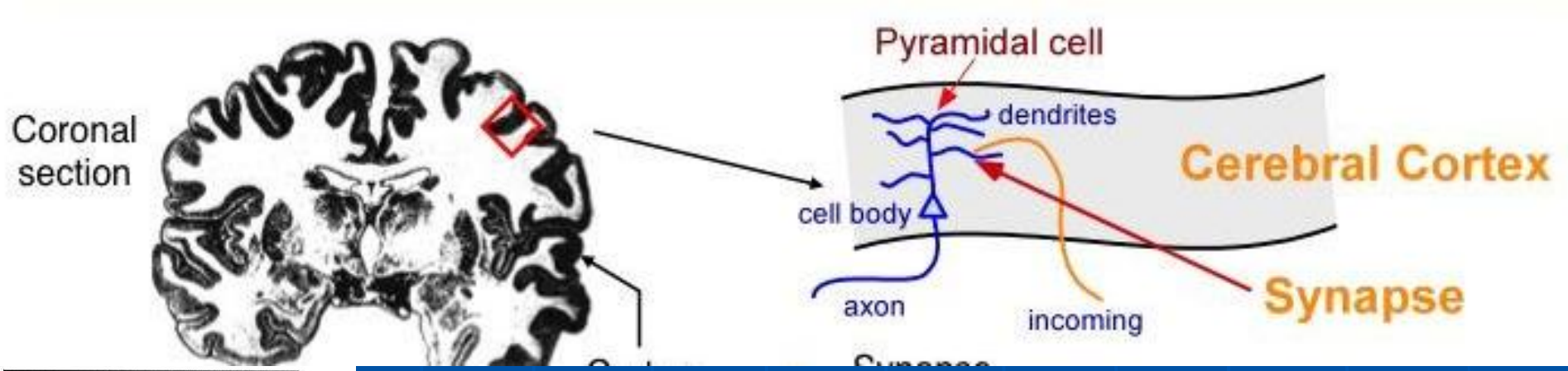

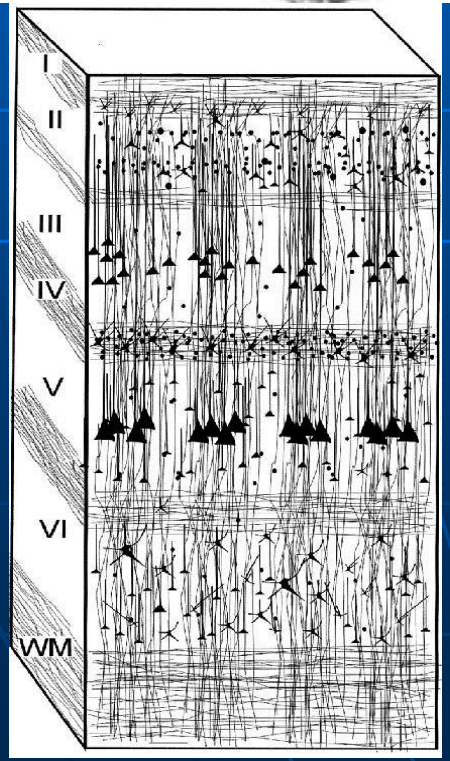

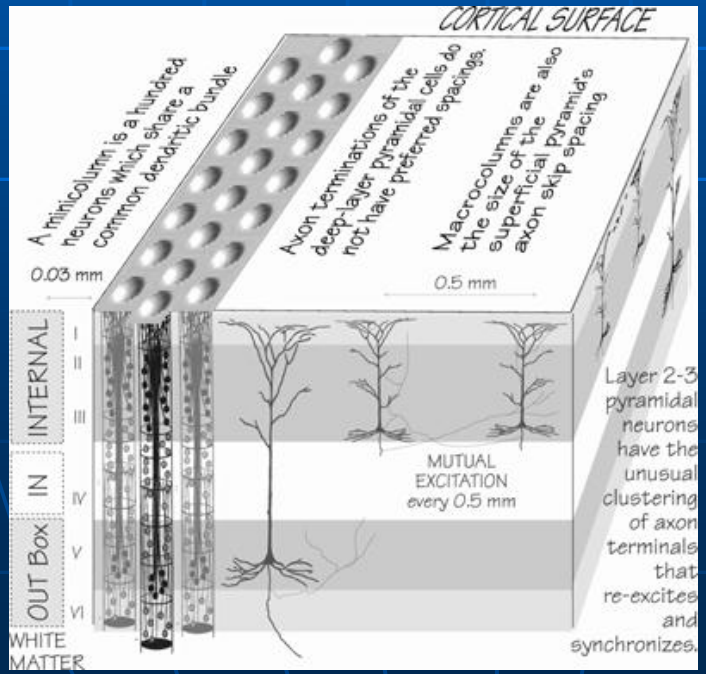

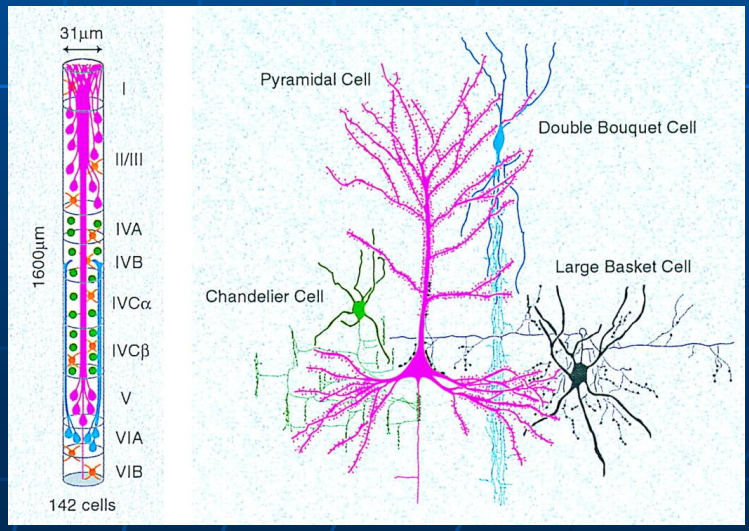

Dipoles

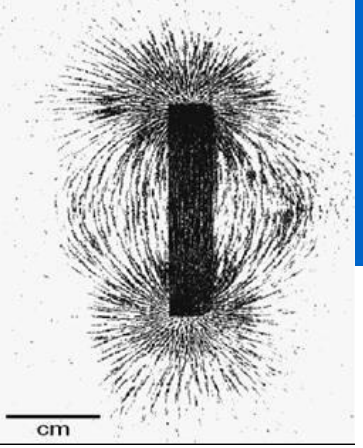

EEG Amplifier

EEG Electrode

Scalp

Skull

Dura Mater

Arachnoid

Subarachnoid Space

Pia Matter

Active Synapses

Efferent Axon

Pyramid cells

Simulation neural oscillations

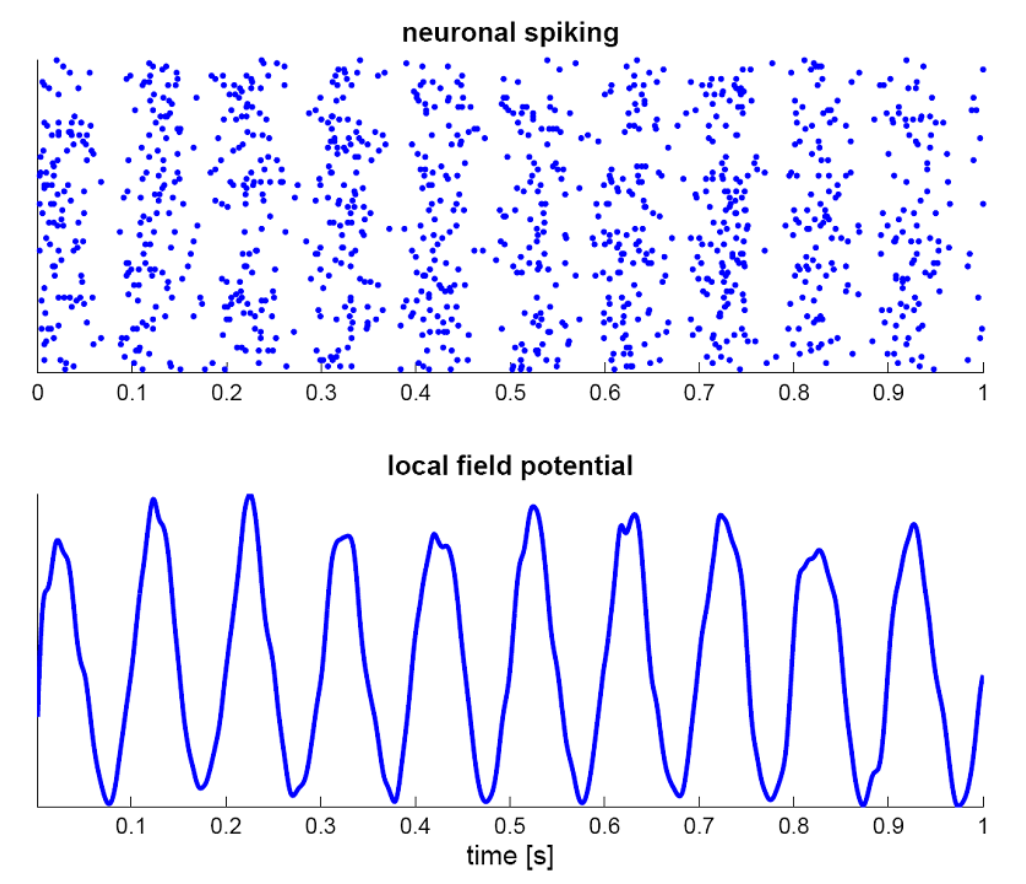

In large-scale oscillations (EEG), amplitude changes are considered to result from changes in synchronization within a neural ensemble, also referred to as local synchronization.
Neural ensembles can generate oscillatory activity endogenously through local interactions between excitatory and inhibitory neurons.

Large-scale synchronization

Synchronized activity (by phase reset, with higher amplitudes as a result) in large-scale neuronal networks has been linked to perception, cognitive functions and behavior.

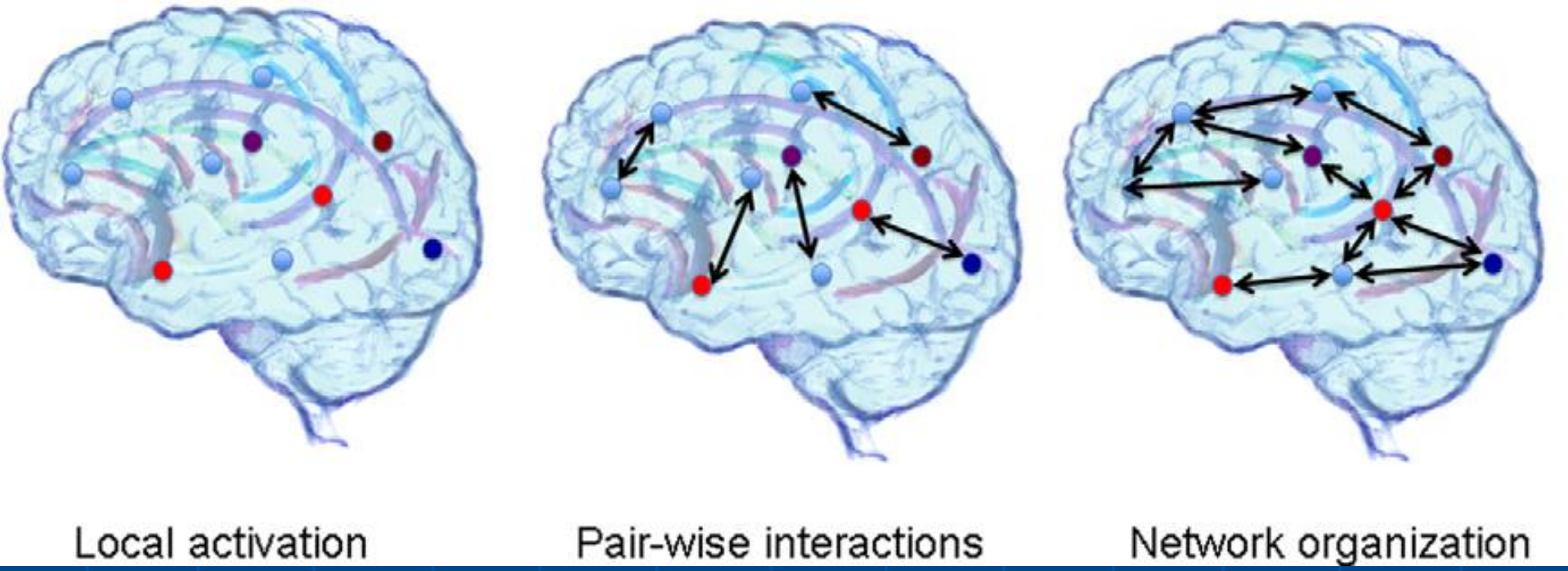

INTERACTION LEVEL

Zero order

First order

Second and higher order
(interactions of interactions)

Van Straaten E.C.W., 2014

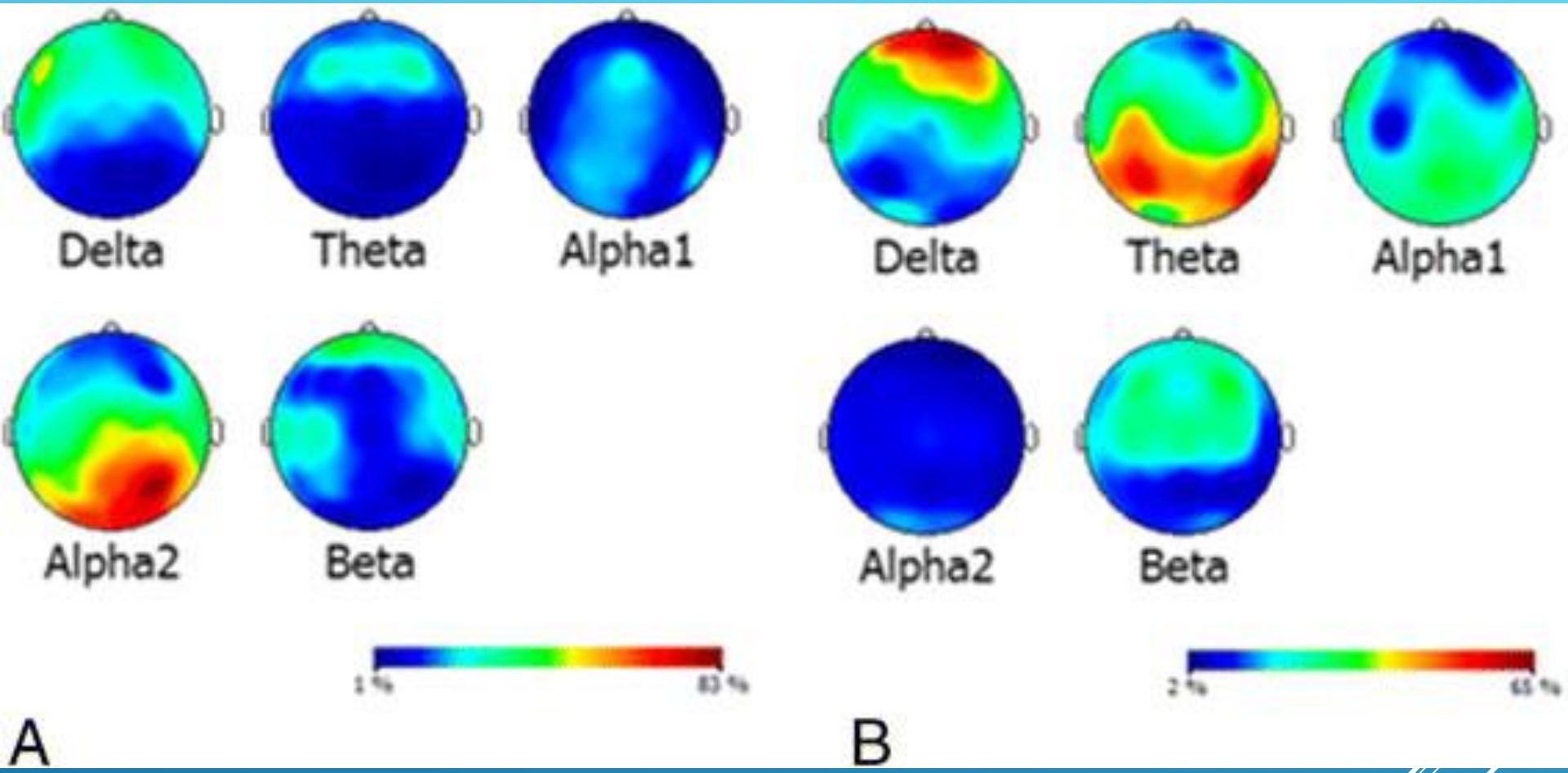

NORMAL AD

With respect to topography in the antero-posterior direction, sources of alpha and beta activity shifted more anteriorly in AD patients compared to both the controls and MCI subjects. No significant difference was found between MCI and controls. Combined alpha and theta GFP were the best discriminating variables between AD patients and controls (84% correct classification) and AD and MCI subjects (78% correctly classified) (Huang C., 2000).

Integration of multiple biomarkers (1st year) using logistic regression predicts Alzheimer's disease at the MCI stage. Simon-Shlomo P., 2013

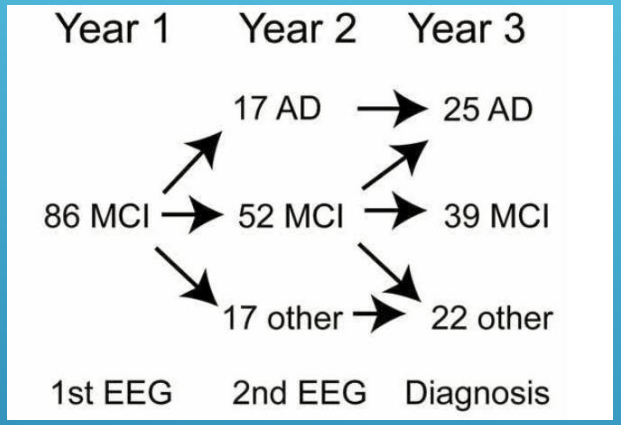

SE.Sensitivity; SP.Specificity; PPV. Positive predictive value; MCC. Matthews Correlation Coefficient; AUC.Area under the receiver operator curve.

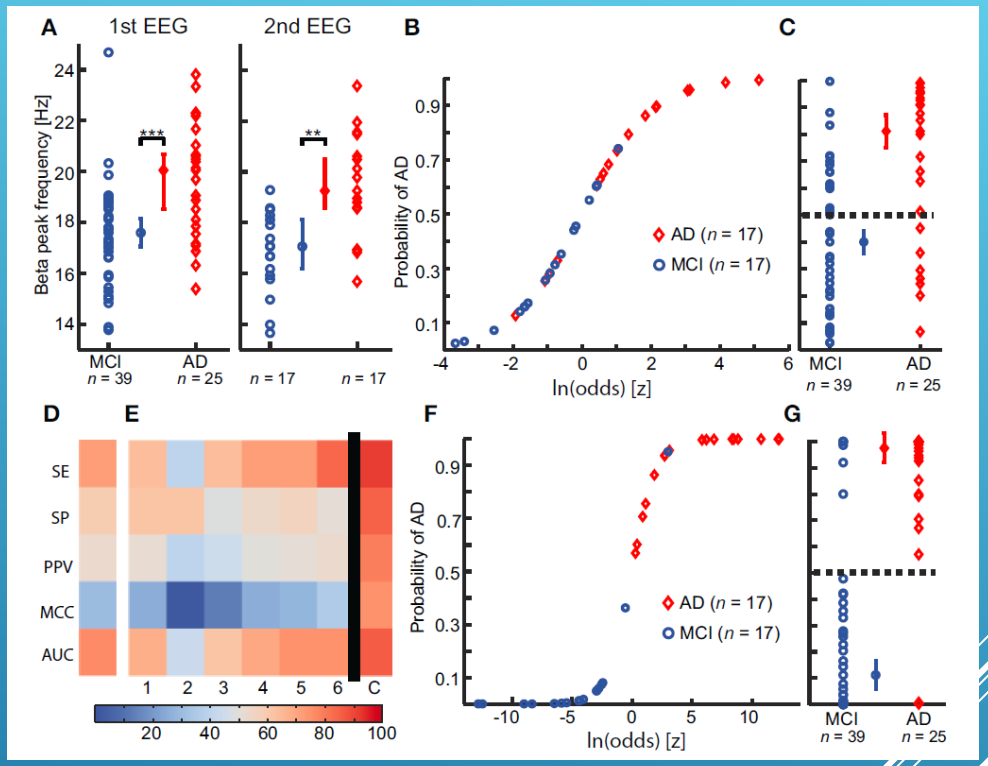

We clearly see that the combined outcome is better than the classification using the individual biomarkers. 1. Peak width of dominant beta peak; 2. Range of amplitude values in beta (13–30 Hz); 3. Bandwidth of subject-specific beta frequency; 4. Ratio between theta and alpha power; 5. Alpha relative power (normalized with 1–45 Hz broadband); 6. Amplitude correlations with Cz in beta (13–30 Hz).

Integration of multiple biomarkers (1st year) using logistic regression predicts Alzheimer's disease at the MCI stage. Simon-Shlomo P., 2013

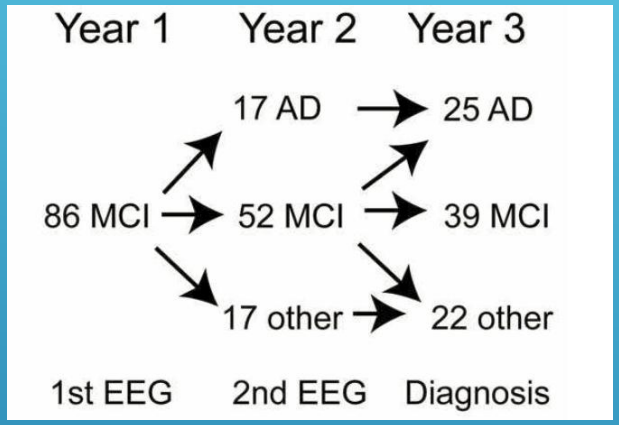

SE.Sensitivity; SP.Specificity; PPV. Positive predictive value; MCC. Matthews Correlation Coefficient; AUC.Area under the receiver operator curve.

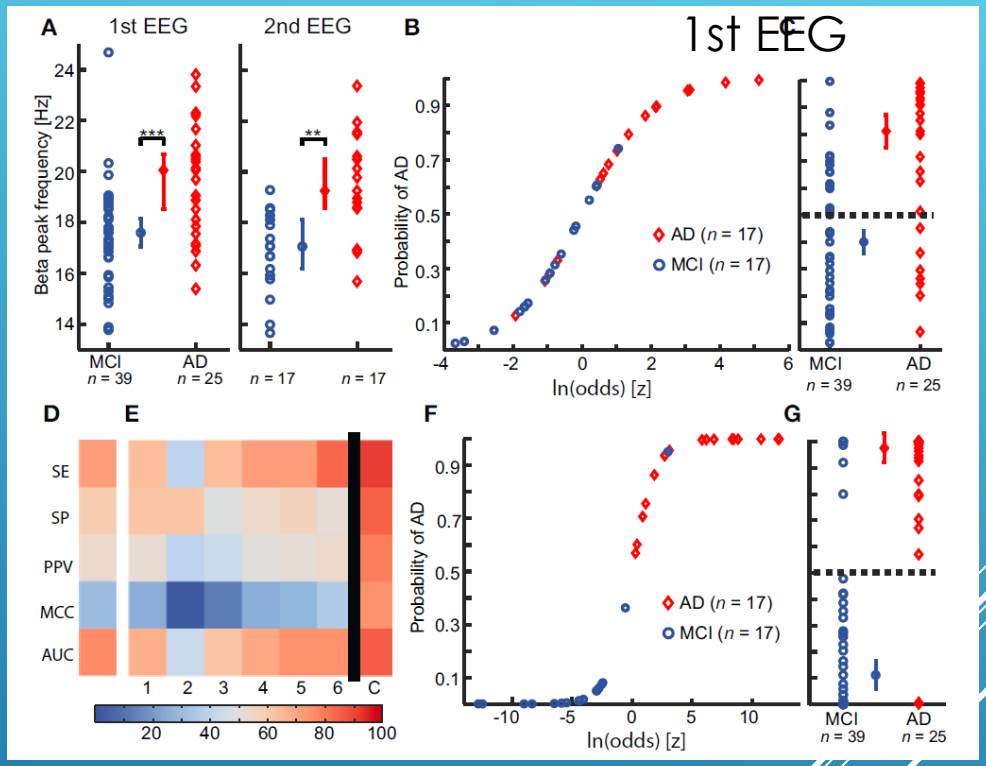

The retrospective testing on first-year data using the classifier model trained on the second-year data gave a **SE of 92%, 85% SP,79% PPV** (MCI-stable, n = 39; ADconvert, n = 25), which indicates that even at this very early stage differences between AD-converters and MCI-stable can be identified.

Integration of multiple biomarkers using logistic regression predicts of Alzheimer's disease at the MCI stage.

Simon-Shlomo P., 2013

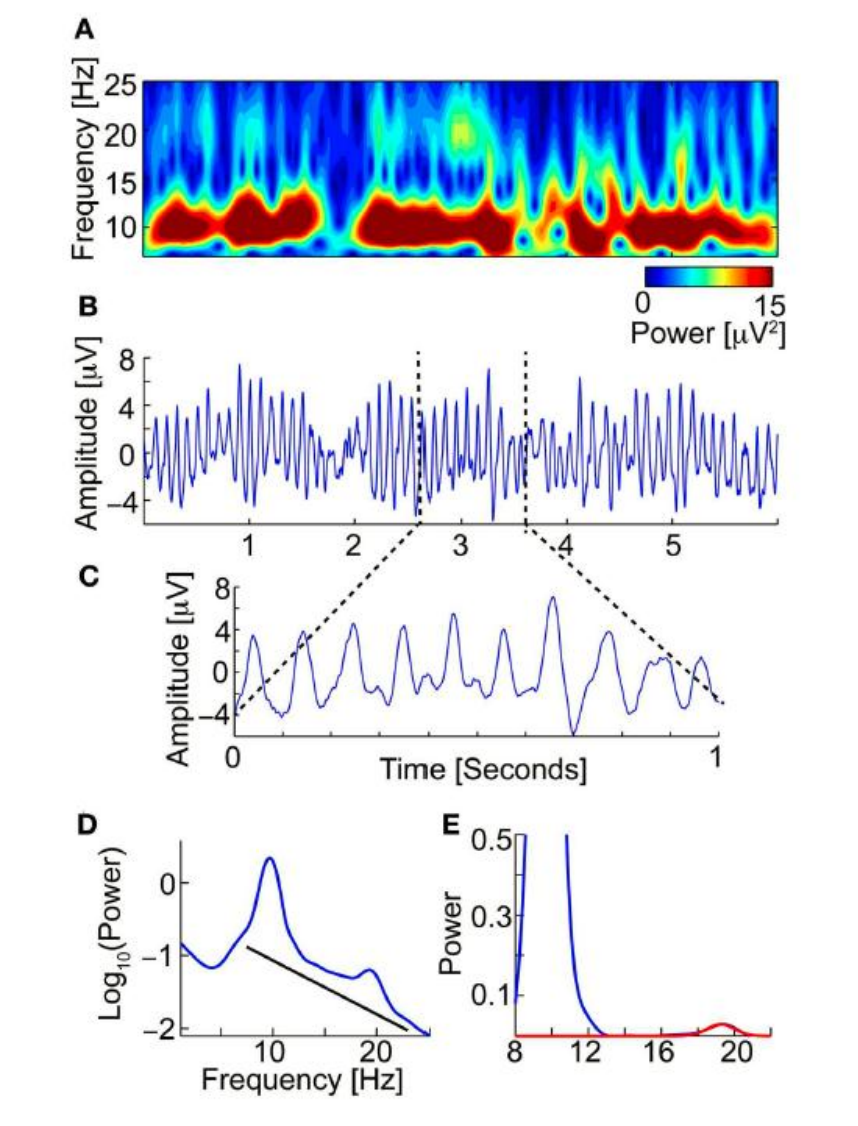

Integration of multiple biomarkers using logistic regression predicts of Alzheimer's disease at the MCI stage. Simon-Shlomo P., 2013

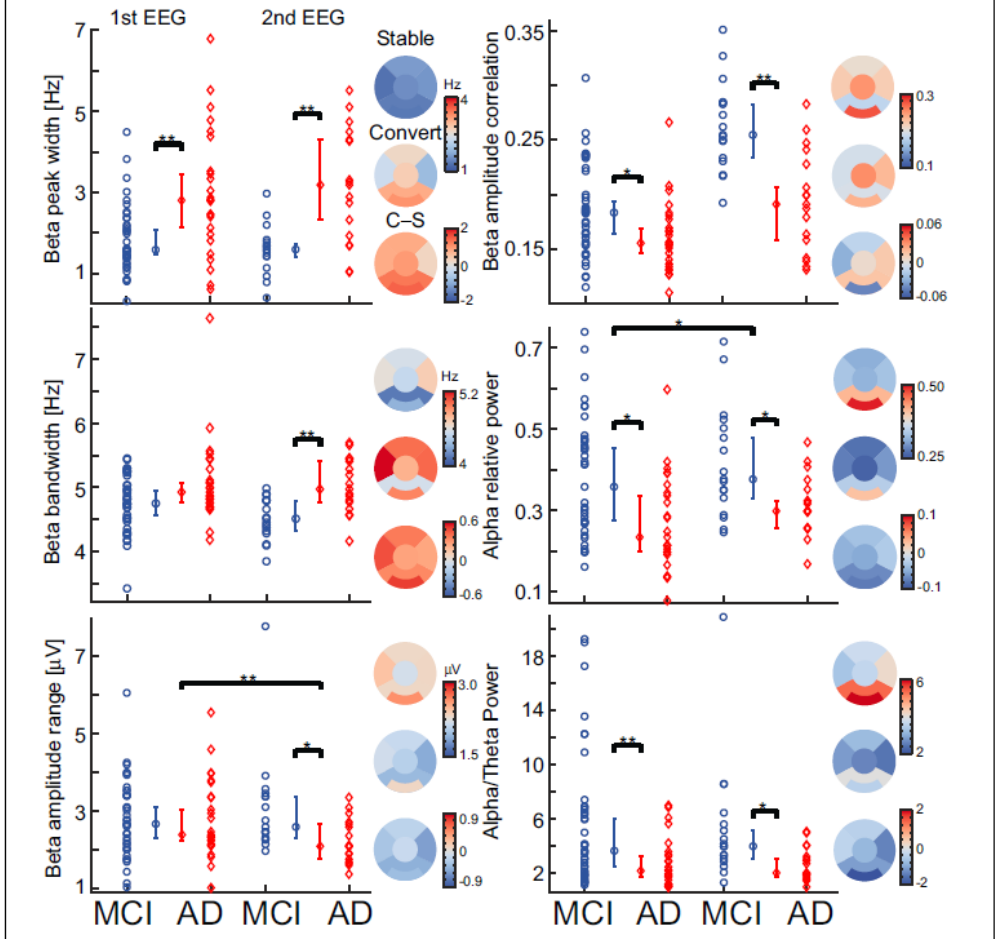

FIGURE 4 | Most biomarkers in the diagnostic index have differences between the MCI-stable (MCI) and AD-converter (AD) groups, and only two have longitudinal changes. For each biomarker, a separation plot is

Topograms based on 2nd EEG

Integration of multiple biomarkers using logistic regression predicts of Alzheimer's disease at the MCI stage.

Simon-Shlomo P., 2013

Apart from relative alpha power and the theta/alpha power ratio, which may reflect early changes toward the well-known slowing of the EEG in AD, our optimal set of biomarkers is derived from the beta frequency band (13–30 Hz).

Beta-band changes have previously been observed in Alzheimer's disease, e.g., by **a more anterior distribution** (Huang et al., 2000). The **larger width of the beta peak and bandwidth** could potentially be linked with a less stable beta frequency, and, therefore, also a less efficient working memory (Kopell et al., 2011).

Hyperexcitability of the cortex has also been observed in AD, which our finding of **higher beta frequency** also suggests.

Relationship between hippocampal hyperactivity and cortical thinning (structural MRI) in clinically normal and MCI older adults (61-83 y.)

Putcha D., 2012

Hippocampal hyperactivity showed a significant association with thinner cortex, specifically in the **precuneus and lateral temporoparietal cortices**. This cortical pattern of thinning has been observed in AD dementia, prodromal AD, and in presymptomatic amyloid-positive individuals. There is evidence from functional and anatomical connectivity work linking the MTL to these regions of the neocortex. Furthermore, this specific network has been implicated in playing a crucial role in episodic memory formation and has been implicated as being targeted by the neurodegenerative process of AD.

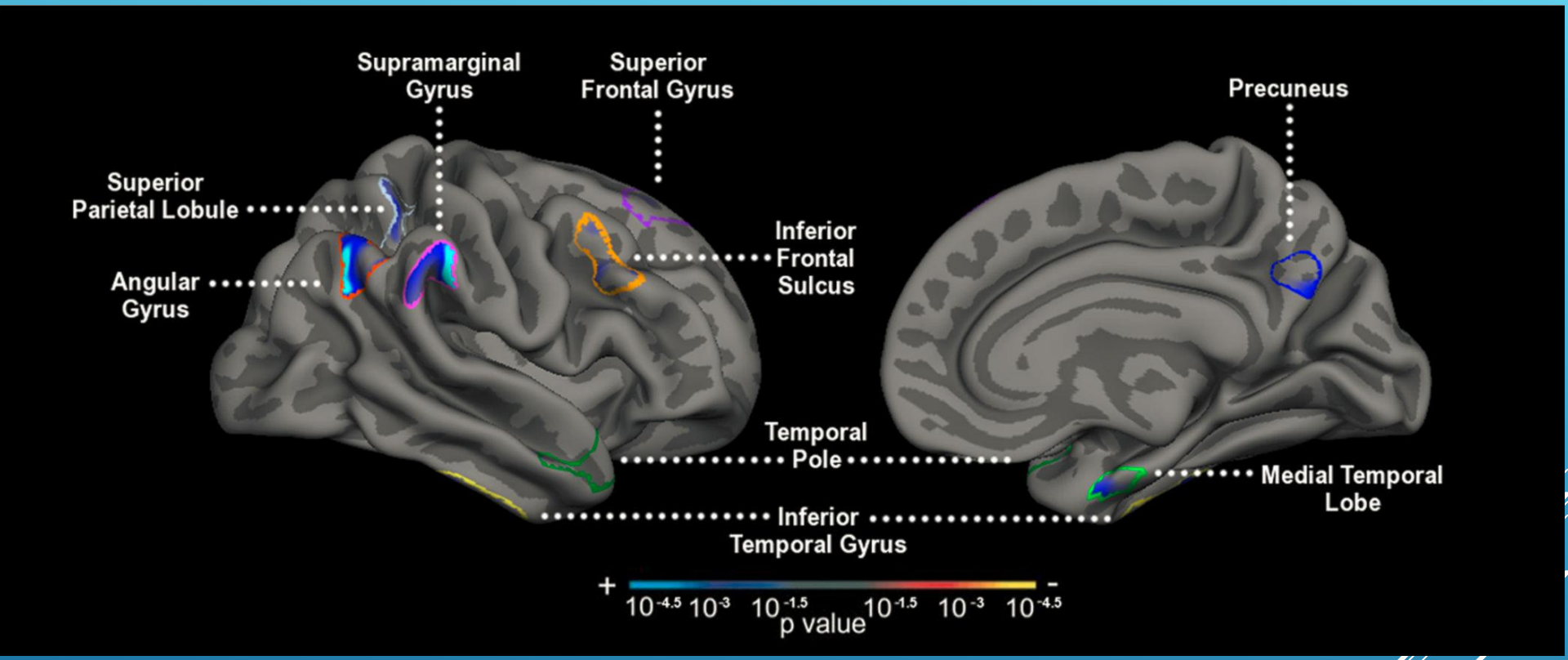

ROI-restricted thickness correlation map of hippo-campal activation and cortical thickness with an AD signature mask.

Levetiracetam and hippocampal activity in MCI
Bakker A., 2012

Greater hippocampal activation in MCI relative to the control group was isolated to the DG/CA3 region consistent with earlier studies.

Treatment with low dose levetiracetam (125 mg BID, 2 weeks) significantly reduced that excess activity (fMRI), such that hippocampal activation in 17 patients on drug did not differ from 17 age-matched control subjects.

Additionally, drug treatment significantly improved 3-choice recognition performance. Memory errors attributable to DG/CA3 dysfunction, which differed between the groups when MCI subjects were on placebo, were significantly reduced by levetiracetam.

Mechanisms tied to AD amyloid pathology demonstrate that fluctuations in neural activity dynamically regulate levels of A-beta in the interstitial fluid (Bero et al., 2011). Such findings support the regulation of neural activity as a possible therapeutic modality to modify disease progression.

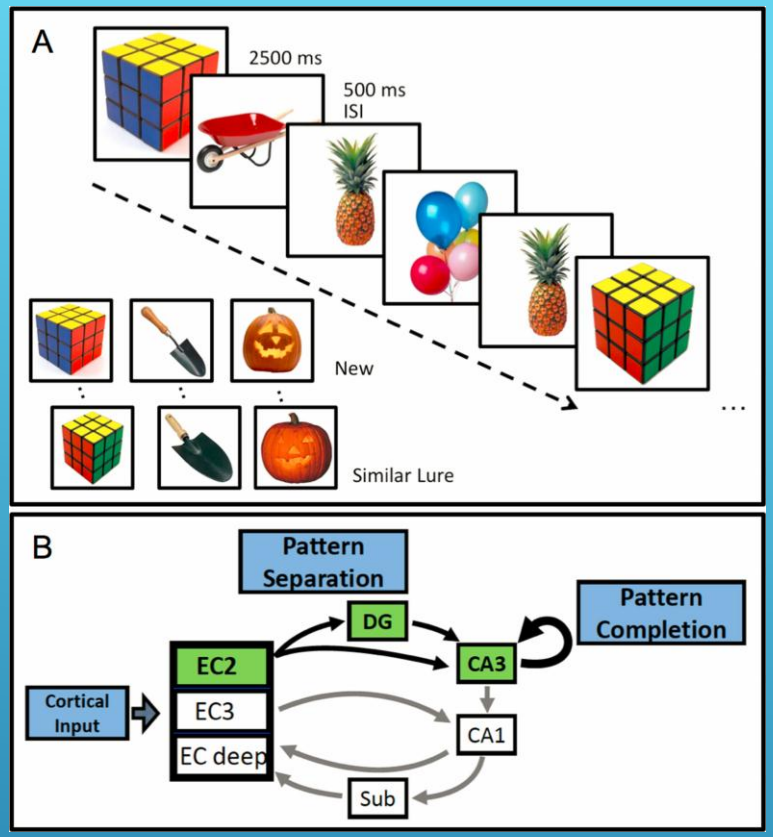

The lure items in the memory task are designed to assess the balance of pattern separation and pattern completion mediated by the DG/CA3. In memory-impaired aged rats with excess CA3 activity, the CA3 pyramidal neurons activate representations tied to prior experiences and fail to encode distinctive representations for new information, indicating a shift in network function toward greater pattern completion and diminished pattern separation (Wilson et al., 2006). A similar condition in humans would be expected to produce more errors with lures incorrectly identified as repetitions of prior items rather than correctly identified as similar but distinctive, only sharing features with prior items in the task. We found this specific profile in the aMCI patients.

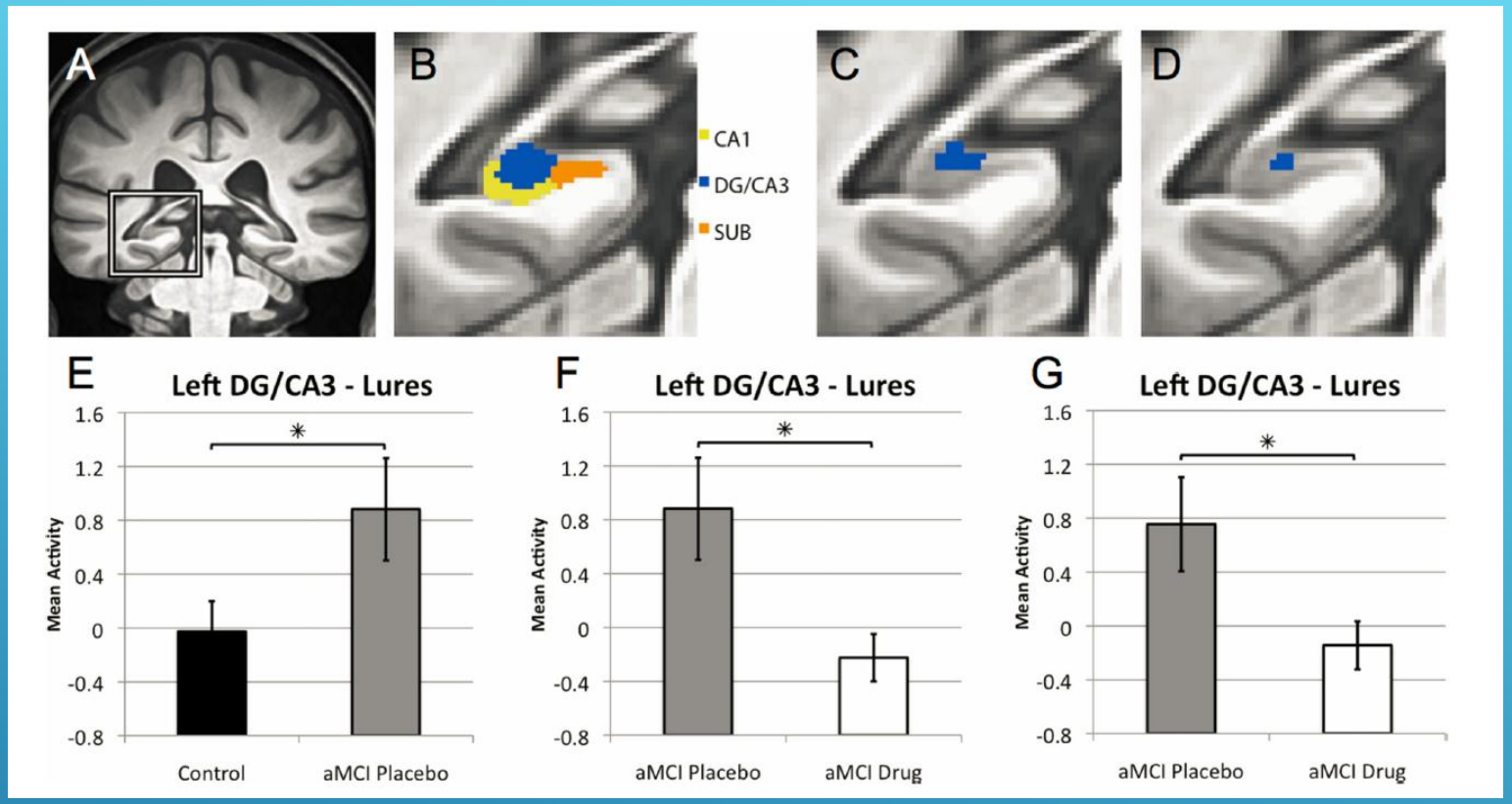
A
B
CA1
DG/CA3
SUB
C
D
E
Left DG/CA3 - Lures
Mean Activity
1.6
1.2
0.8
0.4
0
-0.4
-0.8
*
Control
aMCI Placebo
F
Left DG/CA3 - Lures
aMCI Placebo
aMCI Drug
G
Left DG/CA3 - Lures
aMCI Placebo
aMCI Drug

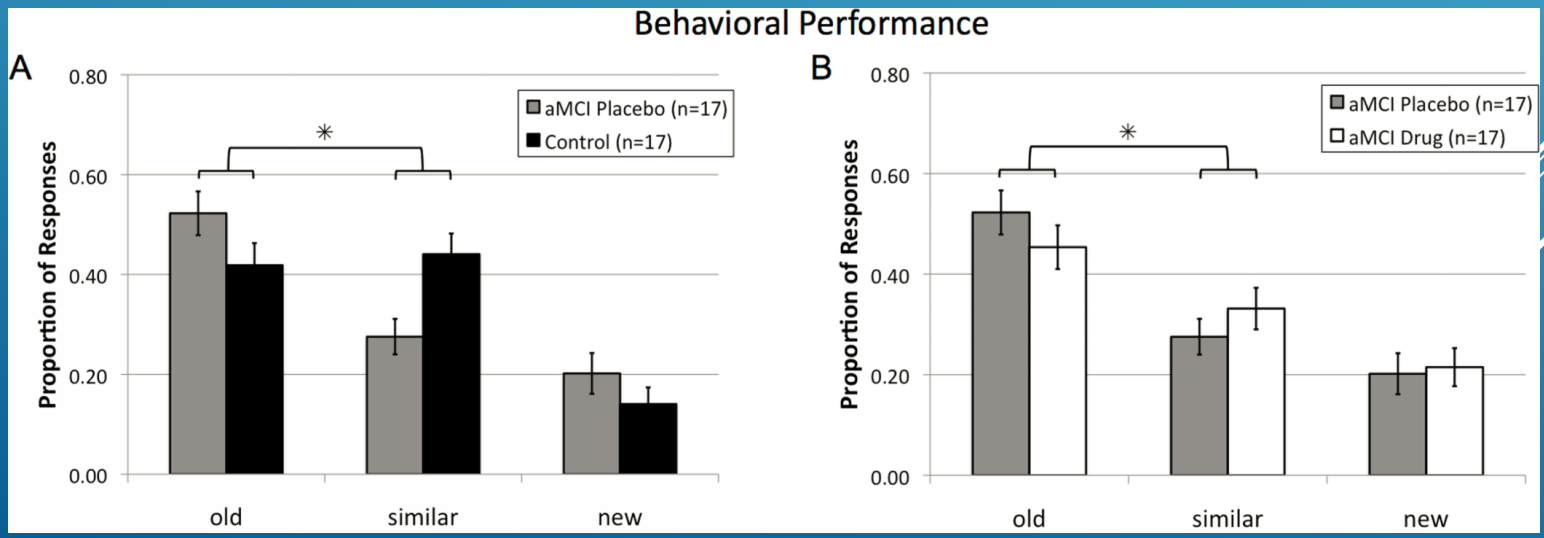
Behavioral Performance
A
Proportion of Responses
0.80
0.60
0.40
0.20
0.00
aMCI Placebo (n=17)
Control (n=17)
*
old
similar
new
B
aMCI Placebo (n=17)
aMCI Drug (n=17)

A Perfect Storm: Converging Paths of Epilepsy and Alzheimer's Dementia Intersect in the Hippocampal Formation

Noebels J.L., 2011

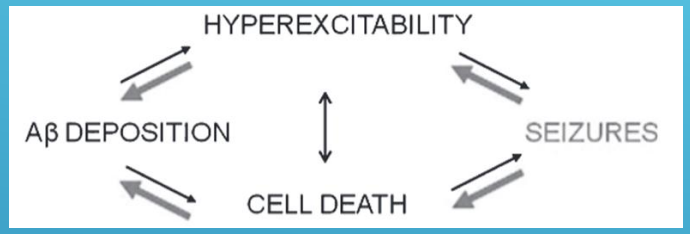

When active inhibitory mechanisms fail early, the resulting disinhibition may destabilize network oscillatory activity at formative stages of AD.

Critical new evidence implicating cellular hyperexcitability, hypersynchronous circuit activity, extensive rewiring of hippocampal networks, and subclinical temporal lobe "silent" seizures identified in validated mouse models of AD implicates a new level of circuit-based pathophysiology that could lead to the appearance of epilepsy and further aggravate memory loss.

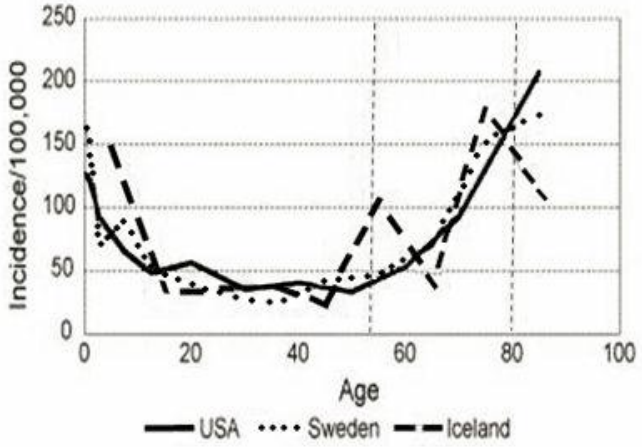

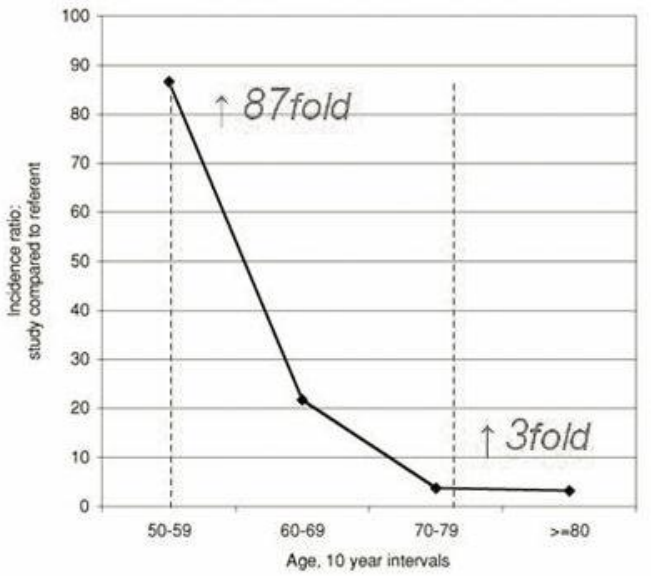

Cortical Atrophy

TLE

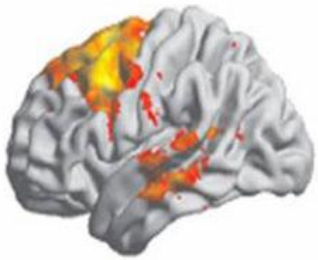

Bernhardt et al, 2008

AD

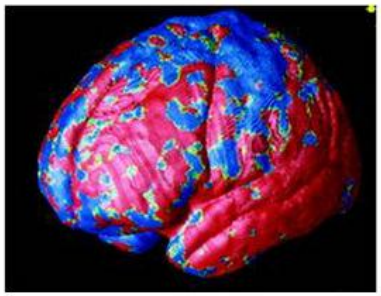

Thompson et al, 2003

Hypometabolism

TLE

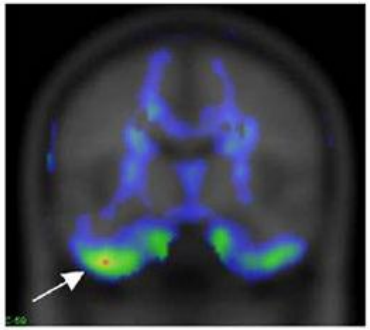

Carne et al, 2007

AD

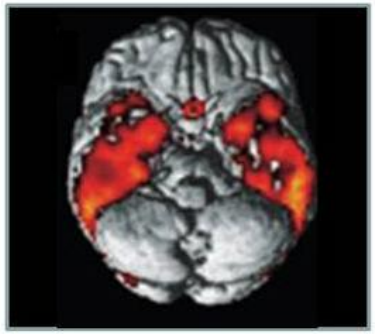

Edison et al, 2007

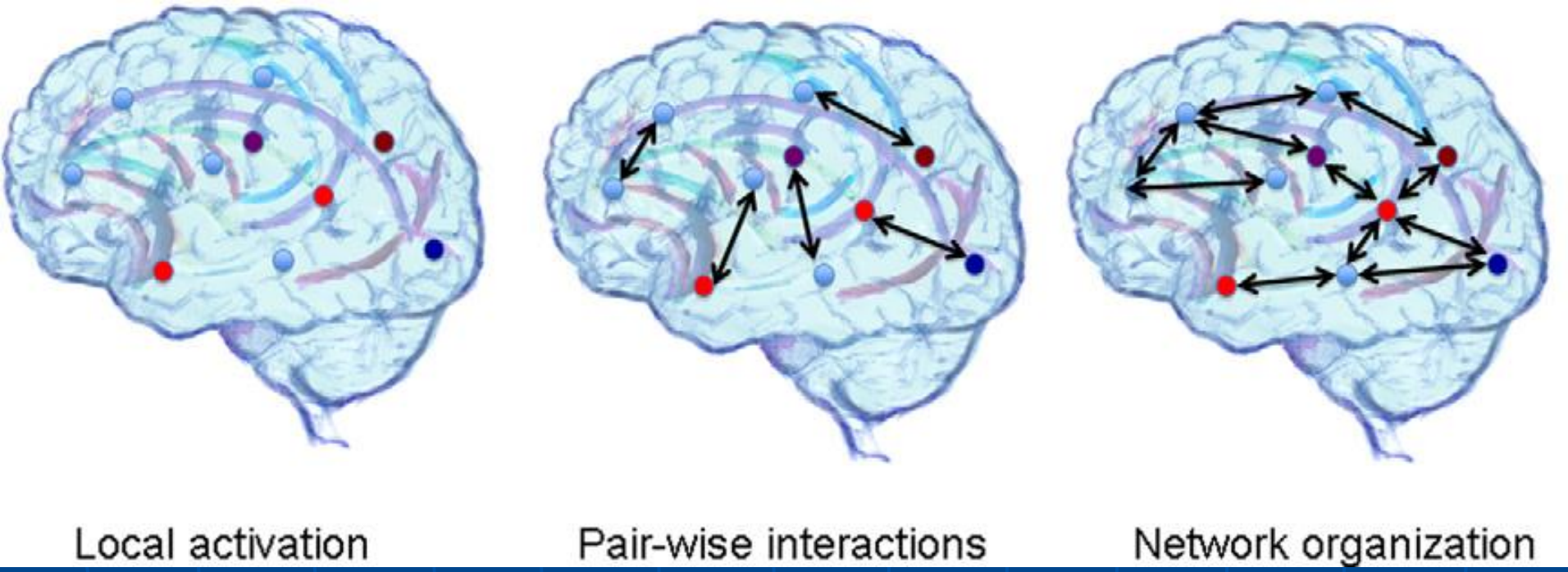

INTERACTION LEVEL

Zero order

First order

Second and higher order
(interactions of interactions)

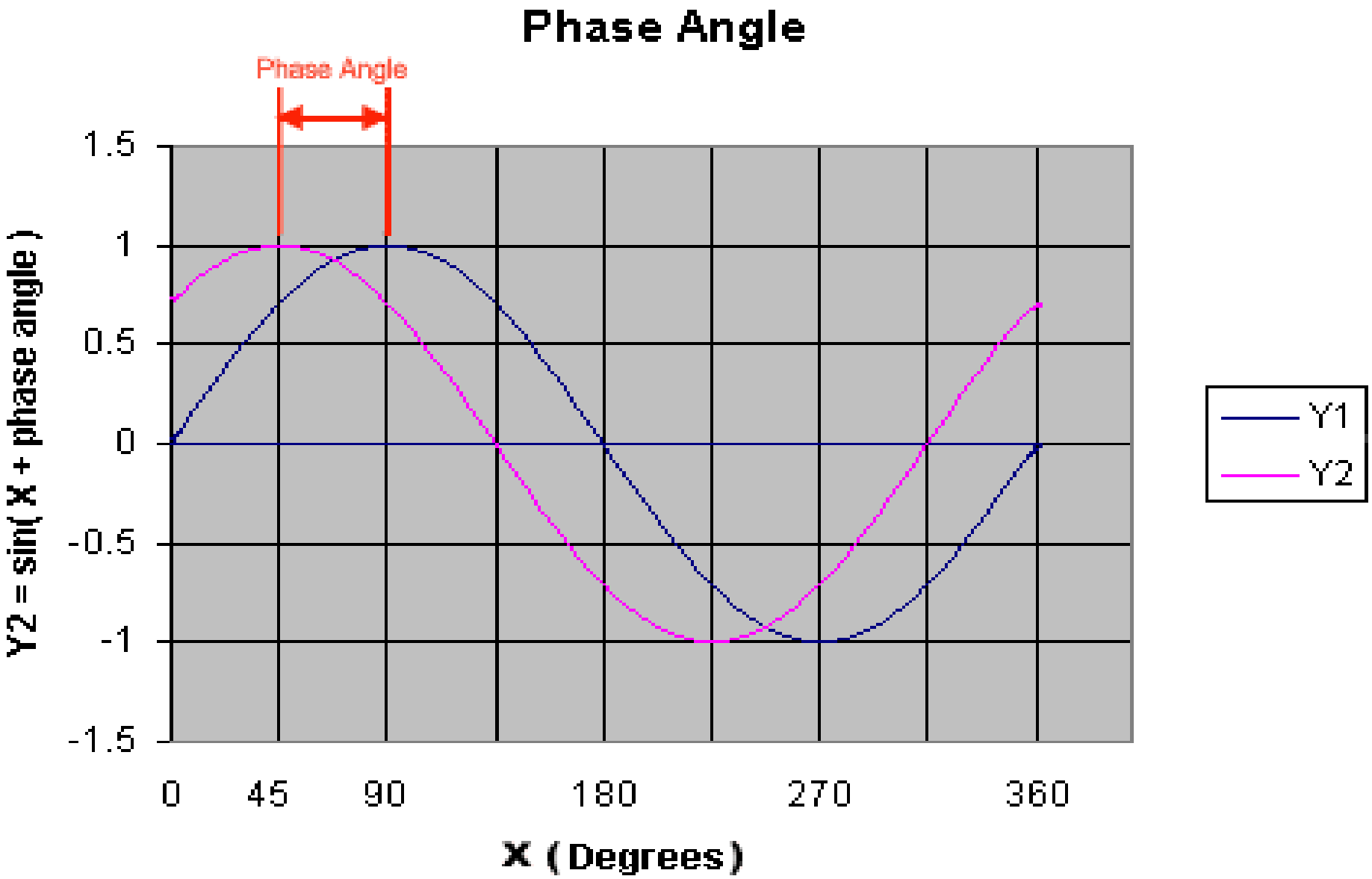
Phase Angle
Phase Angle
1.5
1
0.5
0
-0.5
-1
-1.5
0
45
90
180
270
360
Y2 = sin(x + phase angle)
x (Degrees)
Y1
Y2

Z-score coherence

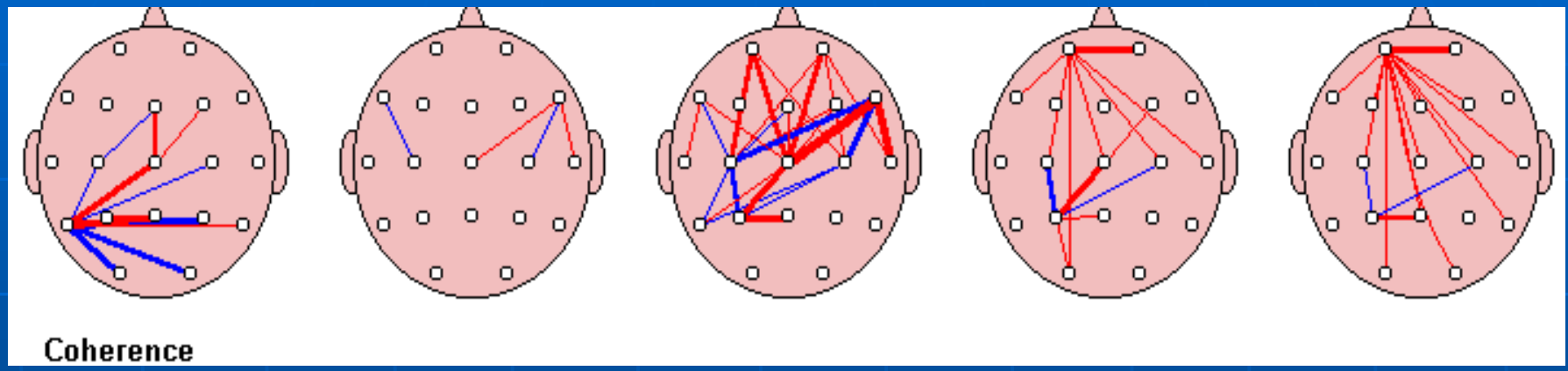

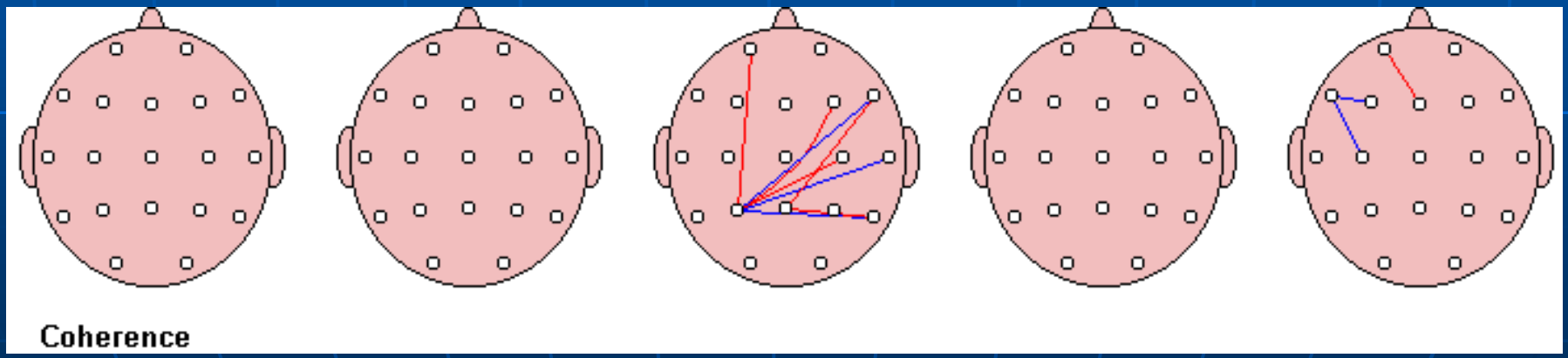

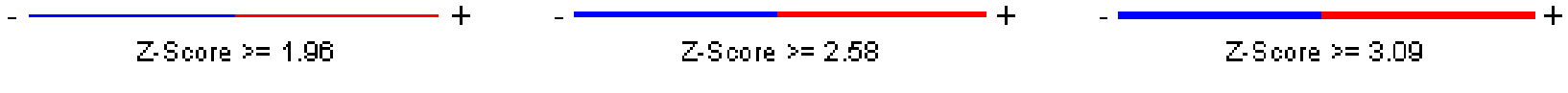

Hippocampal atrophy and interhemispheric hypercoherence in MCI

Moretti D.V., 2011

In MCI subjects, hippocampal atrophy is linked to an **increase of inter-hemispheric coherence seen on frontal (delta) and – earlier - temporal (delta, theta, alpha) regions**.

An increase of neuronal excitability could explain the increased temporal functional coupling.

This hypothesis could receive a support from studies demonstrating a dys-regulation of inhibitory GABA-ergic system following the hippocampal atrophy.

Through the hippocampal commissure, the increase of excitability could spread over the two hemispheres. Our results confirm this view because the increase of coherence between temporal regions is present only in the MCI subjects with the greater hippocampal atrophy.

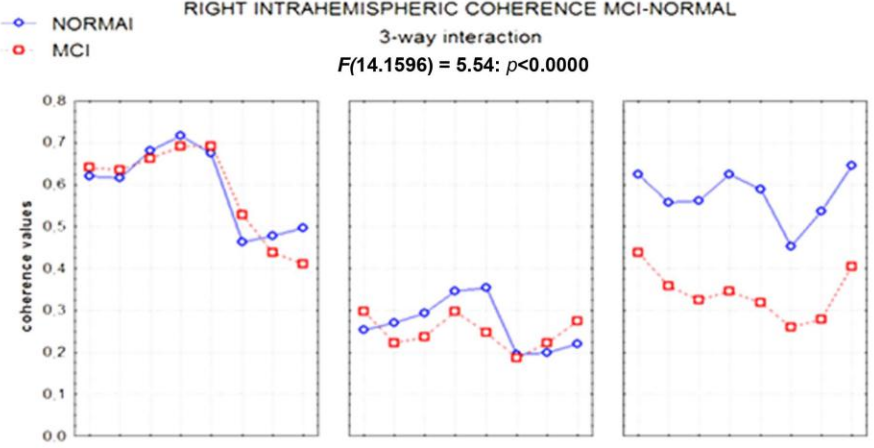
NORMAL
MCI
RIGHT INTRAHEMISPHERIC COHERENCE MCI-NORMAL
3-way interaction
F(14.1596) = 5.54: p<0.0000
coherence values

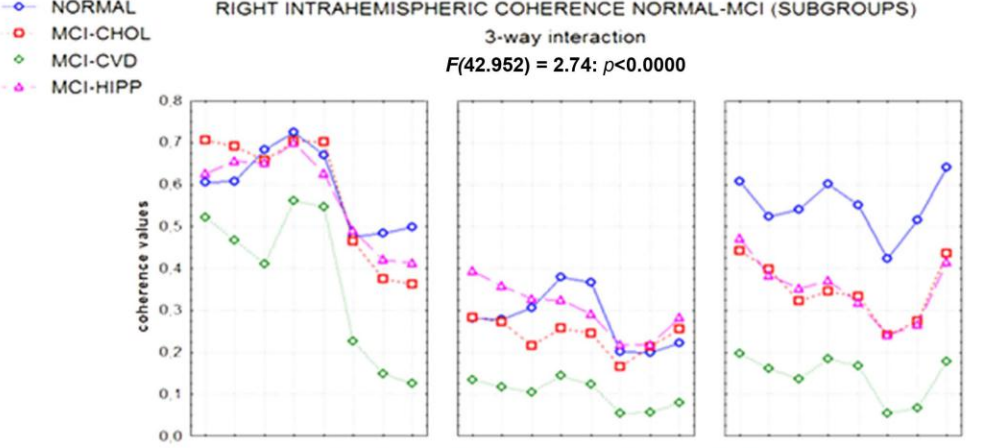
NORMAL
MCI-CHOL
MCI-CVD
MCI-HIPP
RIGHT INTRAHEMISPHERIC COHERENCE NORMAL-MCI (SUBGROUPS)
3-way interaction
F(42.952) = 2.74: p<0.0000
coherence values

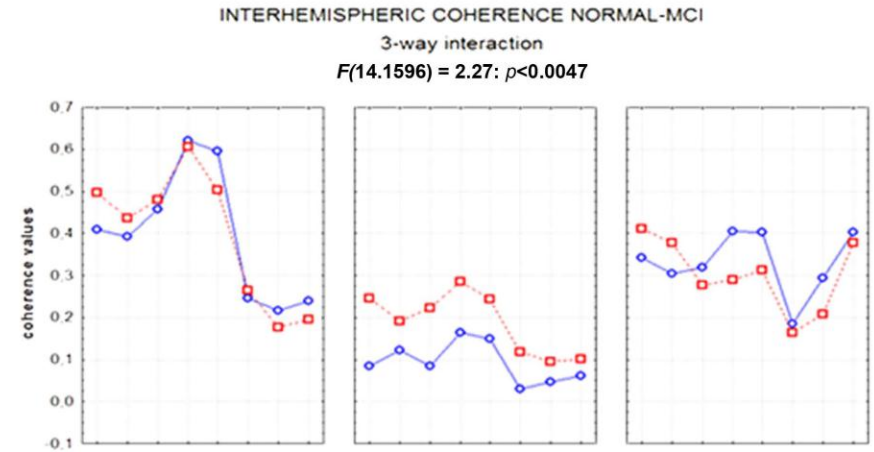
INTERHEMISPHERIC COHERENCE NORMAL-MCI
3-way interaction
F(14.1596) = 2.27: p<0.0047
coherence values

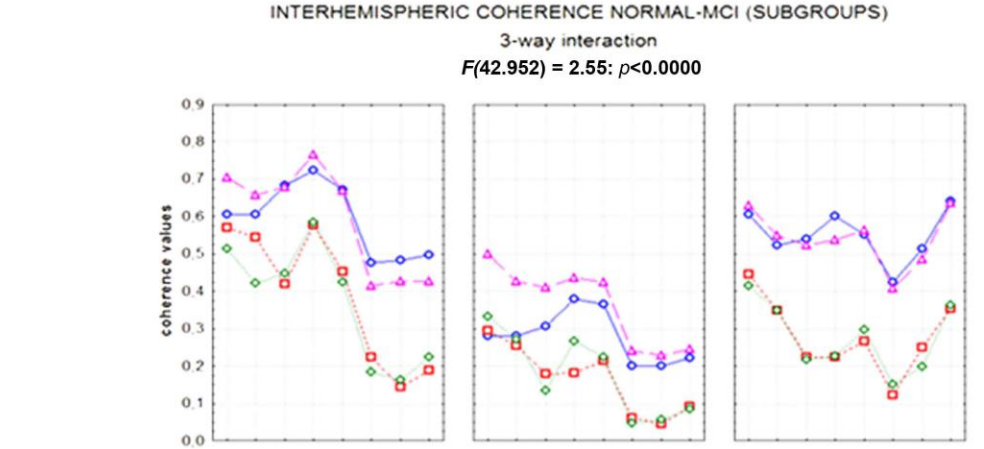
INTERHEMISPHERIC COHERENCE NORMAL-MCI (SUBGROUPS)
3-way interaction
F(42.952) = 2.55: p<0.0000
coherence values

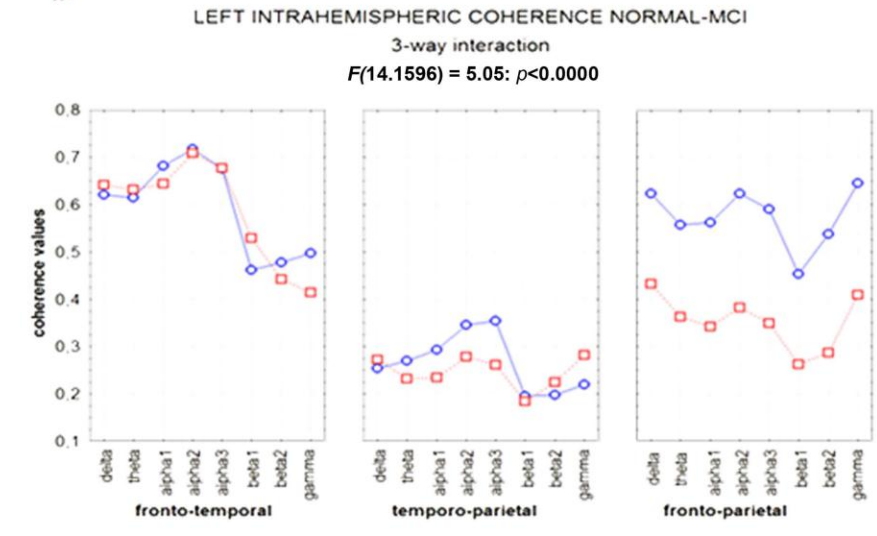
LEFT INTRAHEMISPHERIC COHERENCE NORMAL-MCI
3-way interaction
F(14.1596) = 5.05: p<0.0000
coherence values
delta
theta
alpha1
alpha2
alpha3
beta1
beta2
gamma
fronto-temporal
temporo-parietal
fronto-parietal

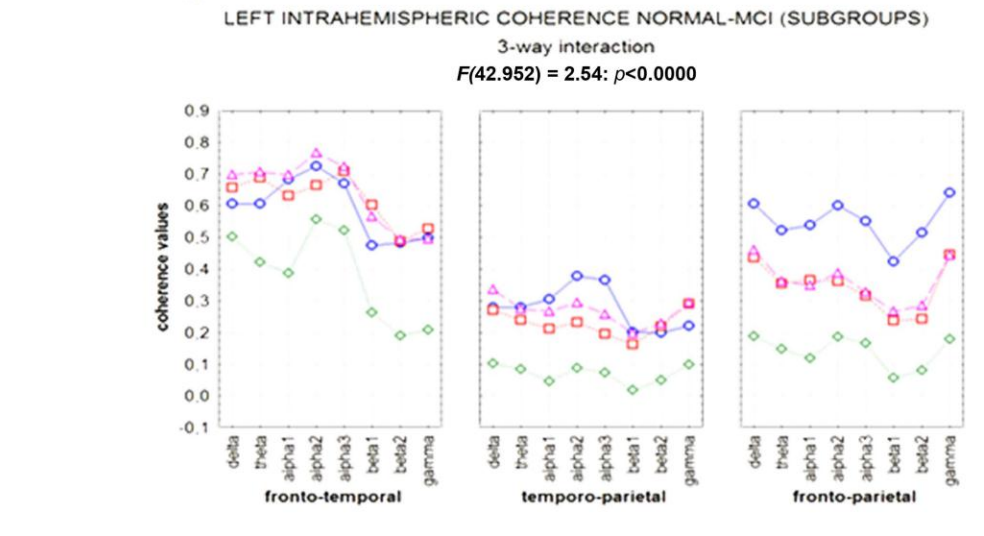
LEFT INTRAHEMISPHERIC COHERENCE NORMAL-MCI (SUBGROUPS)
3-way interaction
F(42.952) = 2.54: p<0.0000
coherence values
delta
theta
alpha1
alpha2
alpha3
beta1
beta2
gamma
fronto-temporal
temporo-parietal
fronto-parietal

A decrease of fronto-parietal coherence characterized MCI with hippocampal atrophy.

A possible explanation is that the increase of excitability in medial temporal areas subsequent to the hippocampal atrophy creates a sort of "temporal areas wall" impairing the long-range, fronto-parietal functional connections within each hemisphere.

Obstacles to EEG source location

electrical reference depresses near sources

EEG

poorly conductive skull blurs spatially scalp potentials

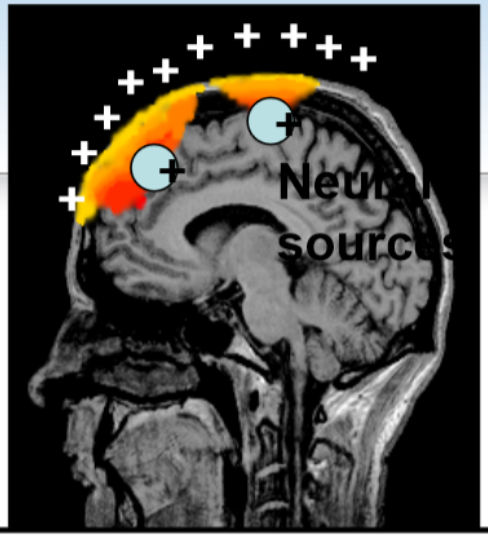

- Neural activity is conducted through the brain volume to the scalp and sensors by *Volume Conduction*
- Volume conduction is linear
- Each sensor measures a (weighted) sum of each neuron's activity

Volume Conduction

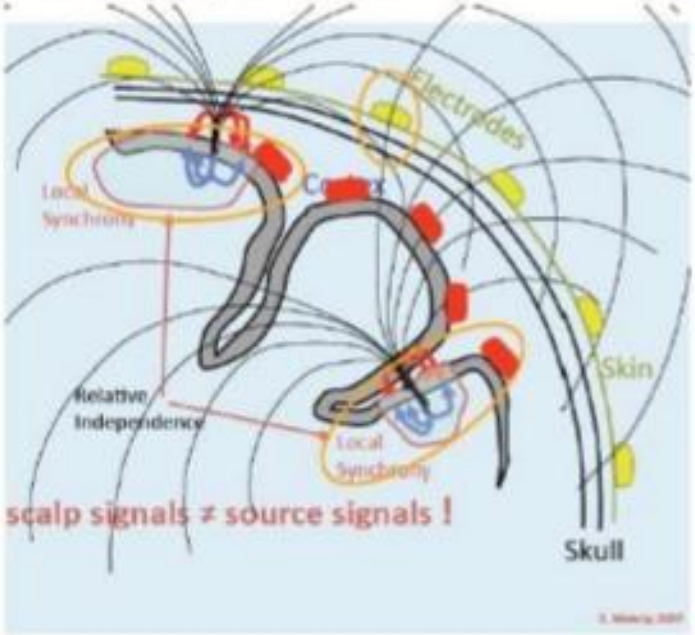

Limitations of scalp EEG

- Scalp electrode EEG activity is contaminated by far-field generators by volume conduction.
- Reference problems prevent exact localization and make phase/coherence calculations ambiguous.
- Blurring of the signal by the skull (solution: Laplacian montage).
- Coherence inflation by phase delay = 0 volume conduction (solution: lagged phase synchrony; phase lag index).

A Lagged Phase Synchronization

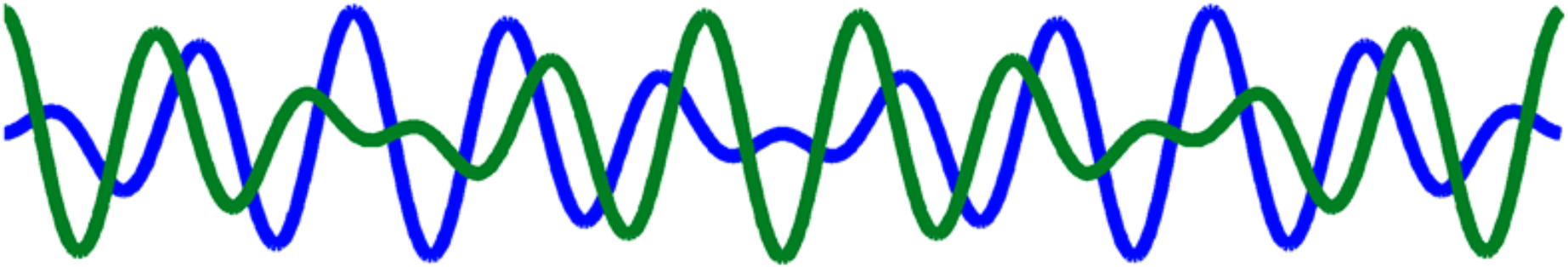

Source Localization from EEG

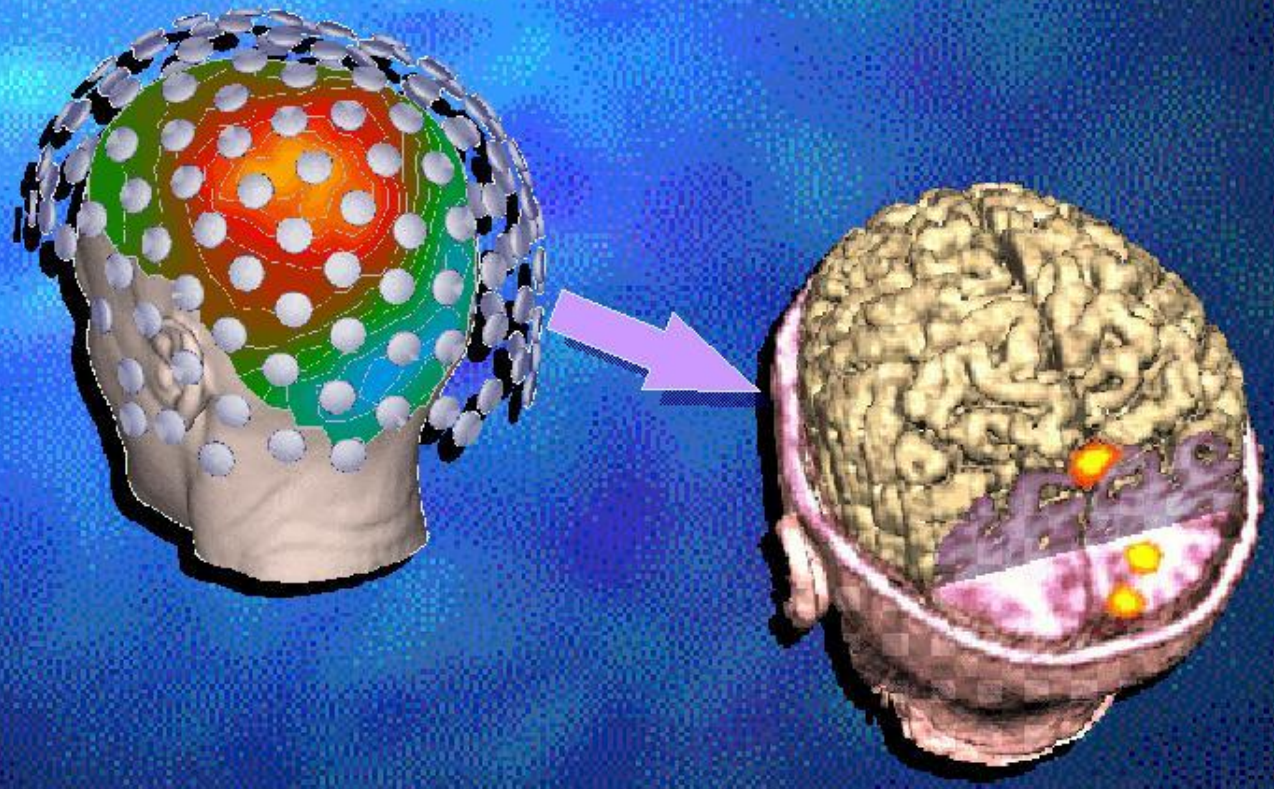

Inverse solution: two reasons

- Solving ambiguity of scalp problem of volume conduction and reference
- Electrical Neuro-Imaging

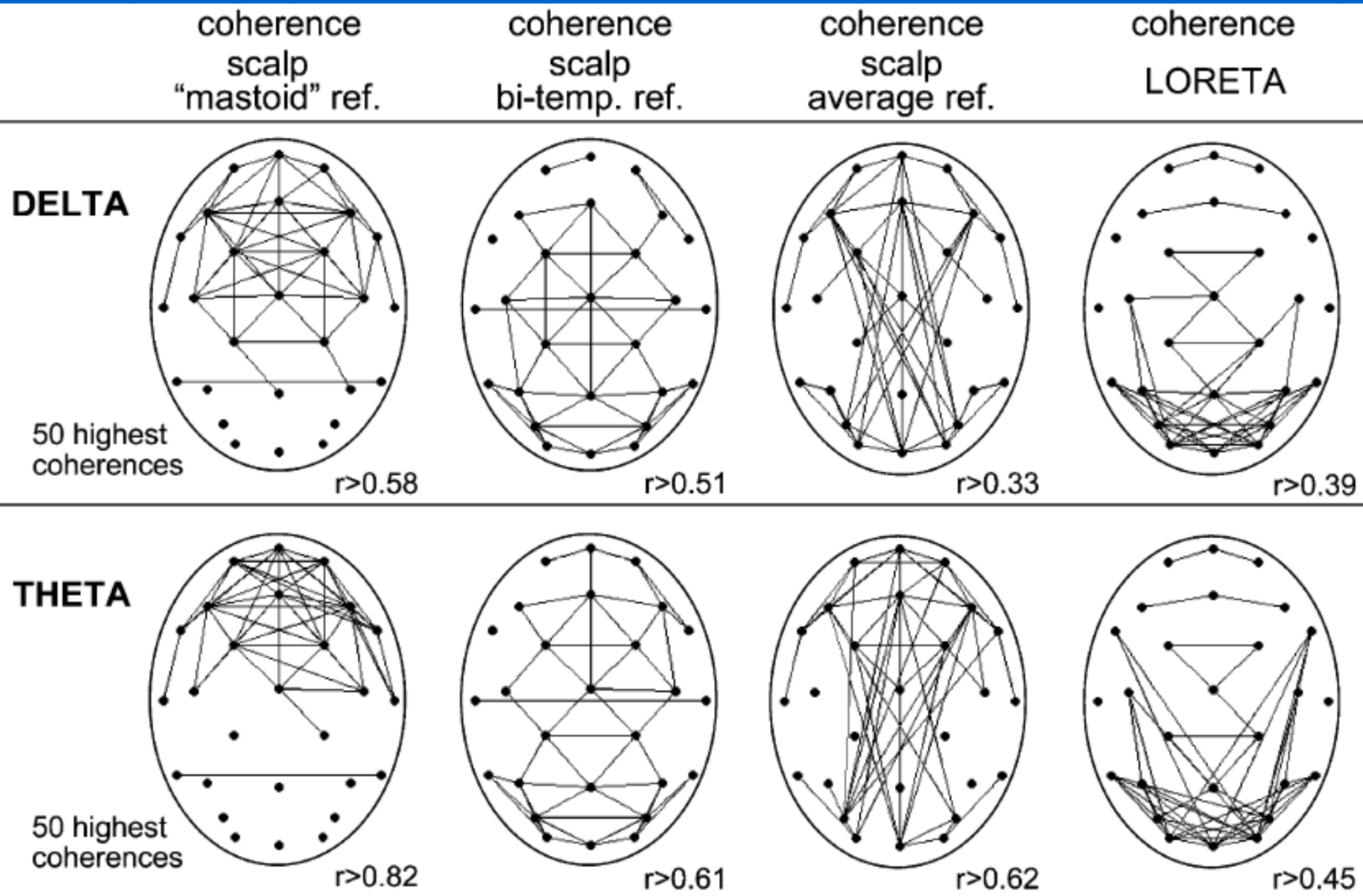
coherence
scalp
"mastoid" ref.
coherence
scalp
bi-temp. ref.
coherence
scalp
average ref.
coherence
LORETA
DELTA
50 highest
coherences
r>0.58
r>0.51
r>0.33
r>0.39
THETA
50 highest
coherences
r>0.82
r>0.61
r>0.62
r>0.45

The Inverse Problem:

Any measured scalp electromagnetic distribution may be described by an infinite number of possible source distributions

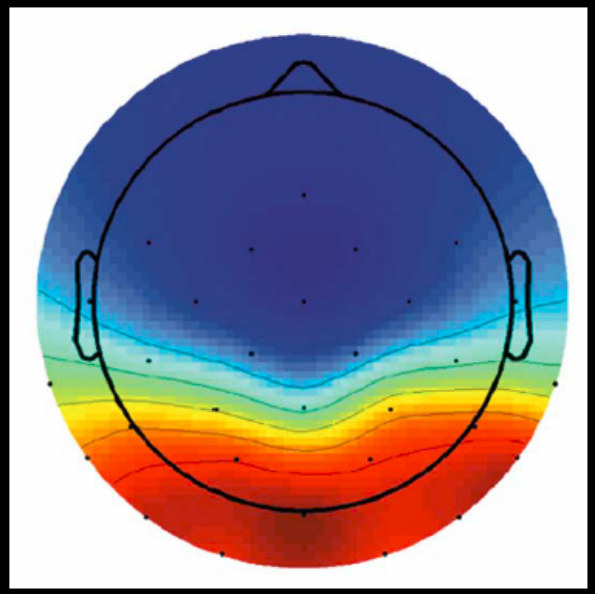

?

=

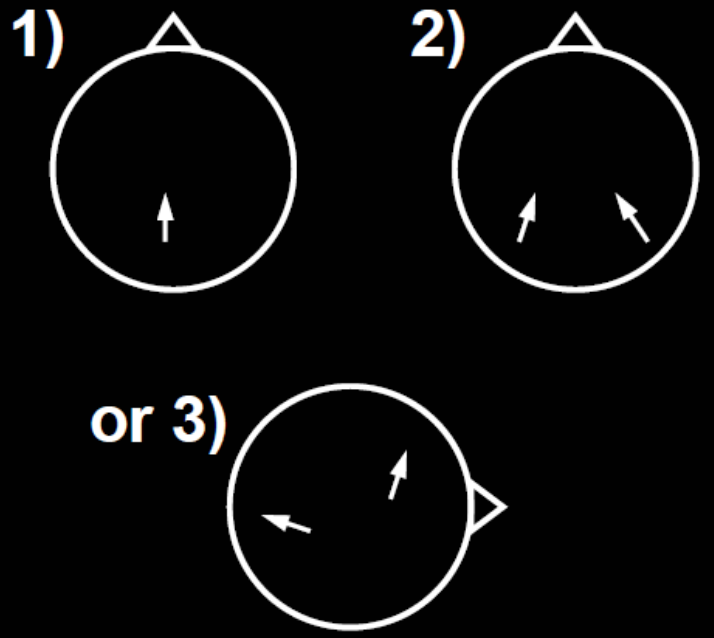

Must use functional–anatomical criteria to constrain the number of possible source distributions

Inverse solution

- Neuroanatomical constraints: cortex
- Electrophysiological constraint: 40-200 mm2 cortical area is needed to produce a well-defined potential at the scalp
- Electrophysiological constraint: electrical activity mostly occurs in a whole Brod-mann area (88 BAs)
- LORETA: distributed solution of dipoles
- Laplacian operator: 2nd spatial derivative = current density
- Validation with EP and with fMRI, DTI

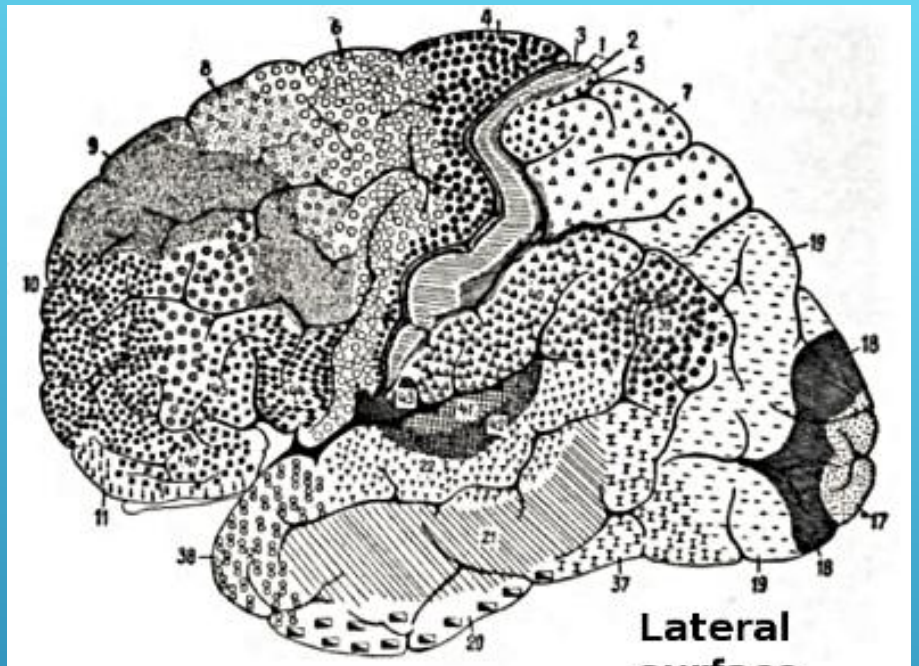
Lateral surface

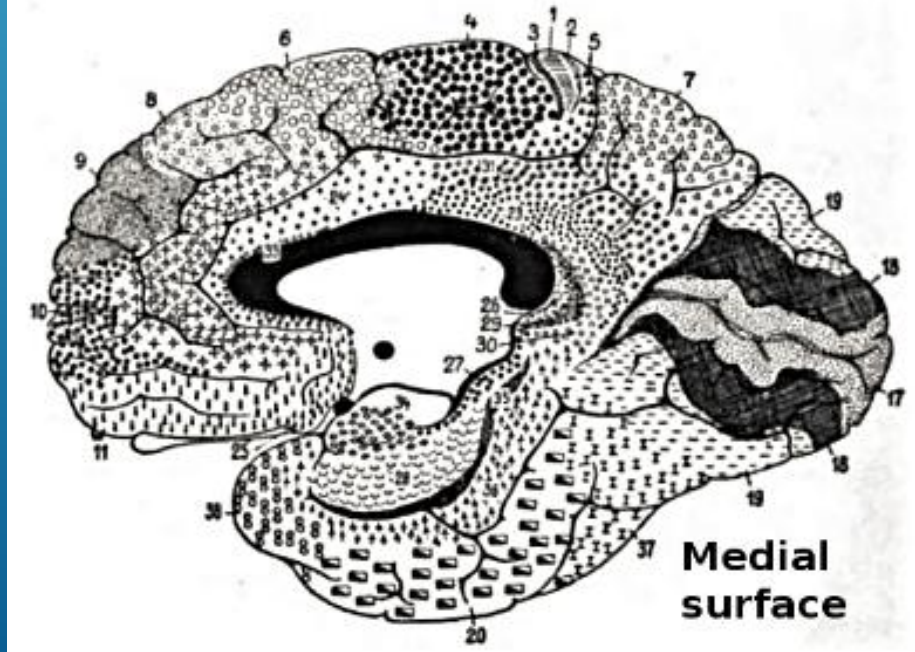
Medial surface

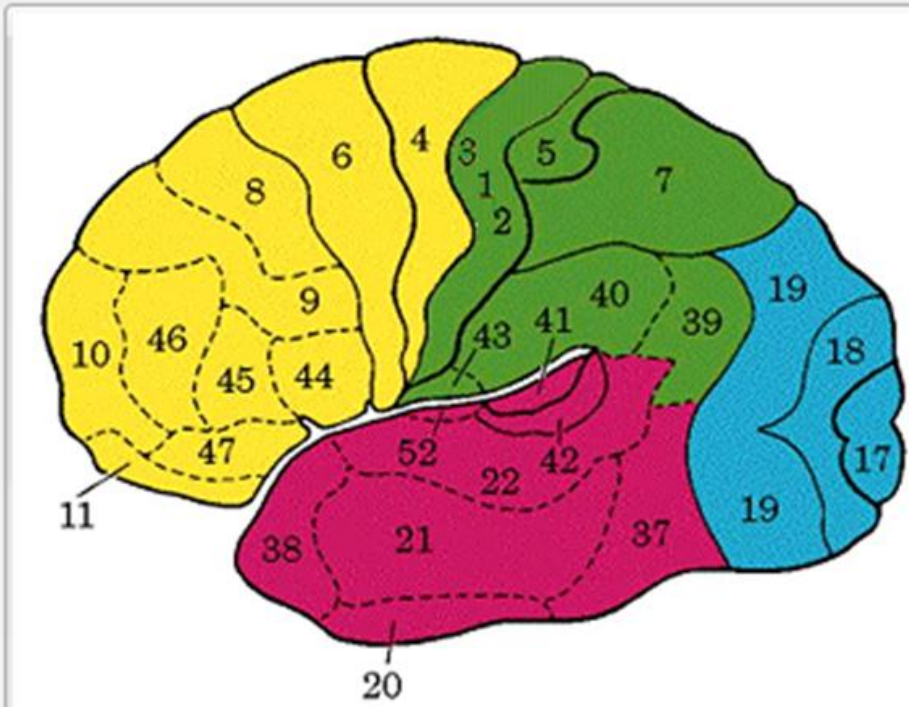
1
2
3
4
5
6
7
8
9
10
11
17
18
19
20
21
22
37
38
39
40
41
42
43
44
45
46
47
52

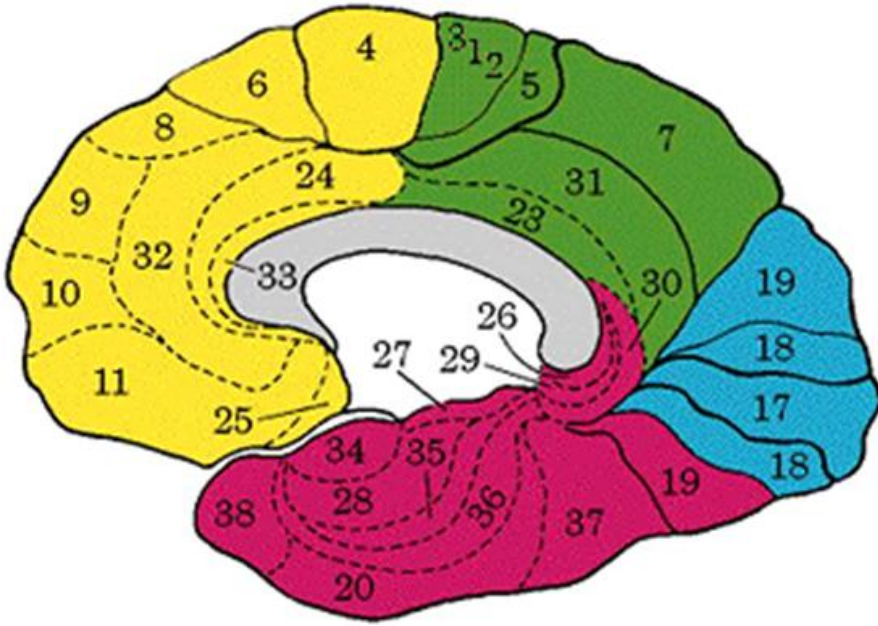
1
2
3
4
5
6
7
8
9
10
11
17
18
19
20
23
24
25
26
27
28
29
30
31
32
33
34
35
36
37
38

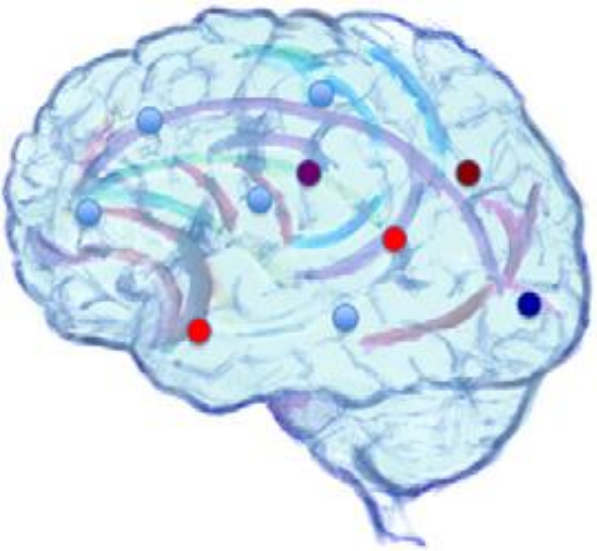

Local activation

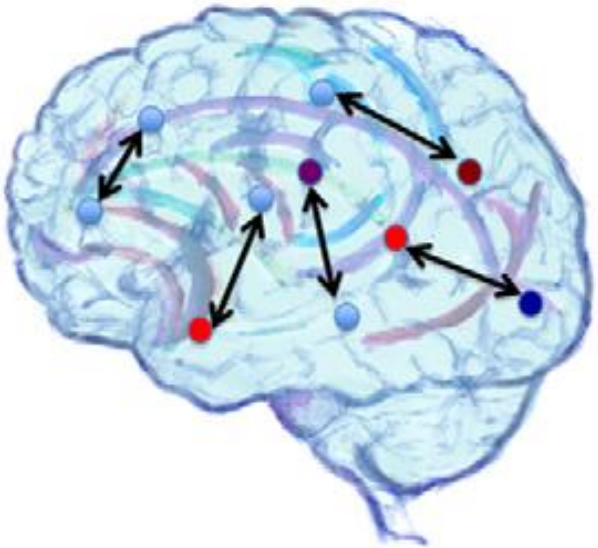

Pair-wise interactions

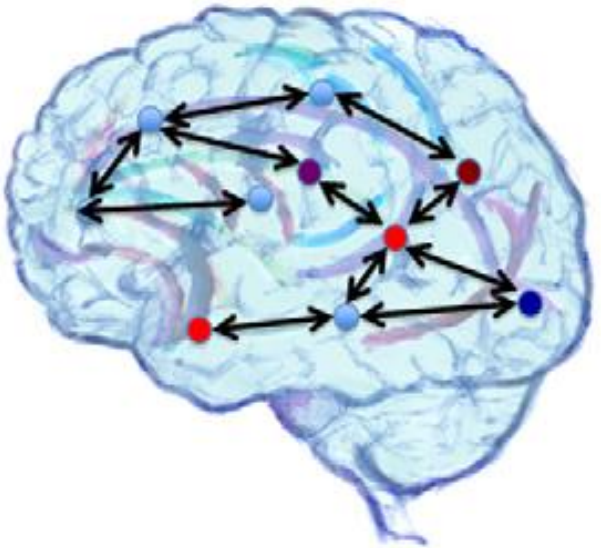

Network organization

INTERACTION LEVEL

Zero order

First order

Second and higher order
(interactions of interactions)

OPEN ACCESS Freely available online

PLOS ONE

Resting-State Network Disruption and *APOE* Genotype in Alzheimer's Disease: A *lagged* Functional Connectivity Study

Leonides Canuet[1]*, Ivan Tellado[1], Veronica Couceiro[1], Carmen Fraile[1], Lucia Fernandez-Novoa[2], Ryouhei Ishii[3], Masatoshi Takeda[3], Ramon Cacabelos[1,2]

1 EuroEspes Biomedical Research Center, Institute for CNS Disorders and Genomic Medicine, Corunna, Spain, **2** EuroEspes Biotechnology Division (Ebiotec), Institute for CNS Disorders and Genomic Medicine, Corunna, Spain, **3** Department of Psychiatry, Osaka University Graduate School of Medicine, Suita city, Osaka, Japan

The main advantage of the regional analysis of LORETA solutions is that this modelling can disentangle rhythms of contiguous cortical areas.

Reference free: unambiguous localization and unambiguous phase/ coherence calculations.

Table 2. Cortical regions of interest (ROIs) determined by eLORETA.

Scalp electrodes	ROI centroid MNI coordinates[a]			Anatomical regions	BAs
	x	*y*	*z*		
Fp1	−25	65	−5	Left frontopolar cortex	10,11
Fp2	25	65	−5	Right frontopolar cortex	10,11
F7	−50	40	−10	Left IFG/ATC	45,47,38
F3	−45	40	30	Left MFG (DLPFC)	9,46
Fz	5	45	50	Superior frontal gyrus (mPFC)	8,9
F4	45	40	30	Right MFG (DLPFC)	9,46
F8	50	40	−10	Right IFG/ATC	45,47,38
T7/T3	−65	−15	−15	Left STG/MTG	21,22,42
C3	−50	−20	60	Left precentral/postcentral (CC)	1,2,3,4,6
Cz	5	−10	70	Medial frontal cortex	4,6
C4	55	−20	55	Right precentral/postcentral (CC)	1,2,3,4,6
T8/T4	70	−20	−10	Right STG/MTG	21,22,42
P7/T5	−60	−65	−5	Left posterior temporal cortex (TOJ)	19,22,37
P3	−40	−70	45	Left inferior parietal lobe	7,39,40
Pz	−5	−65	65	Medial parietal (Precuneus)	7
P4	45	−70	45	Right inferior parietal lobe	7,39,40
P8/T6	55	−70	0	Right posterior temporal cortex (TOJ)	19,22,37
O1	−20	−100	10	Left occipital cortex	17,18,19
O2	20	−100	5	Right occipital cortex	17,18,19

[a]ROIs included all cortical voxels within a 15 mm radius of the center. BAs, Brodmann areas; IFG, inferior frontal gyrus; ATC, anterior temporal cortex; MFG, middle frontal gyrus; DLPFC, dorsolateral prefrontal cortex; mPFC, medial prefrontal cortex; STG, superior temporal gyrus; MTG, middle temporal gyrus; CC, central cortex; TOJ, temporo-occipital junction.

doi:10.1371/journal.pone.0046289.t002

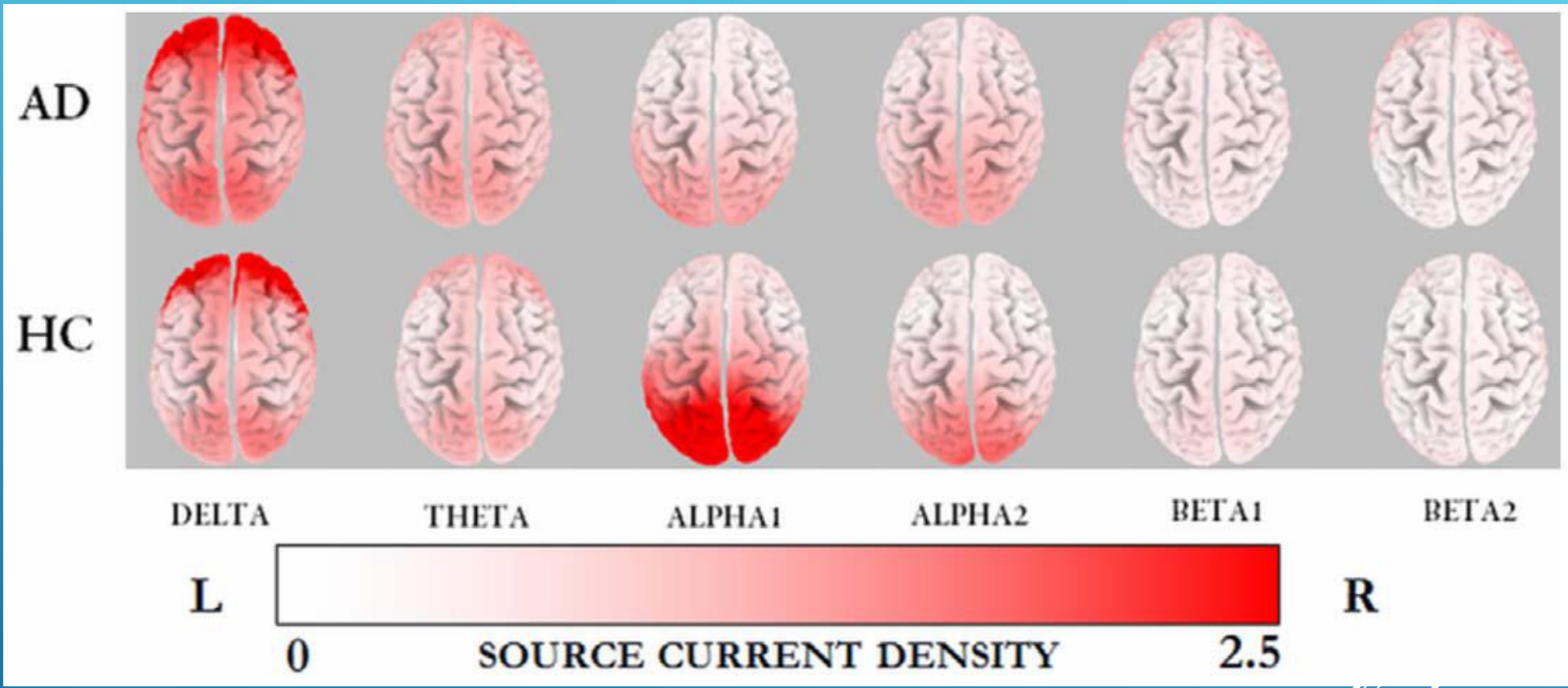
AD
HC
DELTA
THETA
ALPHA1
ALPHA2
BETA1
BETA2
L
R
0
SOURCE CURRENT DENSITY
2.5

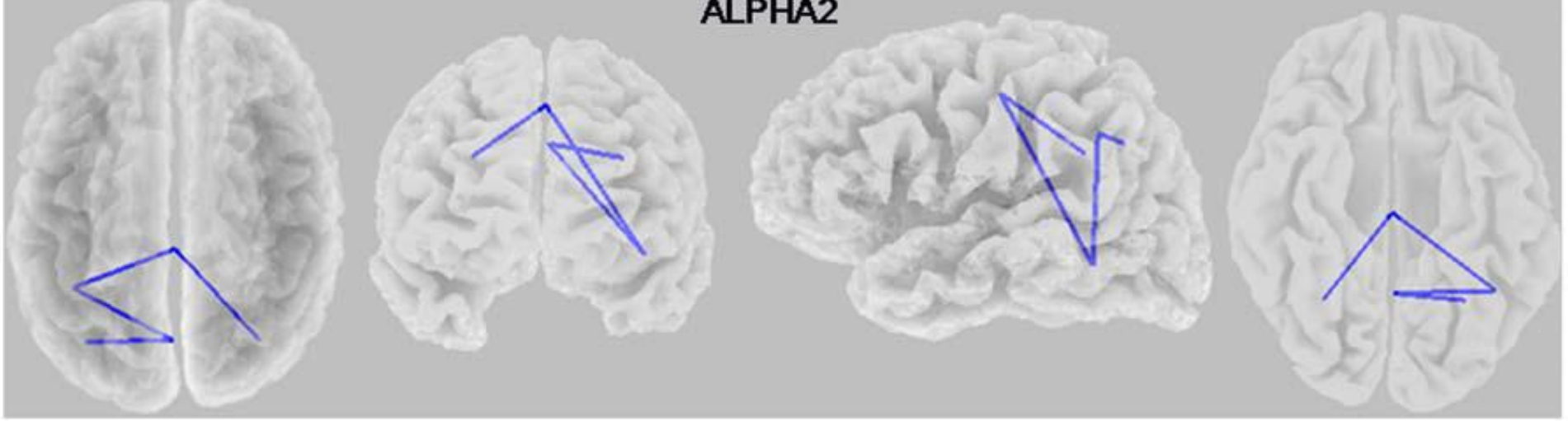

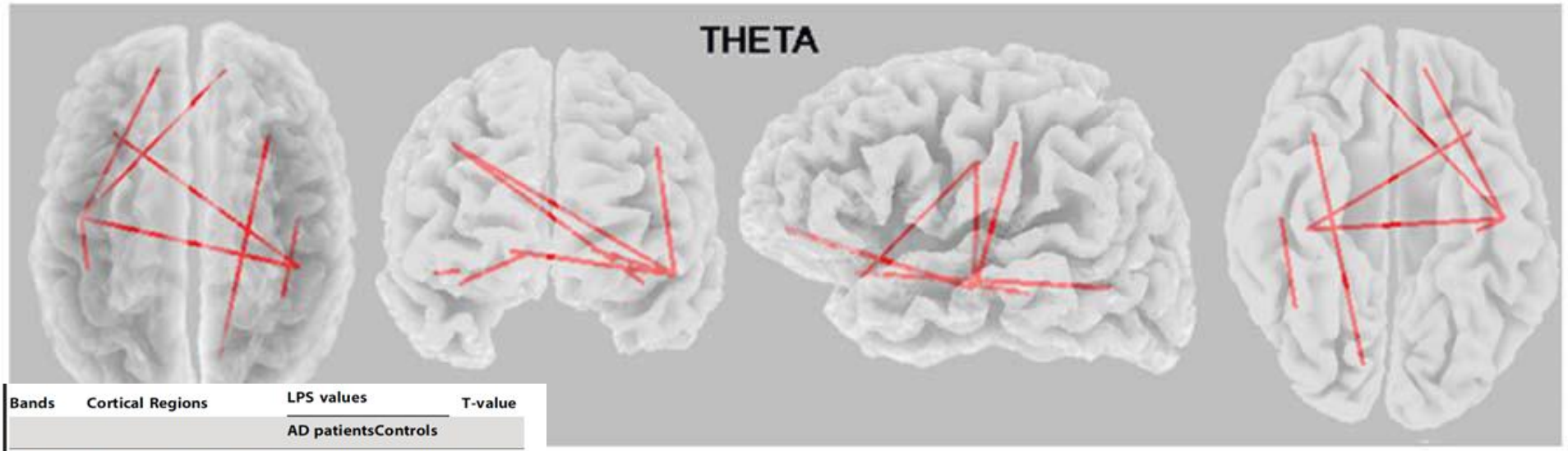

Bands	Cortical Regions		LPS values		T-value
			AD patients	Controls	
Alpha2	L. Temporal	mid-central	0.091±0.067	0.14±0.090	−3.49
(10–13 Hz)	L. Temporal	mid-parietal	0.096±0.063	0.14±0.077	−3.55
	R. Parietal	mid-central	0.11±0.080	0.15±0.082	−3.56
	R. Parietal	mid-parietal	0.071±0.052	0.10±0.051	−3.52
Theta	L. Temporal	L. Prefrontal	0.074±0.040	0.051±0.027	4.27
(4–8 Hz)	L. Temporal	R. Prefrontal	0.098±0.056	0.063±0.029	5.06
	L. Temporal	L. Central	0.089±0.055	0.060±0.033	4.32
	L. Temporal	R. Central	0.087±0.043	0.067±0.019	4.30
	L.ant. Temporal	R. Central	0.070±0.036	0.050±0.017	4.65
	R. Temporal	R. inf. Parietal	0.076±0.044	0.051±0.030	4.60
	R.ant. Temporal	R. Occipital	0.094±0.055	0.066±0.031	4.39

front left bottom

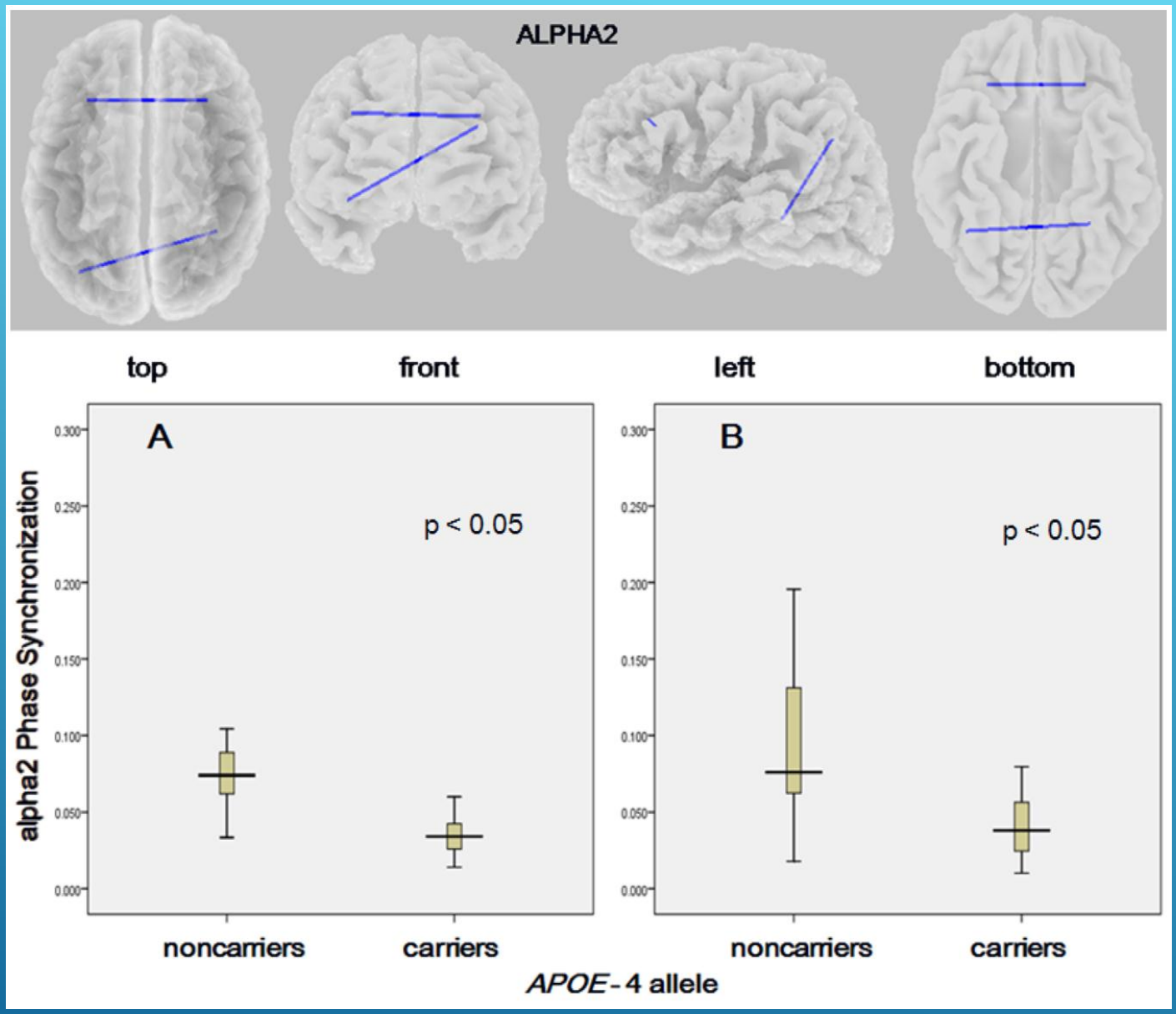

Early AD

A. Lateral PFC

B.L Temporal-R.Parietal

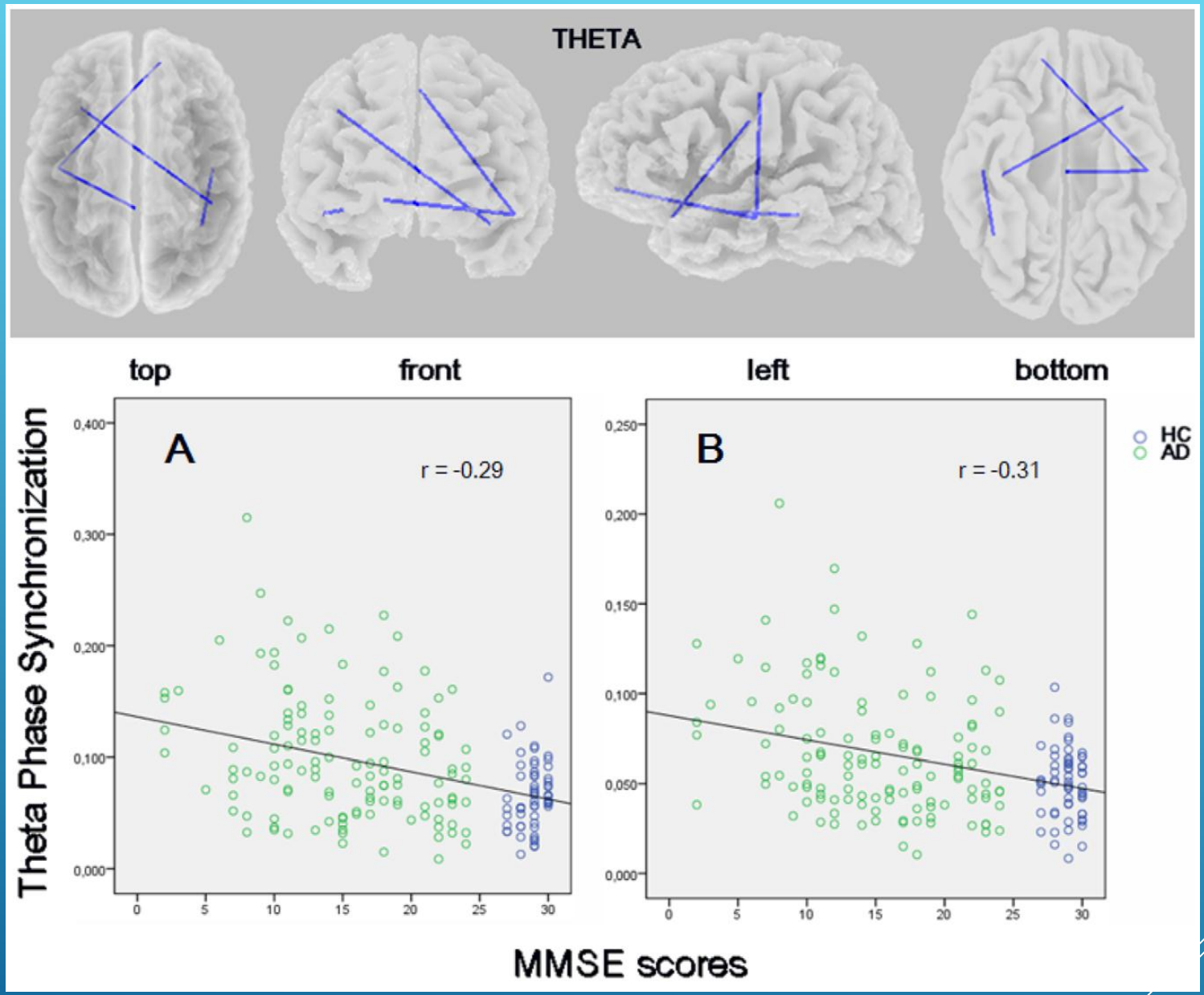

L TEMP.-R PF L ANTEROTEMP.-R CENTR.

Knyazeva M.G., 2010

MPS (multivariate phase synchronization) measures the degree of phase synchronization within a multivariate time series and allows synchronization mapping in spatially extended systems.

In early AD, whole-head mapping reveals a specific landscape of synchronization characterized by **a decrease in MPS over the fronto-temporal region and an increase over the temporo-parieto-occipital region predominantly of the left hemisphere**.

These features manifest themselves through the EEG delta–beta bands and **discriminate patients from controls with an accuracy of up to 94%.** Moreover, the abnormal MPS in both anterior and posterior clusters correlates with the MMSE score, binding regional EEG synchronization to cognitive decline in AD patients. The MPS technique reveals that the EEG phenotype of early AD is relevant to the clinical picture and may ultimately become its sensitive and specific biomarker.

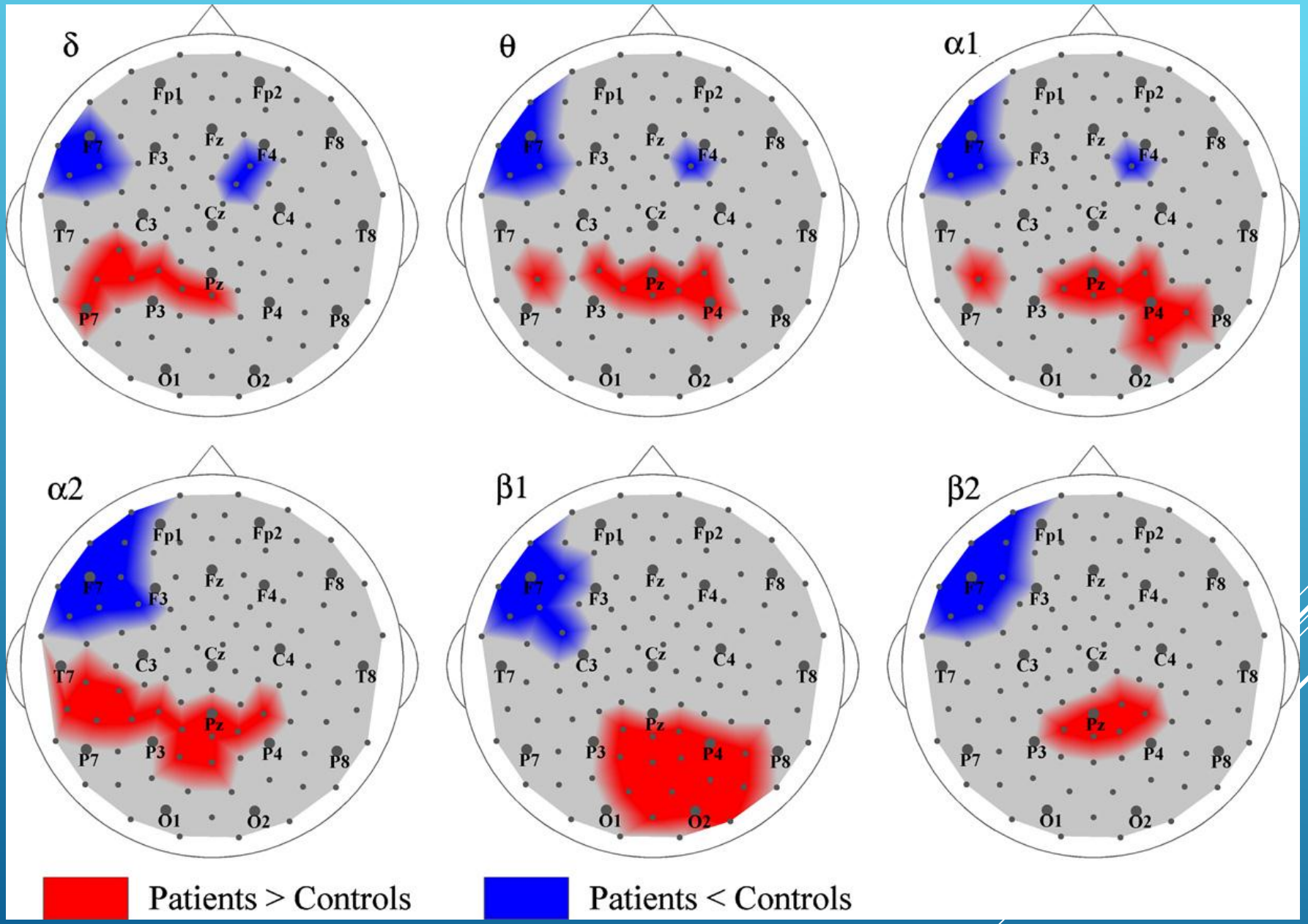
δ
θ
α1
α2
β1
β2
Fp1
Fp2
F7
Fz
F3
F4
F8
T7
C3
Cz
C4
T8
Pz
P7
P3
P4
P8
O1
O2
Patients > Controls
Patients < Controls

Van Straaten E.C.W., 2014

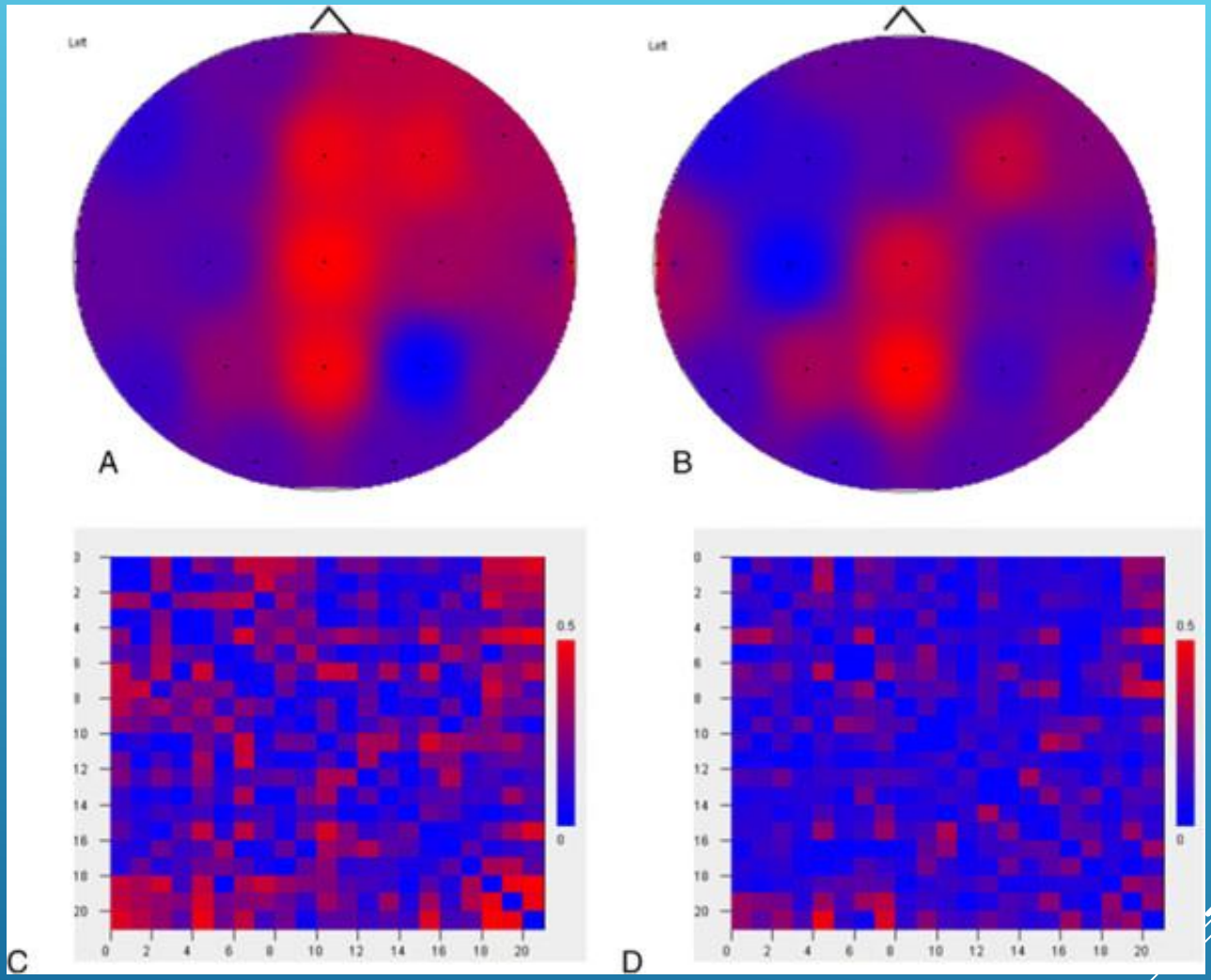

NORMAL AD

ALPHA2 PHASE LAG INDEX

source EEG synchronization in early Alzheimer's disease

Knyazeva M.G., 2013

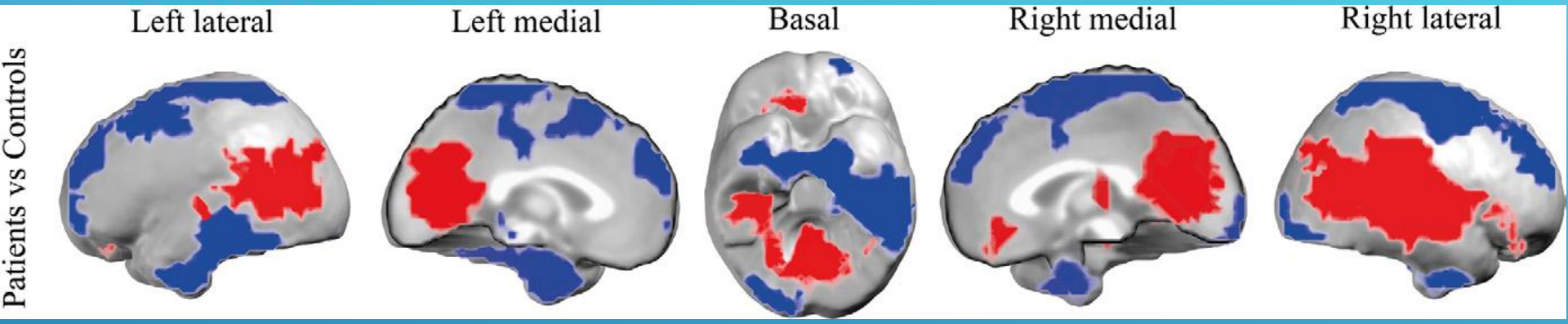

Hyposynchronized clusters in the temporal and prefrontal cortices.

Lateral: superior, middle, and medial frontal gyri bilaterally and the left inferior and middle temporal gyri.

Medial temporal lobe: the uncus bilaterally and the left parahippocampal gyrus together with the left fusiform gyrus. The medial hemispheric surfaces were affected symmetrically.

source EEG synchronization in early Alzheimer's disease

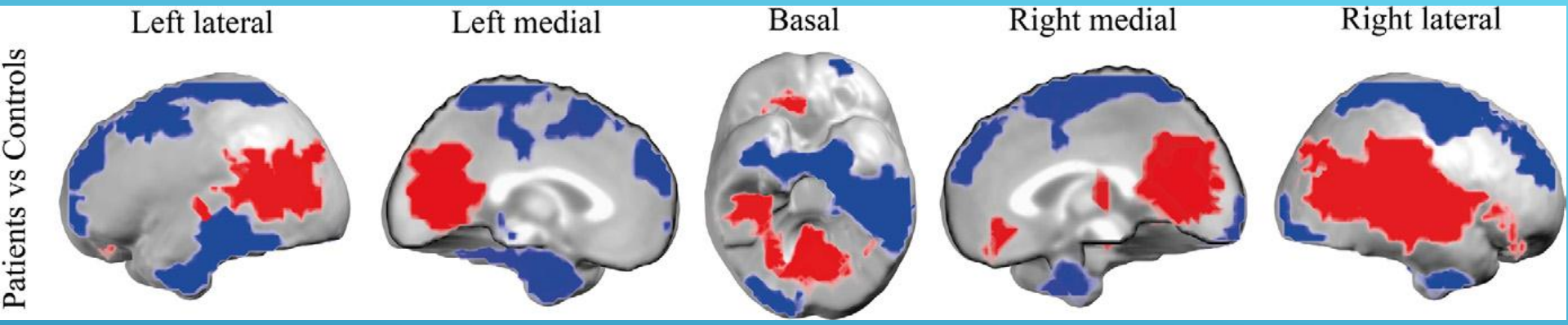

Hypersynchronization in **posterior clusters** located on the medial, basal, and lateral surfaces of both hemispheres, with the largest network on the **right hemispheric convexity**.
This **R cluster** spread from the right inferior and middle occipital gyri posteriorly, covering a significant part of the lateral temporal territories.
The **L cluster** was limited to parietal (SMG) and lateral temporal.

In the **medial surface** hypersynchronized networks covered the posterior cingulate gyrus, precuneus, and cuneus.

On the **basal surface** they were found in the lingual, right fusiform, and right parahippocampal gyri.

2-phase scenario for the evolution of FC with AD progression

Increased EEG **synchronization** is characteristic of early and possibly preclinical AD, and is the result of a loss of inhibitory interneurons. With progression, ongoing degradation of anatomical connectivity ultimately results in hyposynchronization.

Increased EEG synchronization is a manifestation of the hypoactive state of a region in early AD. The clinical significance of this possibility is that the earliest EEG signs of preclinical AD may be hypersynchronization in the posterior cortex (lateral and medial parietal and posterior cingulate cortices, extending into lateral occipital and medial temporal regions). This is a very early event observed at a preclinical stage, when neither cognitive deficits, nor cerebral atrophy are detected.

The networks with decreased intraregional synchronization are in the lateral and medial temporal regions including parahippocampal and fusiform gyri of the left hemisphere and the uncus, which is affected early in AD.

The asymmetry of hyposynchronization with greater effects in the left hemisphere is mirrored by a comparable spatial pattern of demyelination of juxtacortical white matter (U-fibers).

Neuroscience. 2006 Dec;143(3):793-803. Epub 2006 Oct 13.

Conversion from mild cognitive impairment to Alzheimer's disease is predicted by sources and coherence of brain electroencephalography rhythms.

Rossini PM[1], Del Percio C, Pasqualetti P, Cassetta E, Binetti G, Dal Forno G, Ferreri F, Frisoni G, Chiovenda P, Miniussi C, Parisi L, Tombini M, Vecchio F, Babiloni C.

STATISTICAL ANOVA INTERACTION 0F GROUP, BAND, ROI

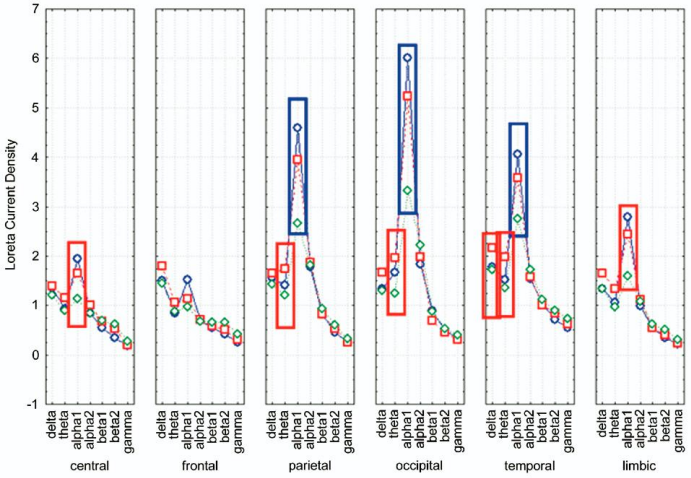

STATISTICAL ANOVA INTERACTION 0F GROUP, BAND, PAIR

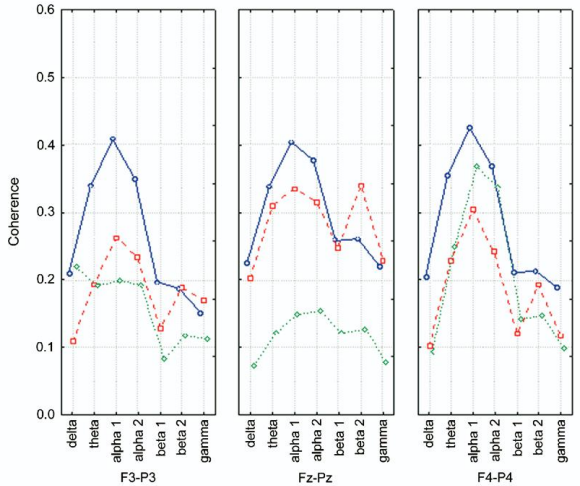

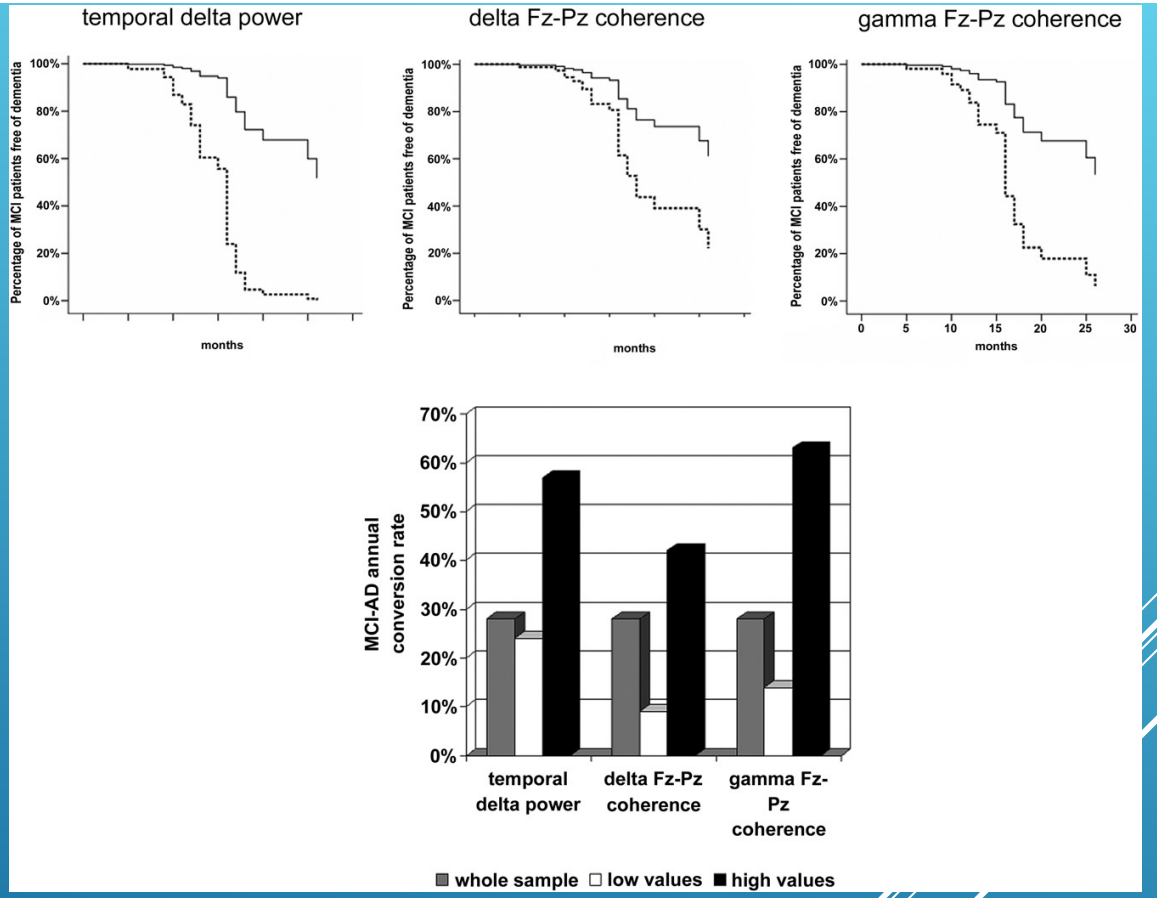

Continuous linebelow, dashed lineabove the estimated cutoffs:
2.57 for temporal delta LORETA current density,
2.07 for Fz–Pz delta log coherence,
and 2.62 for Fz–Pz gamma log coherence.

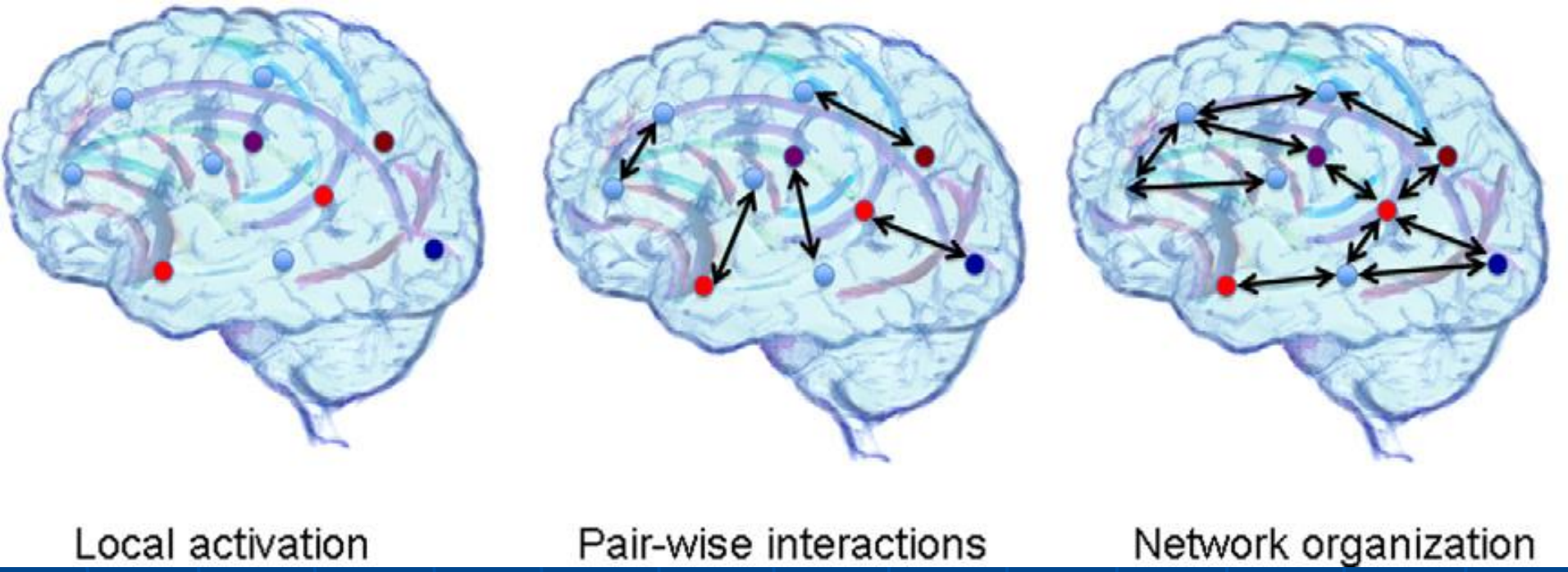

INTERACTION LEVEL

Zero order

First order

Second and higherorder
(interactions of interactions)

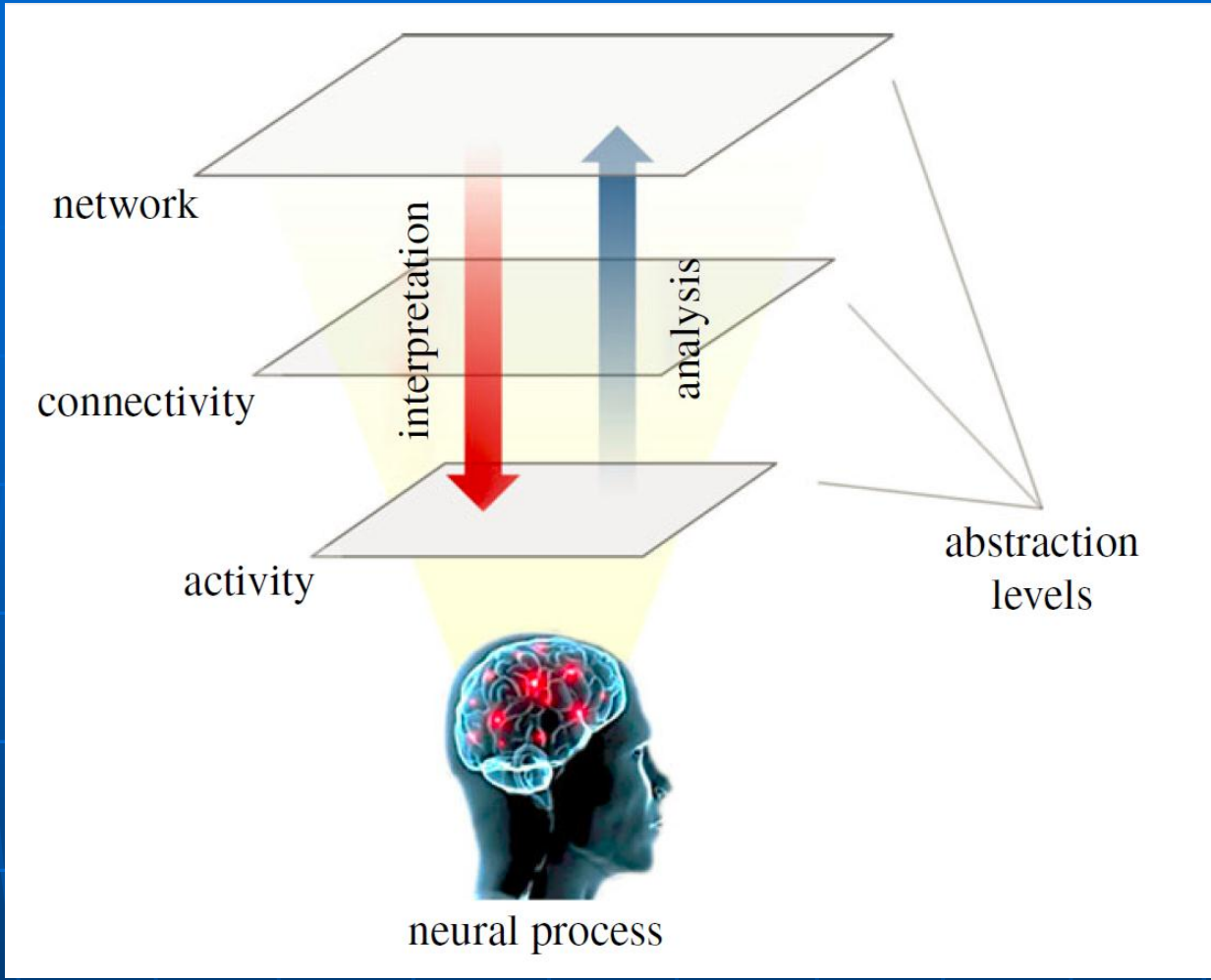

Changes in the neural process generate modifications in the measured brain activity (**univariate analysis, abstraction level 1**).
FC (**bivariate analysis, abstraction level 2**) applies to the measured brain signals.
Graph modelling (**multivariate analysis, abstraction level 3**) applies to FC.

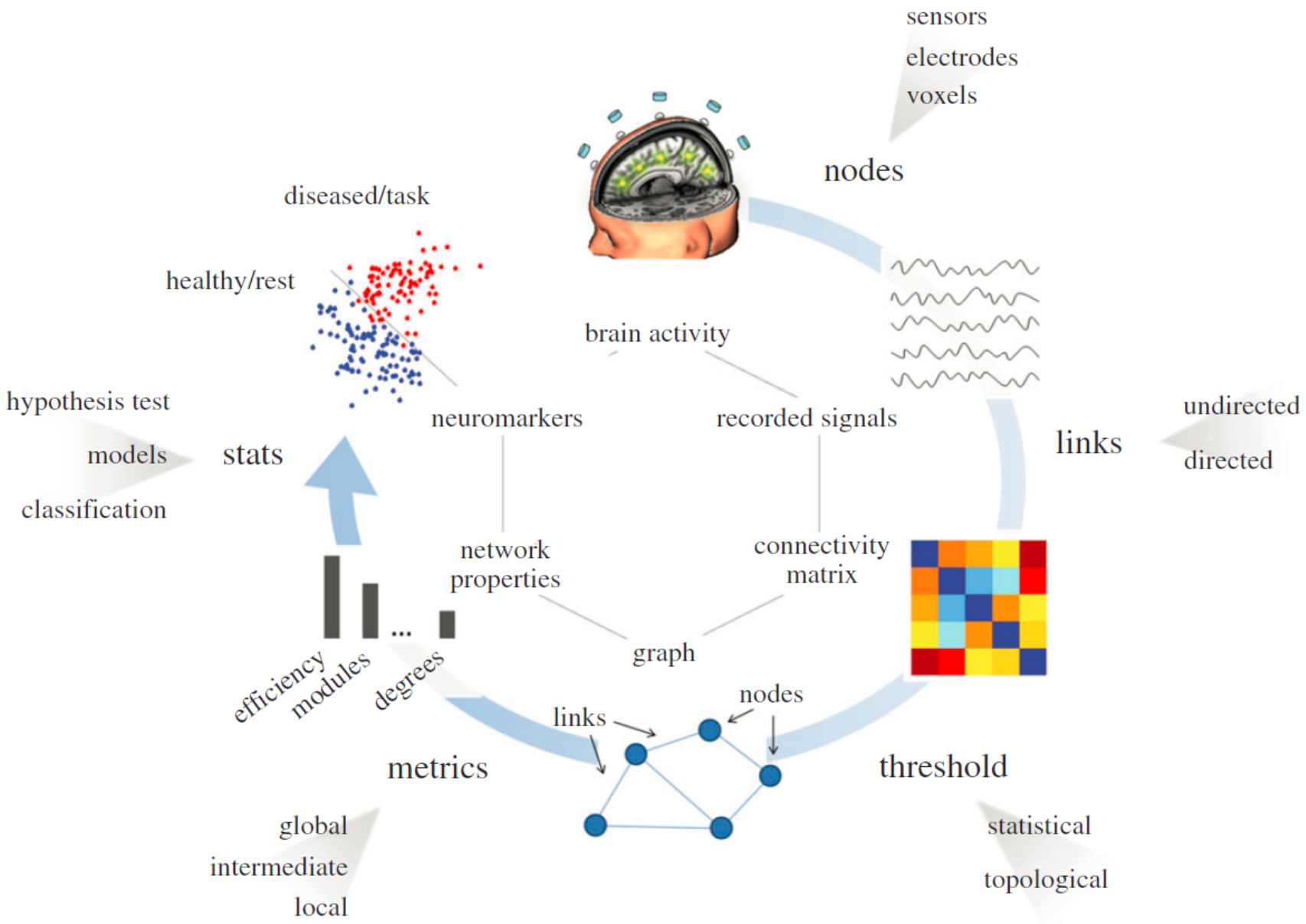

NETWORK (GRAPH) TOPOLOGY

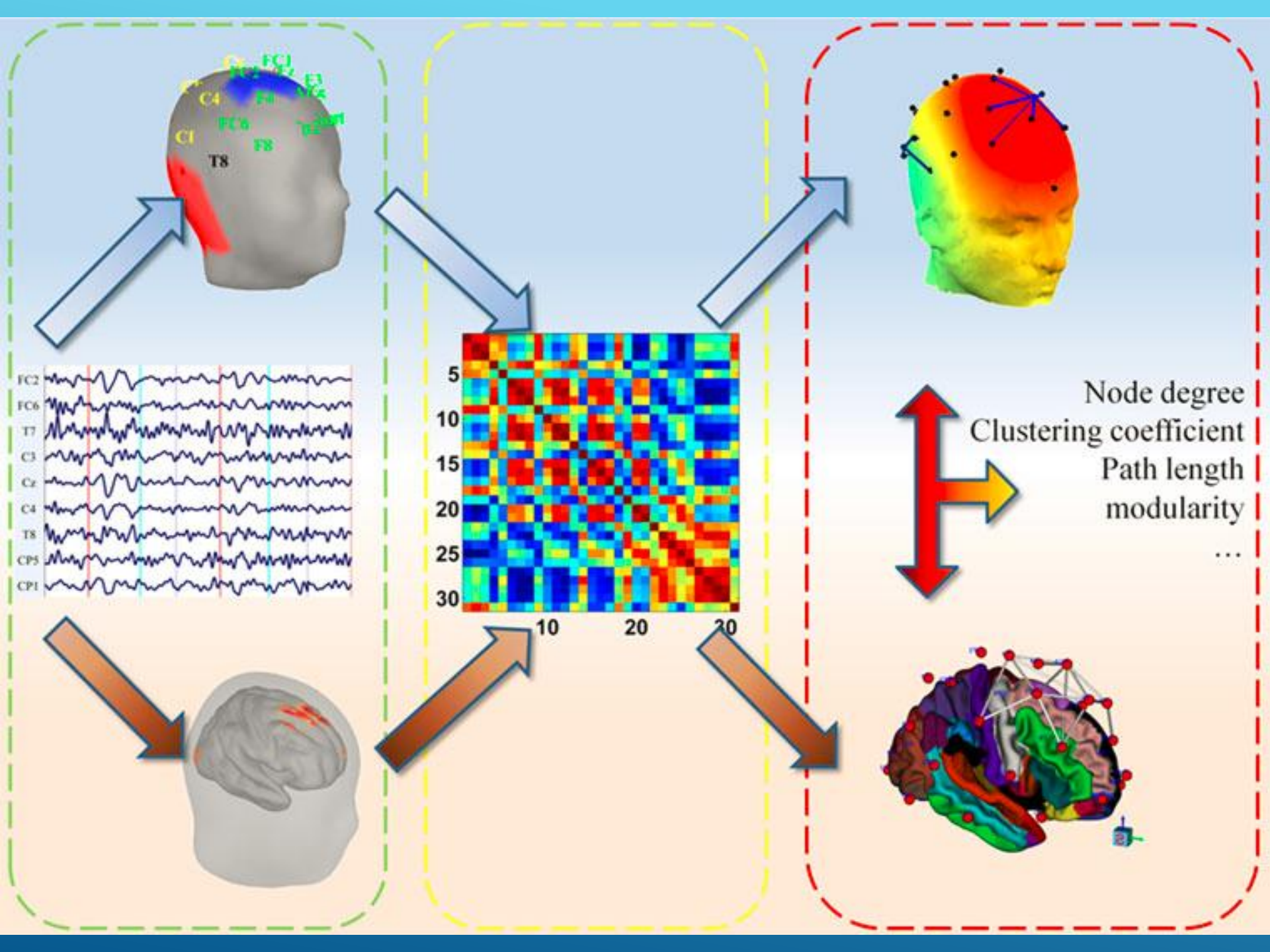
C4
C1
T8
FC2
FC6
T7
C3
Cz
C4
T8
CP5
CP1
5
10
15
20
25
30
10
20
20
Node degree
Clustering coefficient
Path length
modularity
…

- The clustering coefficient C is a measure of the local connectedness of a graph. It can be defined as the number of edges present between the neighbors of a node divided by the total possible number of edges between the neighbors. Normalized C: gamma
- Path length L is the number of edges in the shortest path between two nodes. Nomalized L: Lambda
- Node degree k is it's number of connections
- Network degree K is the average degree of all nodes
- Small worldlness sigma = gamma/lambda. Small world if > 1

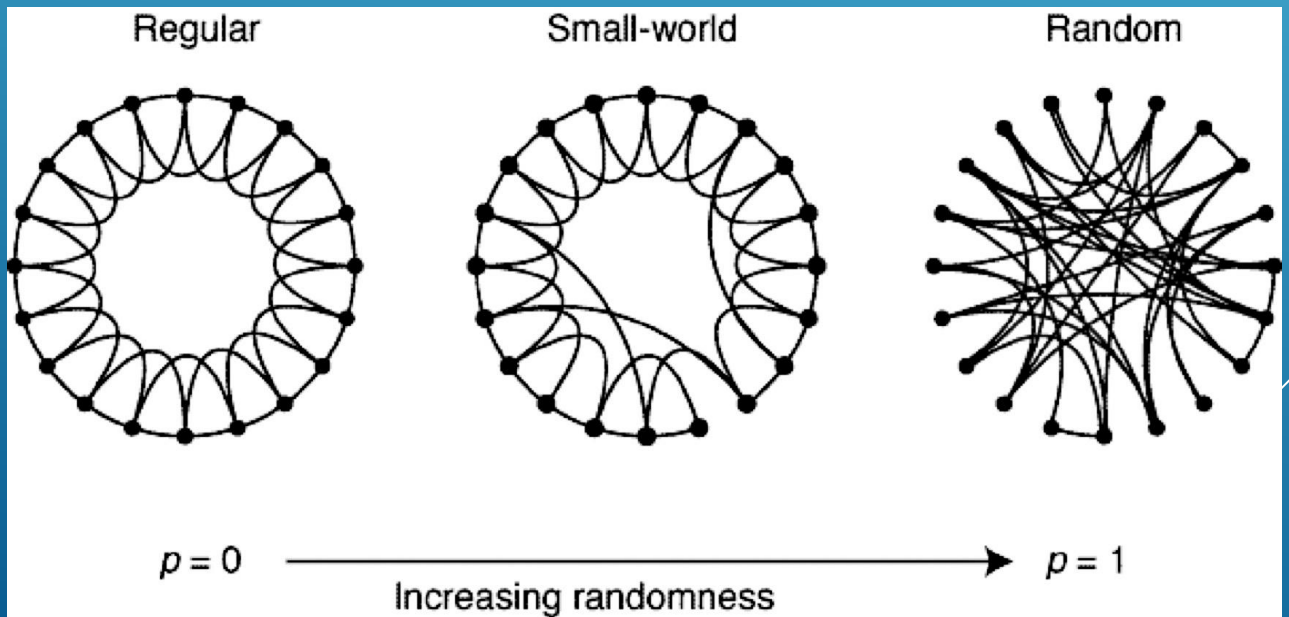

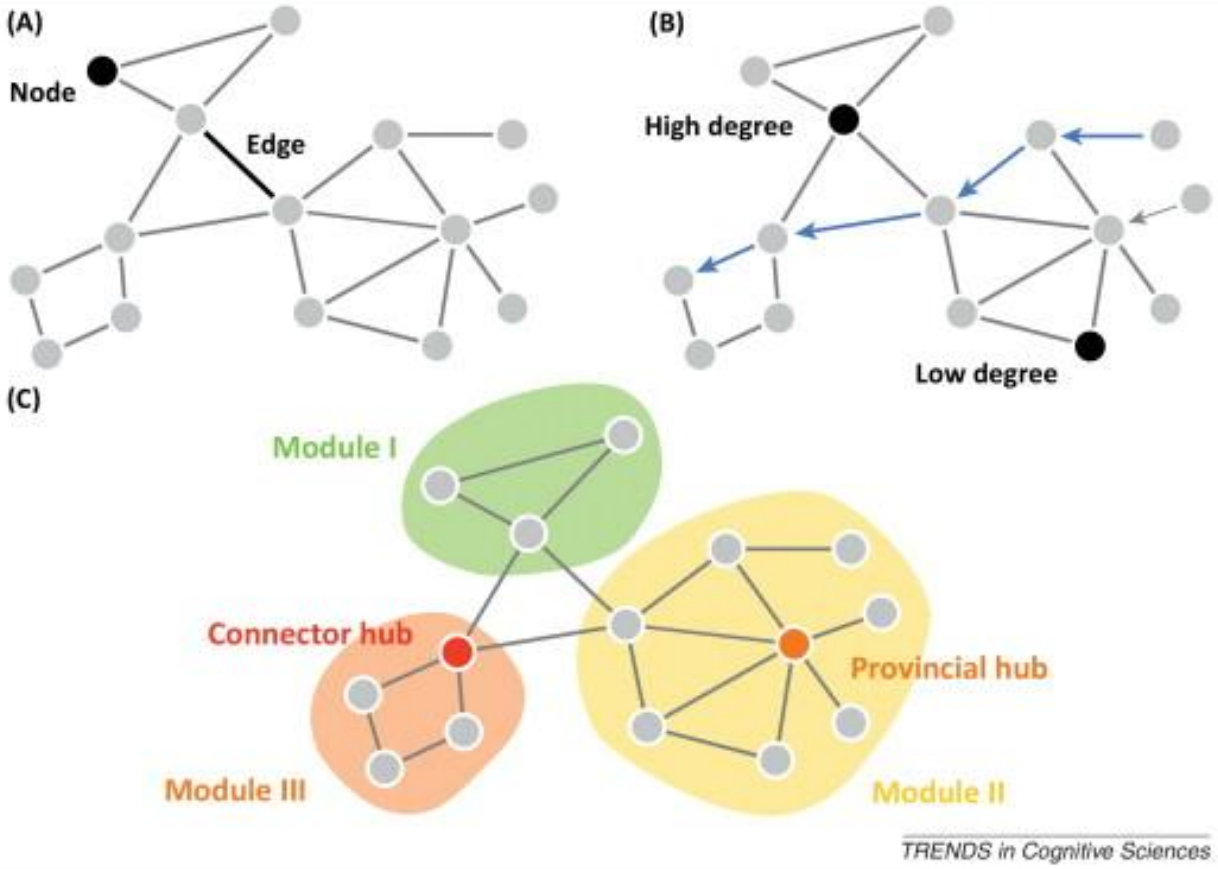
(A)
Node
Edge
(B)
High degree
Low degree
(C)
Module I
Connector hub
Provincial hub
Module III
Module II
TRENDS in Cognitive Sciences

INTEGRATION

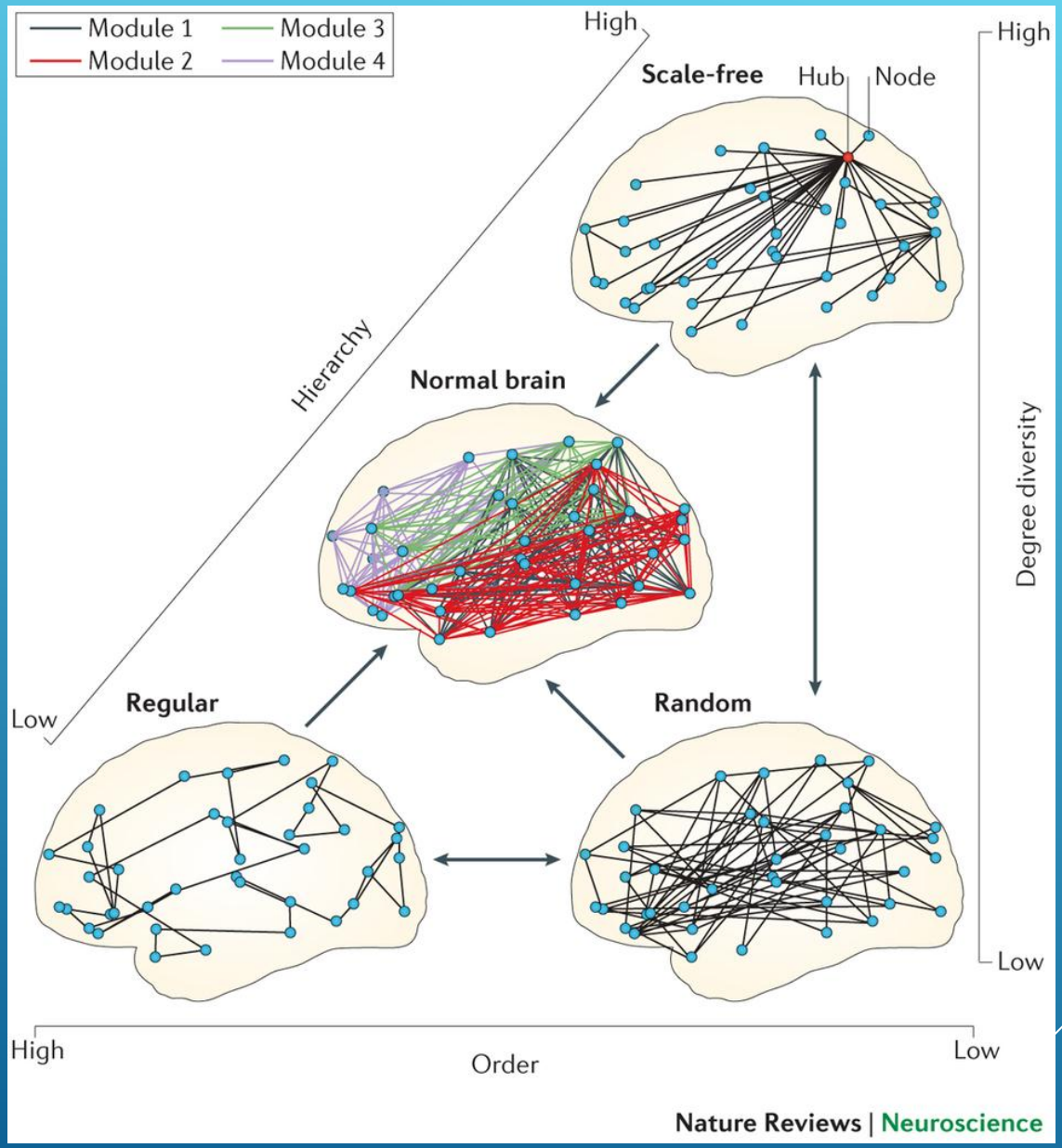

SEGREGATION

RANDOM

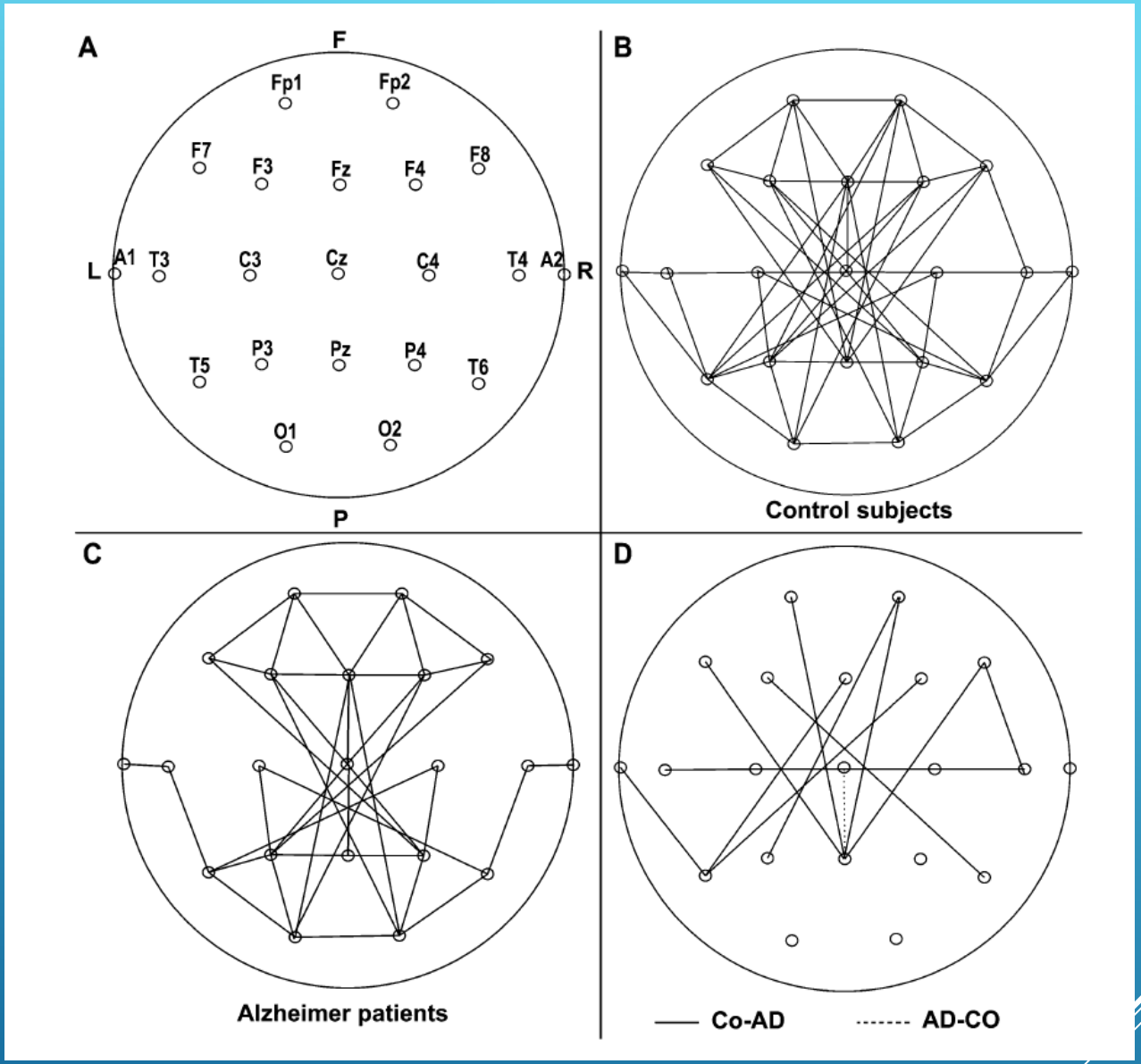

STAM C.J., 2007

Average reference
SL (synchronization likelihood)

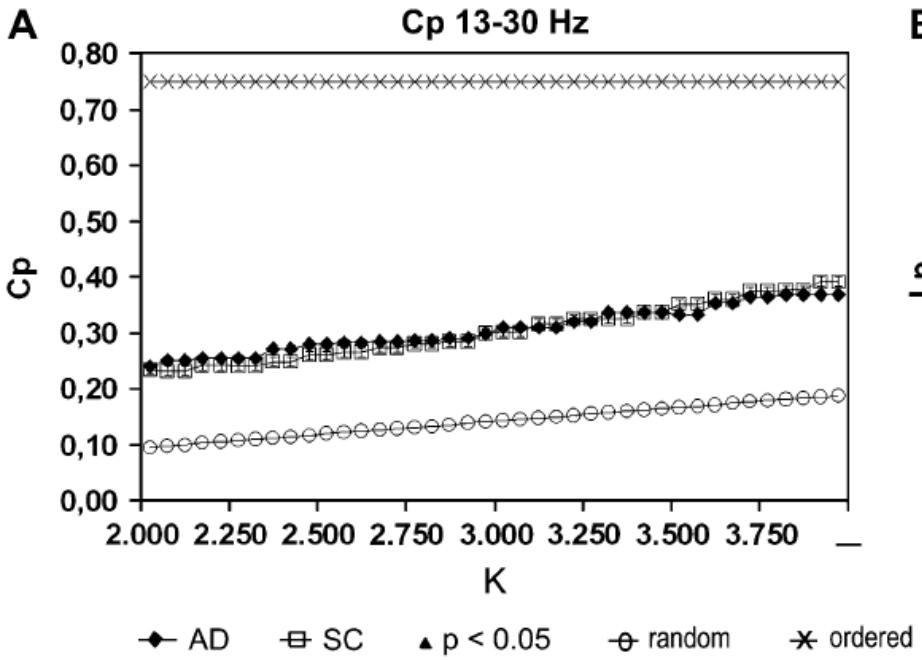
A
Cp 13-30 Hz
Cp
0,80
0,70
0,60
0,50
0,40
0,30
0,20
0,10
0,00
2.000 2.250 2.500 2.750 3.000 3.250 3.500 3.750
K
AD
SC
p < 0.05
random
ordered

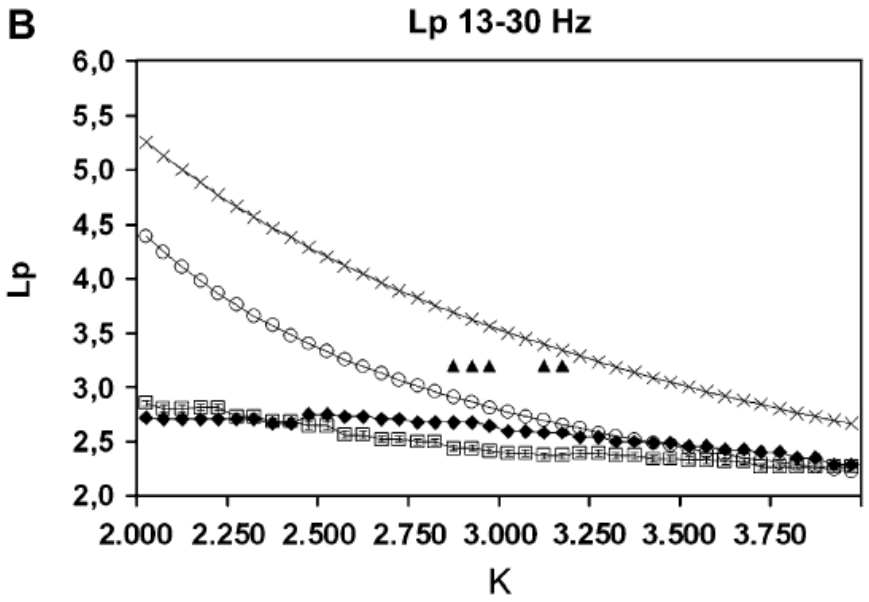
B
Lp 13-30 Hz
Lp
6,0
5,5
5,0
4,5
4,0
3,5
3,0
2,5
2,0
2.000 2.250 2.500 2.750 3.000 3.250 3.500 3.750
K

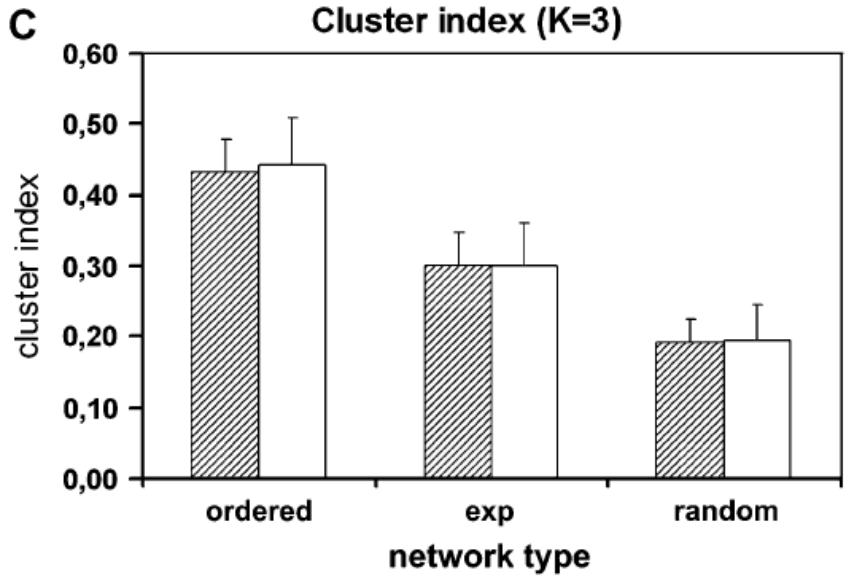
C
Cluster index (K=3)
cluster index
0,60
0,50
0,40
0,30
0,20
0,10
0,00
ordered
exp
random
network type

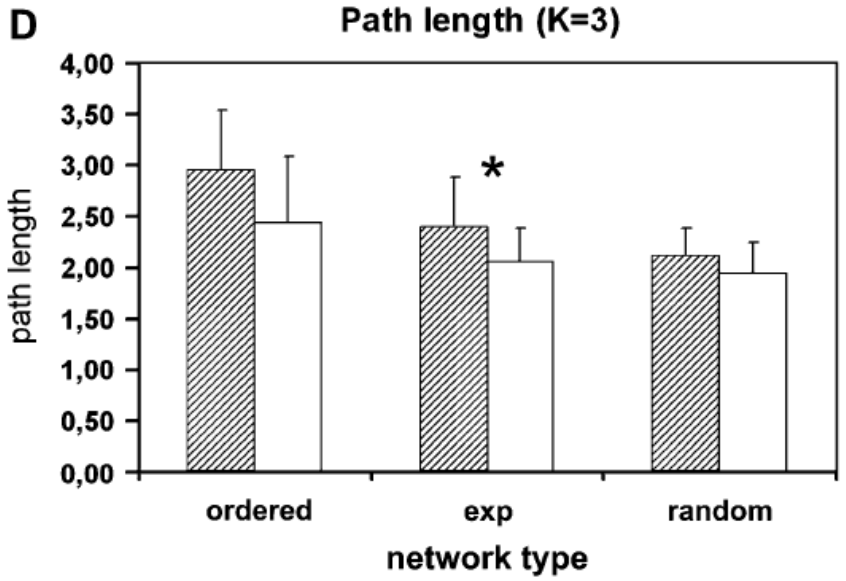
D
Path length (K=3)
path length
4,00
3,50
3,00
2,50
2,00
1,50
1,00
0,50
0,00
*
ordered
exp
random
network type

Both groups showed small-world properties.

AD patients exhibited longer characteristic path length, Lp, over a wide range of thresholds.

There was no significant difference observed in the cluster coefficient, Cp, between the two groups.

Significant negative correlation between MMSE score and network path length of all the subjects.

These results suggest a disruption of small-world organization in the brain functional networks in AD.

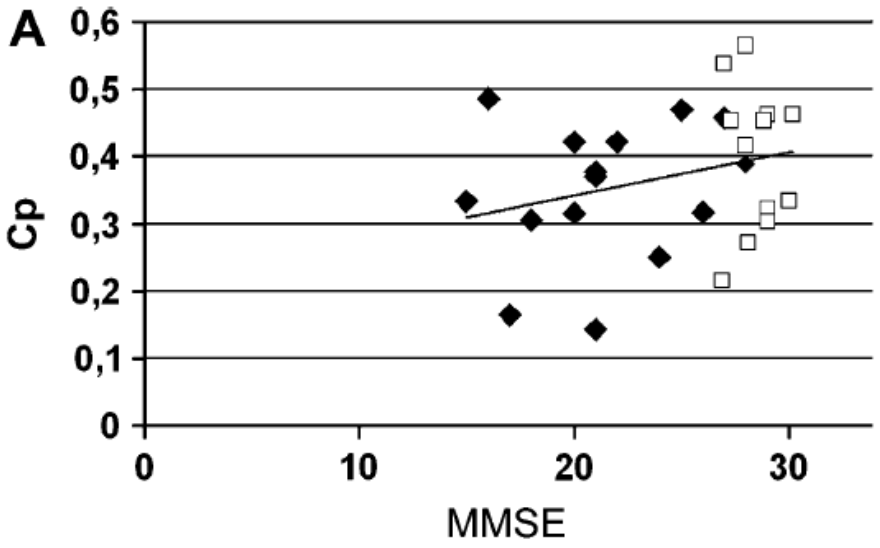
A
Cp
0,6
0,5
0,4
0,3
0,2
0,1
0
0
10
20
30
MMSE

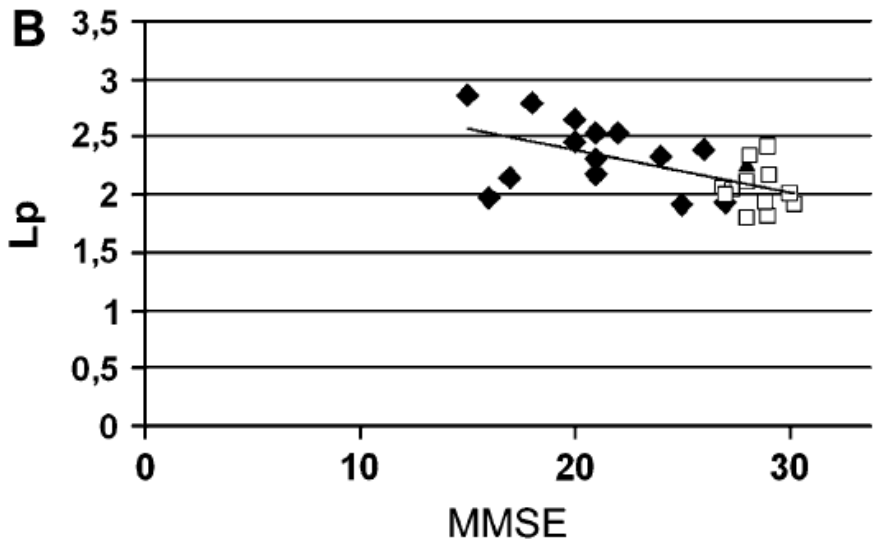
B
Lp
3,5
3
2,5
2
1,5
1
0,5
0
0
10
20
30
MMSE

Network topology in MCI

Xu P., 2004

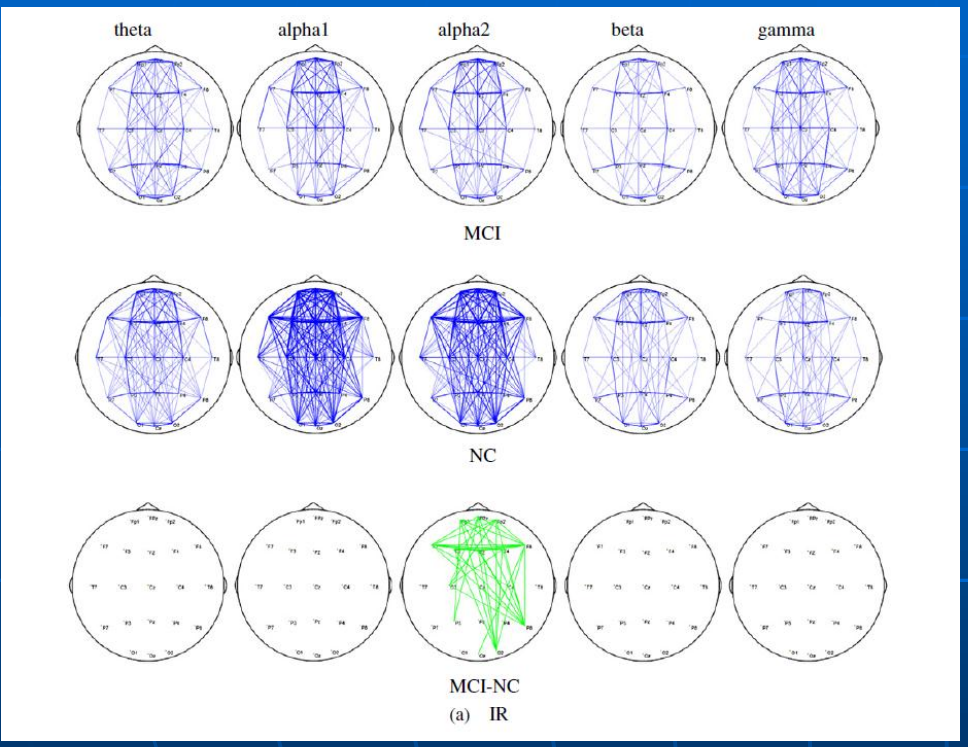

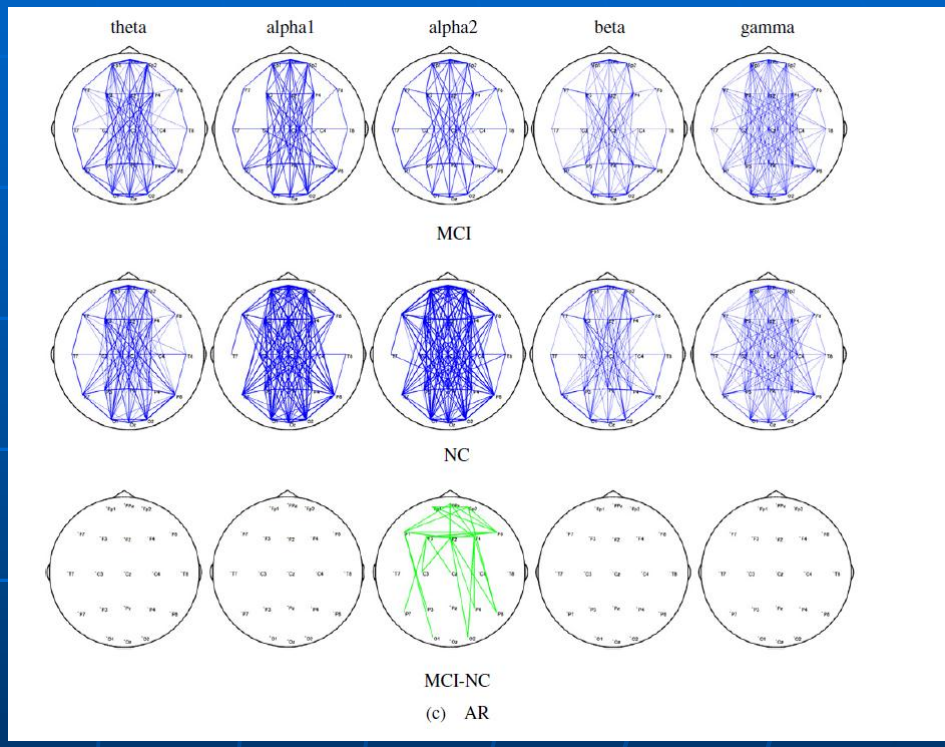

REST (reference electrode Standardization technique)

IR (infinite reference)

Average reference

Network topology in MCI

Xu P., 2004

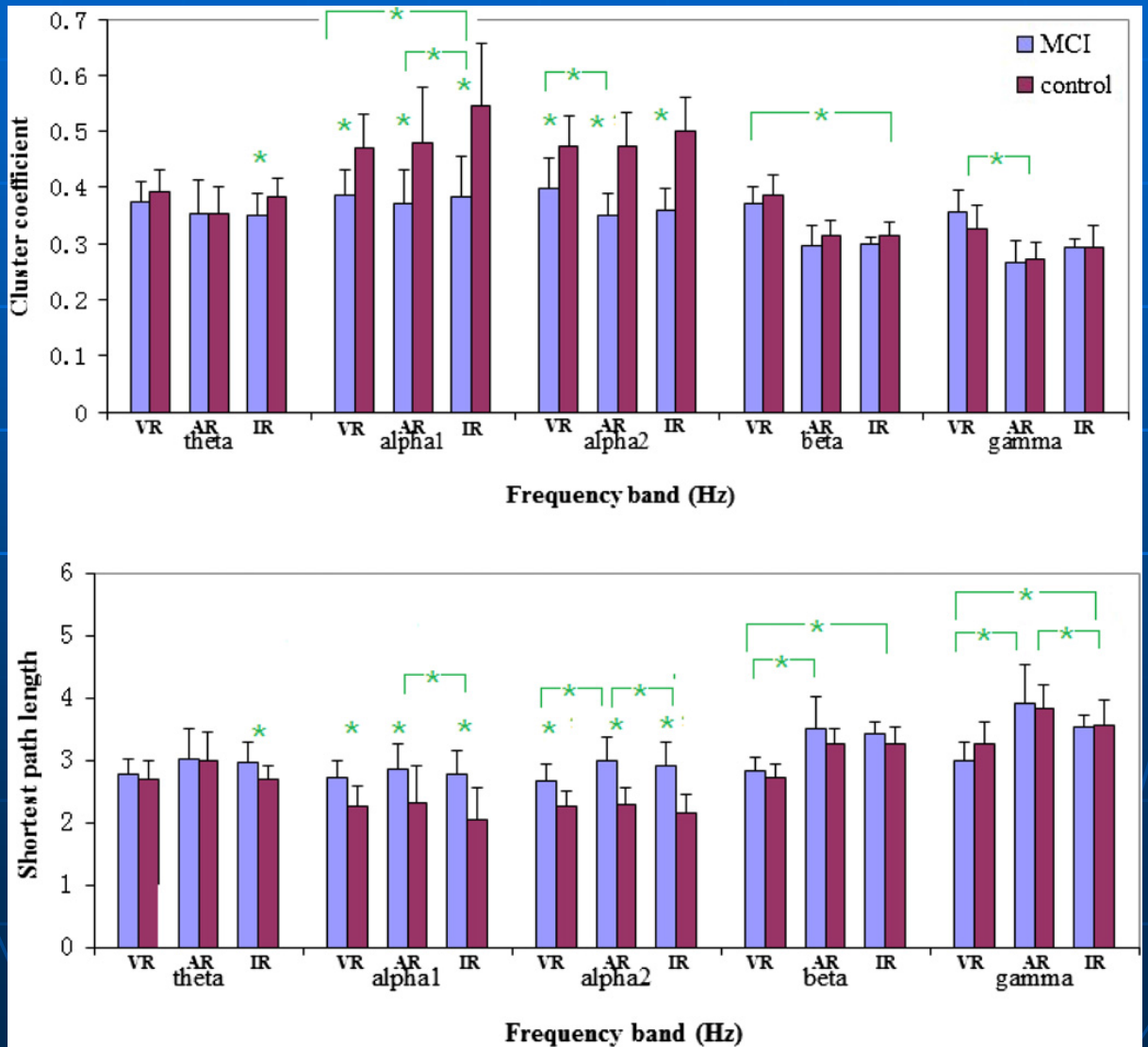

Network topology in MCI

Xu P., 2004

Table 3. The classification performance for MCI recognition.

		Alpha 1						Alpha 2						Alpha1+alpha 2					
		Acc (%)		Spe (%)		Sen (%)		Acc (%)		Spe (%)		Sen (%)		Acc (%)		Spe (%)		Sen (%)	
		NET	MCoh	NET	MCoh	NET	MCoh	NET	MCoh	NET	MCoh	NET	MCoh	NET	MCoh	NET	MCoh	NET	MCoh
LDA	VR	75	70	70	70	80	70	80	75	**90**	70	70	80	**90**	75	**100**	70	80	80
	AR	65	70	60	70	70	70	85	75	80	70	90	80	75	75	70	70	80	80
	IR	**85**	**80**	**80**	**80**	**90**	**80**	**90**	**85**	80	**80**	**100**	**90**	85	**80**	70	70	**100**	**90**
SVM	VR	75	70	70	**70**	**80**	70	75	75	**80**	70	70	80	65	70	60	60	70	**80**
	AR	75	65	70	50	**80**	**80**	80	70	70	60	90	80	75	65	70	50	80	**80**
	IR	**80**	**75**	**80**	**70**	**80**	**80**	**90**	**85**	**80**	**80**	**100**	**90**	**85**	**75**	**80**	**80**	**90**	70

Gomez C., 2009

Coherence mean values were lower in the MCI group than in control group at all frequency bands (delta, theta, alpha-1, alpha-2, beta, and gamma). The highest accuracy (69.8%) was achieved in the beta band.

Network topology in MCI

Xu P., 2004

The conducted studies demonstrate that the resting network of the scalp EEG with a zero reference that is realized by REST can be used to robustly classify the MCI with an Acc of approximately 90%, which is close to the classification obtained using MRI (Fan *et al* 2008, Misra *et al* 2009, Wee *et al* 2012). Compared with the existing MCI classification studies that use EEG, the performance improvement of the current work can be attributed to the following exclusive techniques: (a) first of all, the network properties have more discriminative ability than the traditional Coh for the MCI recognition, possibly because the network view is a better portrayal of the intrinsic neural mechanisms of MCI; and (b) IR-based EEG data can construct networks to save information about the truly existing differences between MCI and NC; in other words, REST can partially recover the lost information that is caused by a non-zero transformation.

The classification Acc using the Mcoh (mean coherence) is 75%-85%.

90% Acc was achieved when the network features in the alpha2 band were adopted.

Network topology in MCI vs. mAD

Lu C.F, 2014

The disruptions of network integrity and reductions of network efficiency in mAD characterized by

lower degree,
decreased clustering coefficient,
higher shortest path length,
reduced global and local efficiencies

in the delta, theta, beta2, and gamma bands are evident.

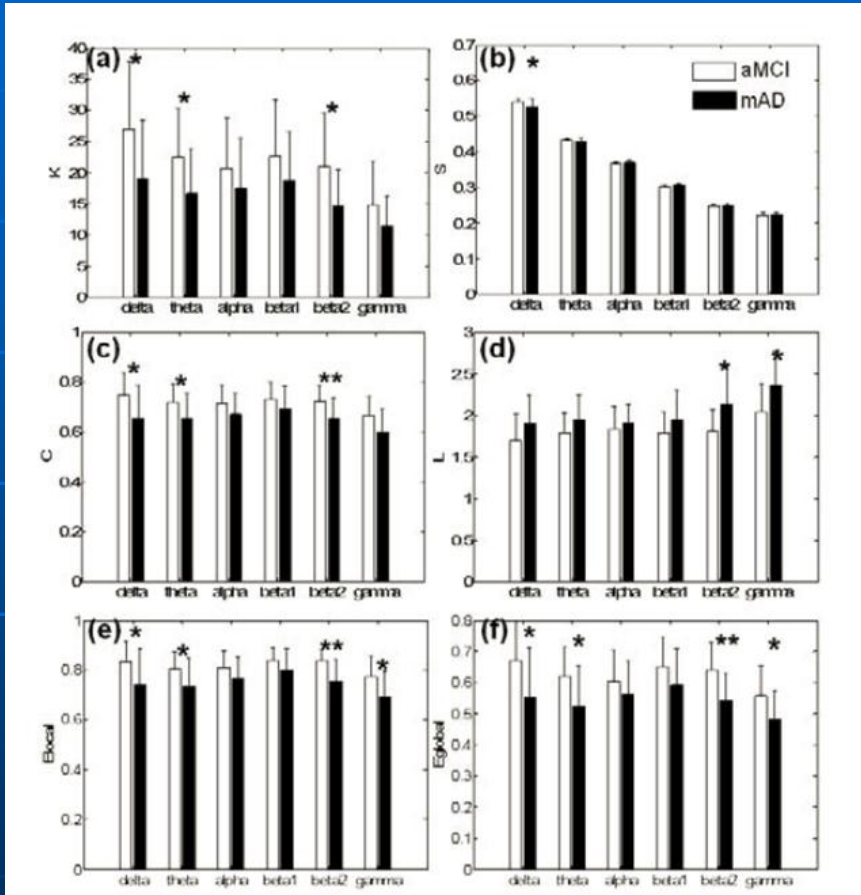

Fig. 2 The global network properties, (a) degree, (b) strength, (c) clustering coefficient, (d) shortest path length, (e) global efficiency, and (f) local efficiency, in each frequency band for aMCI and mAD groups. *, $p < 0.05$; **, $p < 0.005$

Network topology in MCI vs. mAD

19 ch. EEG source reconstruction

Lu C.F, 2014

CORTICAL SURFACE REGIONS AND THEIR ABBREVIATIONS (ALL FOR BOTH HEMISPHERES)

Type	Name	Label	Type	Name	Label
PF	Medial orbitofrontal	MOF	PF	Lateral orbitofrontal	LOF
PF	Parsorbitalis	PO	F	Superior frontal	SF
F	Caudal middle frontal	CMF	F	Rostral middle frontal	RMF
F	Parsopercularis	POP	F	Parstrangularis	PT
C	Paracentral	paraC	C	Precentral	preC
C	Postcentral	postC	P	Precuneus	precun
P	Surperior parietal	SP	P	Inferior parietal	IP
P	Supramarginal	SM	T	Superior temporal	ST
T	Middle temporal	MT	T	Inferior temporal	IT
T	Transverse temporal	TT	T	Insula	insula
T	Parahippocampus	paraH	T	Entrohinal	EC
T	Fusiform	fusiform	L	Rostral anterior cingulate	RAC
L	Caudal anterior cingulate	CAC	L	Posterior cingulate	PC
L	Isthmus cingulate	IC	O	Cuneus	cuneus
O	Lingual	lingual	O	Pericalcarine	periCal
O	Lateral occipital	LO			

PF, prefrontal; F, frontal; C, central; P, parietal; T, temporal; L, limbic; O, occipital.

Network topology in MCI vs. mAD

Lu C.F, 2014

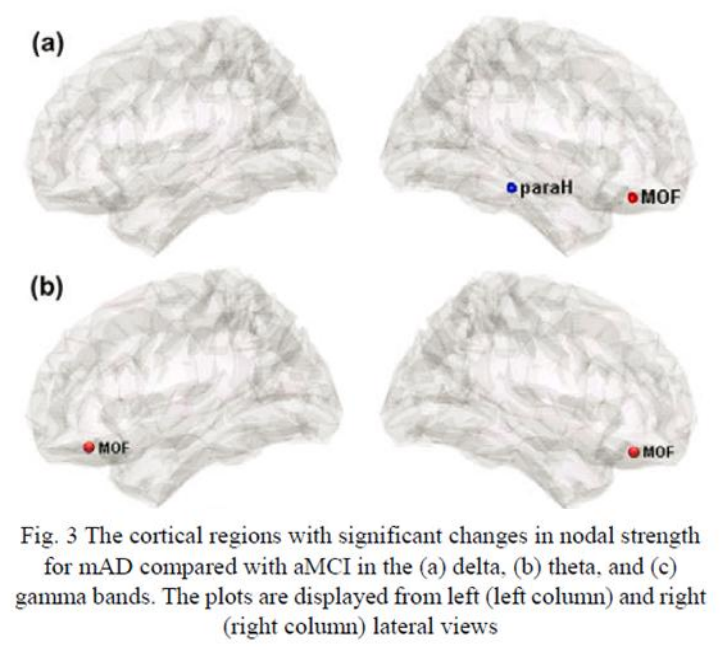

Fig. 3 The cortical regions with significant changes in nodal strength for mAD compared with aMCI in the (a) delta, (b) theta, and (c) gamma bands. The plots are displayed from left (left column) and right (right column) lateral views

Bilateral medial orbitofrontal cortices (MOF) exhibited increases in **nodal strength S** (weighted degree) in the theta and delta bands for mAD. Theta activity, which arises from the hippocampus and oscillates with medial frontal and cingulate cortex, is associated with memory functions. This result suggested that the mAD patients have stronger functional connectivity related to the bilateral medial orbitofrontal regions in the low-frequency fluctuations, which may be compensation to the disruption to the hippocampus-related connectivity.

In contrast, the right parahippocampus exhibited reduced nodal strength in the delta band for mAD. The decline of the nodal strength in parahippocampus gyrus may suggest the impairment of memory encoding and retrieval in mAD patients.

Network topology in MCI vs. mAD

Lu C.F, 2014

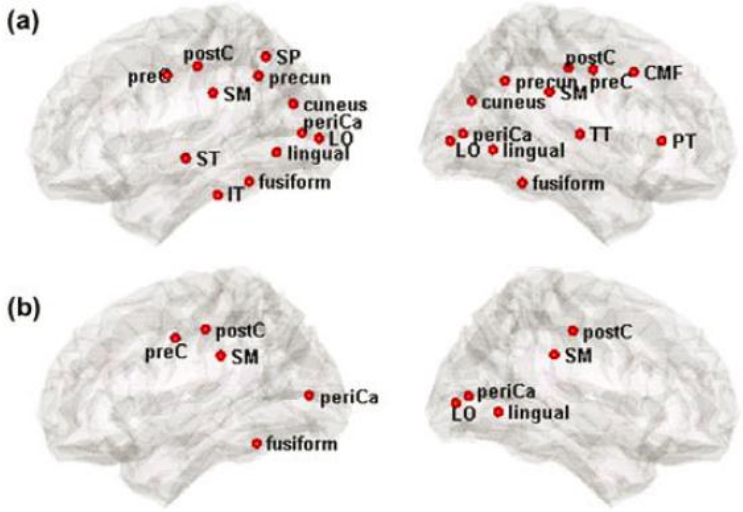

Fig. 5 The cortical regions with significant increases in nodal shortest path length for mAD compared with aMCI in the (a) beta2 and (b) gamma bands. The plots are displayed from left (left column) and right (right column) lateral views

Significant increases in **nodal shortest path length** for mAD were found in several central regions (preC and postC), right middle frontal (CMF), and right inferior frontal regions (PT and PO) in addition to the bilateral parietal and occipital regions in the higher frequency bands, namely, the beta2 and gamma bands.

The increased nodal shortest path length of a node indicated larger separations between it and other nodes in the network, suggesting that the costs for information transmission and integration were expensive in mAD compared with aMCI.

Network topology in MCI vs. mAD

Lu C.F, 2014

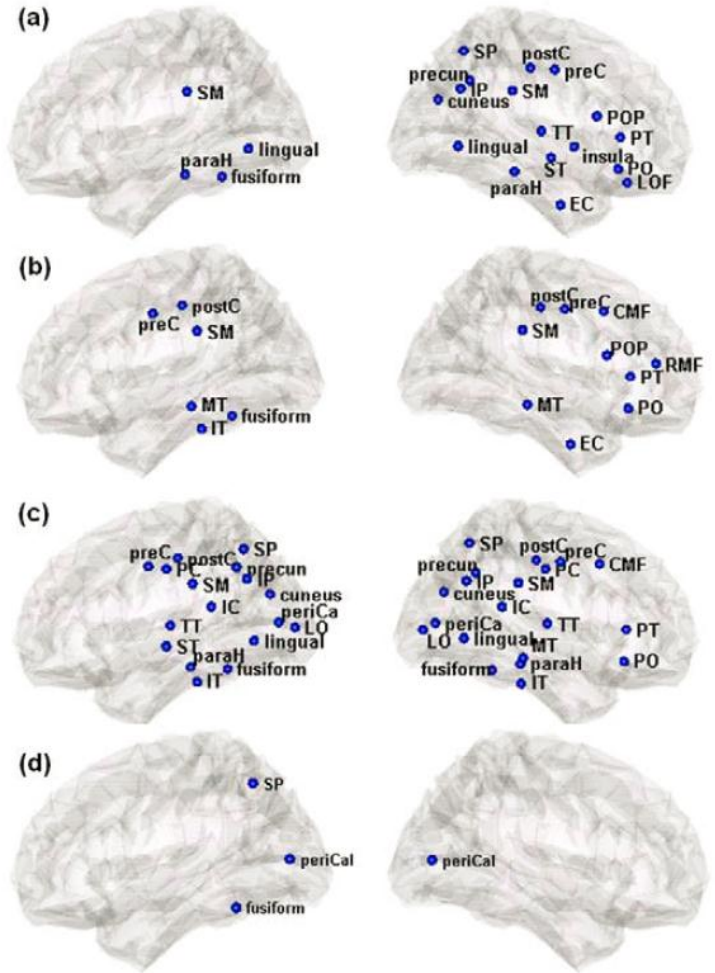

Fig. 6 The cortical regions with significant decreases in nodal efficiency for mAD compared with aMCI in the (a) delta, (b) theta, (c) beta2, and (d) gamma bands. The plots are displayed from left (left column) and right (right column) lateral views

Nodal efficiency quantifies the importance of a node for communication within the network.
For **nodal efficiency**, significant alterations between mAD and aMCI groups were observed in different cortical regions in the delta, theta, beta2, and gamma bands.

In the low-frequency delta band, regions with significantly reduced nodal efficiency in mAD mainly distributed in the right hemisphere, covering right inferior frontal (POP, PT, and PO), temporal (paraH, insula, ST, TT, and EC), parietal, and occipital regions. The delta waves of EEG have been reported to be characterized by right lateralization focused on the thalamus-connected frontal, parietal and temporal cortices.
The distributed regions with significantly decreased nodal efficiency lateralized to the right hemisphere in the delta band may reflect the disrupted connections between the thalamus and multiple cortical regions.

In the high-frequency beta2 band, regions with reduced nodal efficiency in mAD mainly located in bilateral parietal, temporal, occipital regions, and right frontal regions. Two limbic regions (PC and IC) also exhibited significant reduction of nodal efficiency in the beta2 band for mAD.

Stam (2009) further demonstrated that the AD-related network changes in the lower alpha could be better explained by a **"Targeted Attack" model** (assuming that edges connecting high-degree nodes are more vulnerable than others, causing their weight to be reduced first) instead of a "Random Failure" model (assuming that network changes are due to a random decrease in the strength of all edges). His modeling analysis suggests that **those highly connected brain network "hubs" (e.g., association cortex regions/DMN) might be especially at risk in AD**.

The connectivity account would play an important role in revealing the transneural spread of misfolded proteins through neural networks in neuro-degenerative disease. **The multimodal association areas, which have a striking overlap with the default mode network, have the highest level of connectivity, and are the most electrically active**.

In line with this view, **the metabolism hypothesis (MH)** has been proposed, which suggests that changes in the default mode network (DMN, the ongoing low-frequency fluctuations during resting state between the anterior and posterior cingulate cortex as well as the precuneus) stimulate **an activity-dependent or metabolism-dependent cascade** that promotes the development of the AD pathology.

INTRINSIC CORRELATIONS WITHIN THE DEFAULT NETWORK

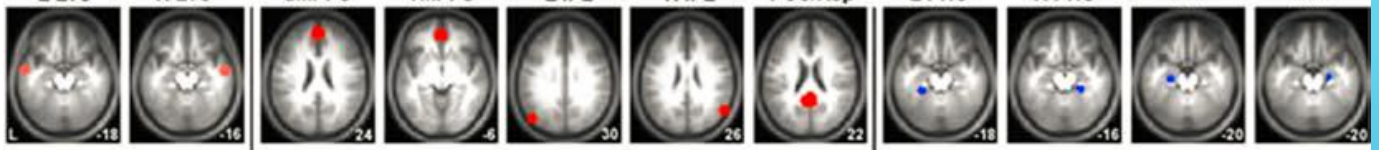

L LTC	1.00	0.41	0.16	0.12	0.14	0.12	0.12	0.11	0.06	0.18	0.14
R LTC		1.00	0.16	0.18	0.07	0.20	0.19	0.08	0.10	0.15	0.17
dMPFC			1.00	0.47	0.22	0.31	0.34	-0.06	-0.10	-0.01	-0.04
vMPFC				1.00	0.27	0.31	0.52	0.11	0.06	0.20	0.16
L IPL					1.00	0.47	0.49	0.25	0.10	0.11	0.06
R IPL						1.00	0.42	0.12	0.05	0.09	0.07
pCC/Rsp							1.00	0.23	0.16	0.26	0.21
L PHC								1.00	0.57	0.31	0.28
R PHC									1.00	0.28	0.28
L HF										1.00	0.61
R HF											1.00

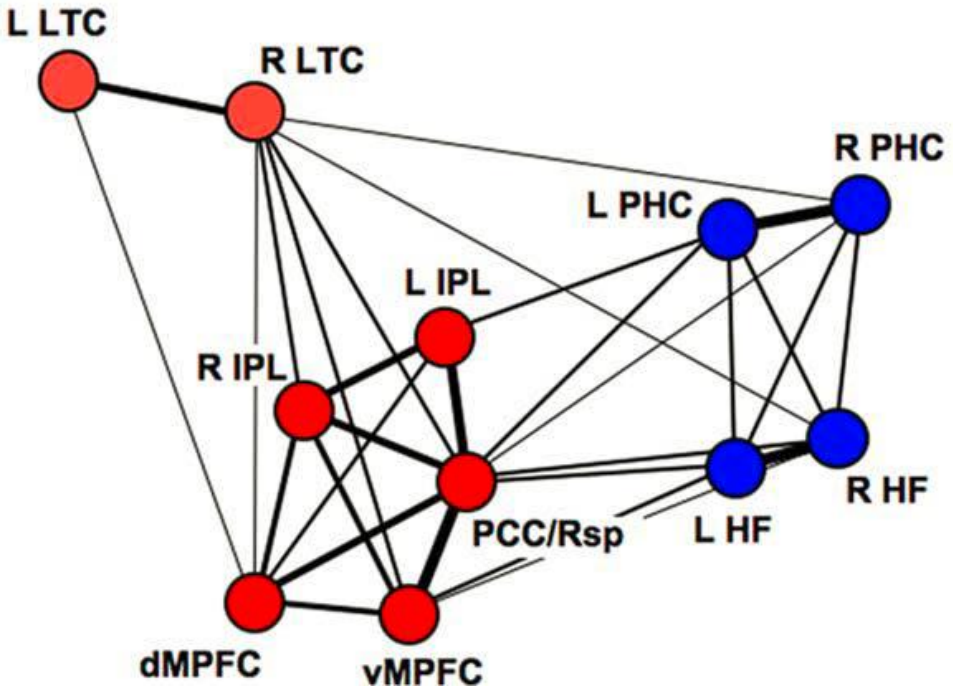

SPONTANEOUS DEFAULT NETWORK ACTIVITY

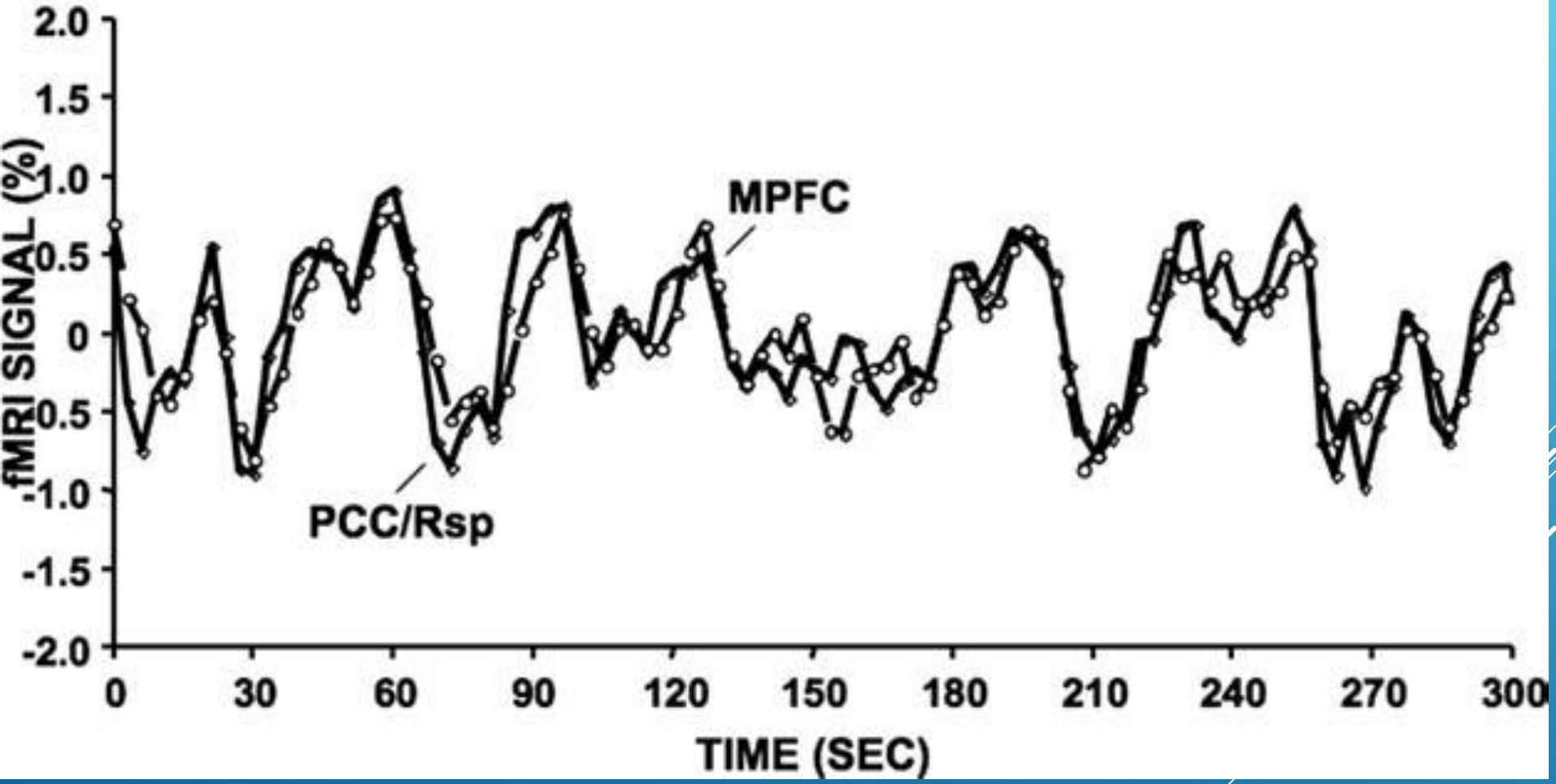

Loreta Default Brain Network

Frontal

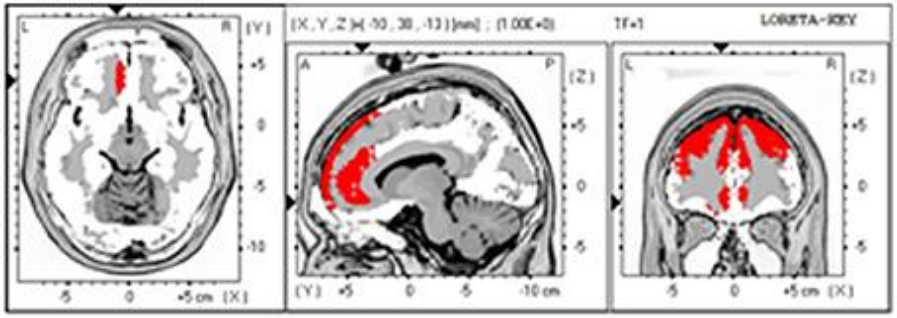

Anterior Cingulate

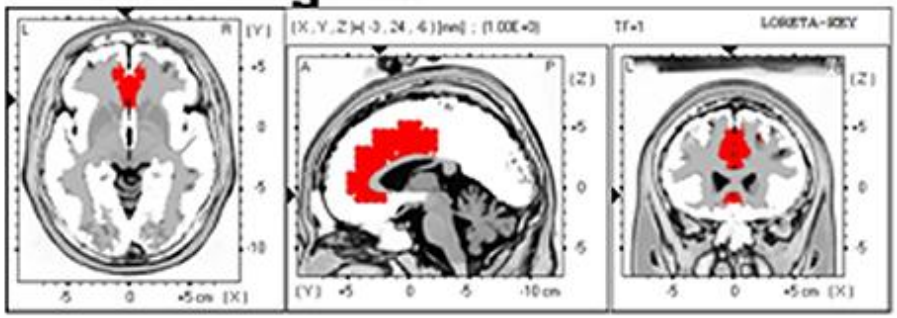

Temporal

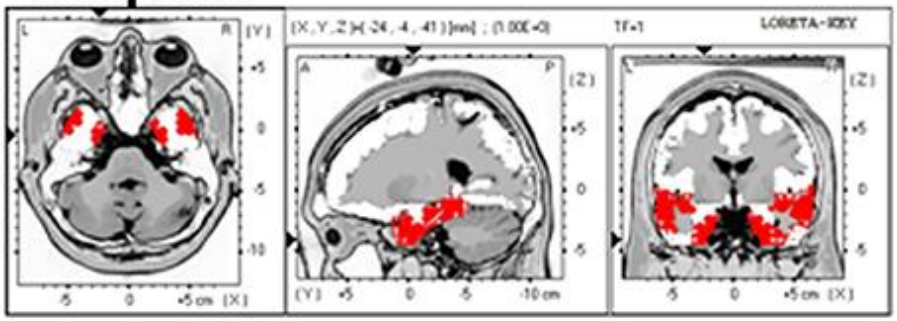

Hippocampus

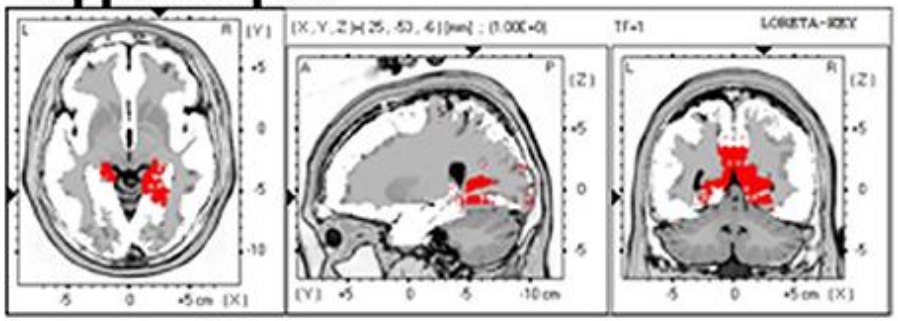

Posterior Cingulate

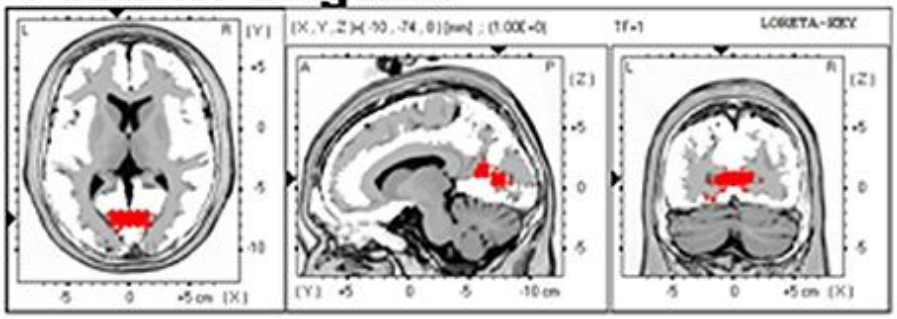

Parietal

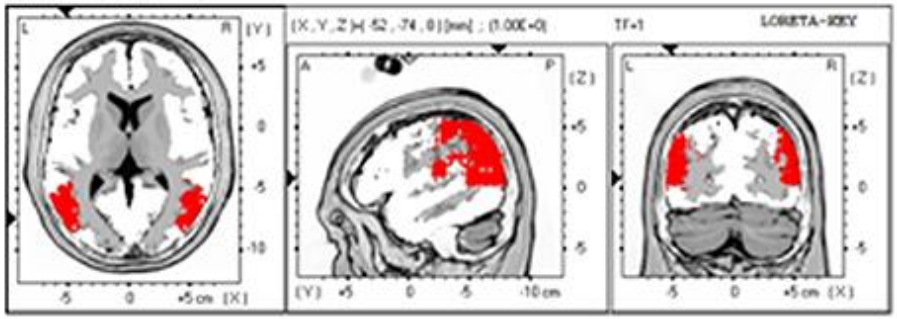

Hyperactive neurons are observed near amyloid plaques in animal models and in humans, connectivity hubs overlap the anatomy of A-β deposition. Abnormal DMN activity discriminates between Mild Cognitive Impairment (MCI), AD and controls, and predicts AD conversion. Thus, default connectivity seems to be a promising approach to reveal novel mechanisms leading to AD.

Early-stage, transient rises of firing rate and functional connectivity in AD matches observations in preclinical AD patients, suggesting that this chain of events is not compensatory but pathological.

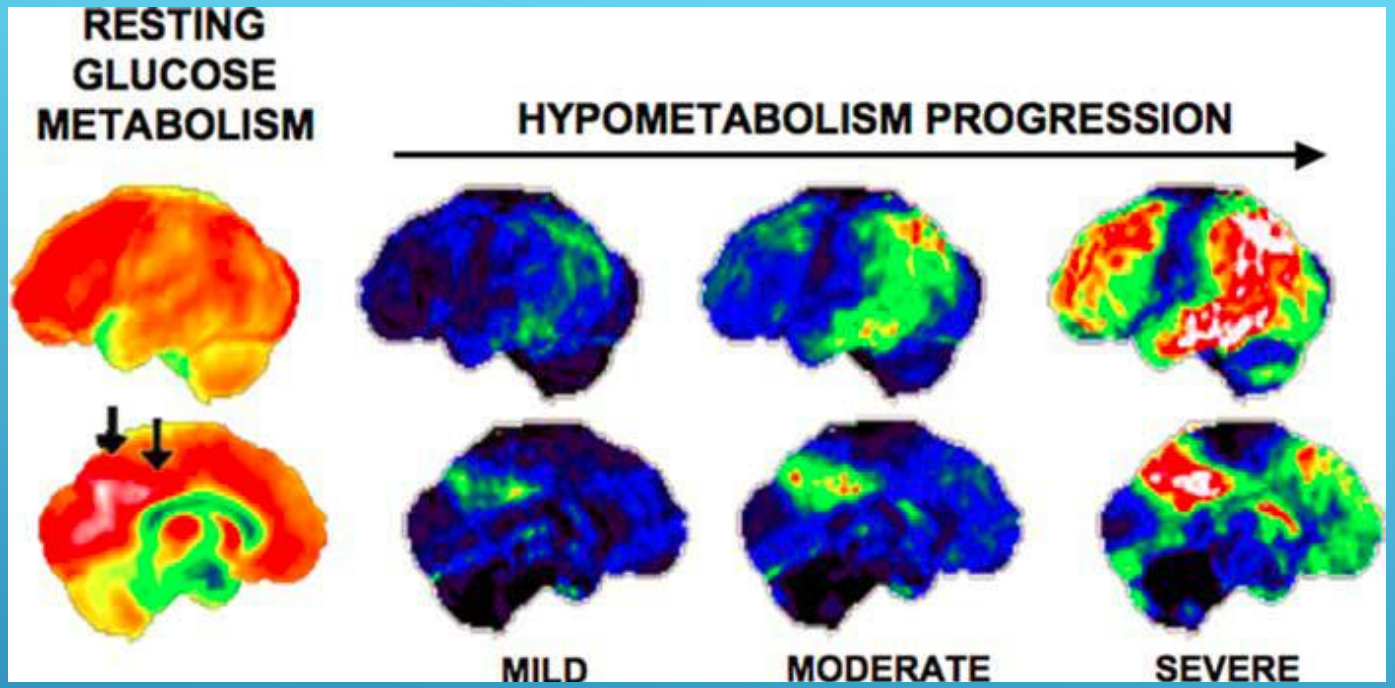

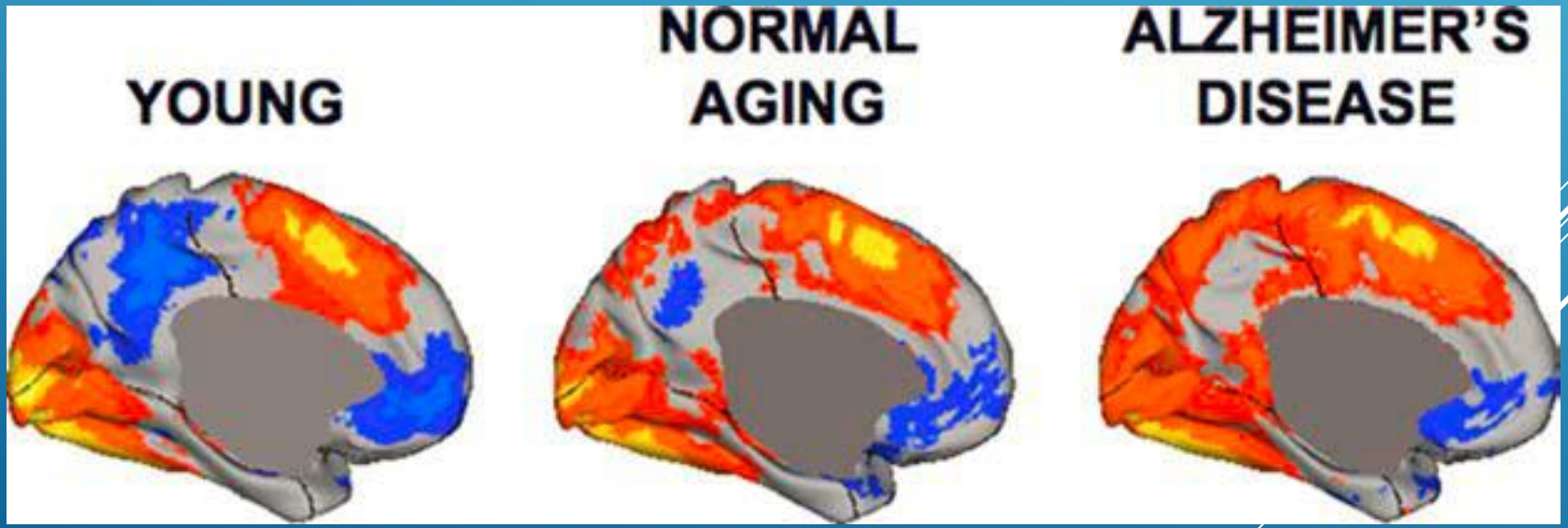

Task increases (red) and decreases (blue) from a simple word classification task referenced to a passive baseline task.

A new reformulation of the Hebbian principle: ‘not only neurons that fire together wire together but also neurons that wire together die together’

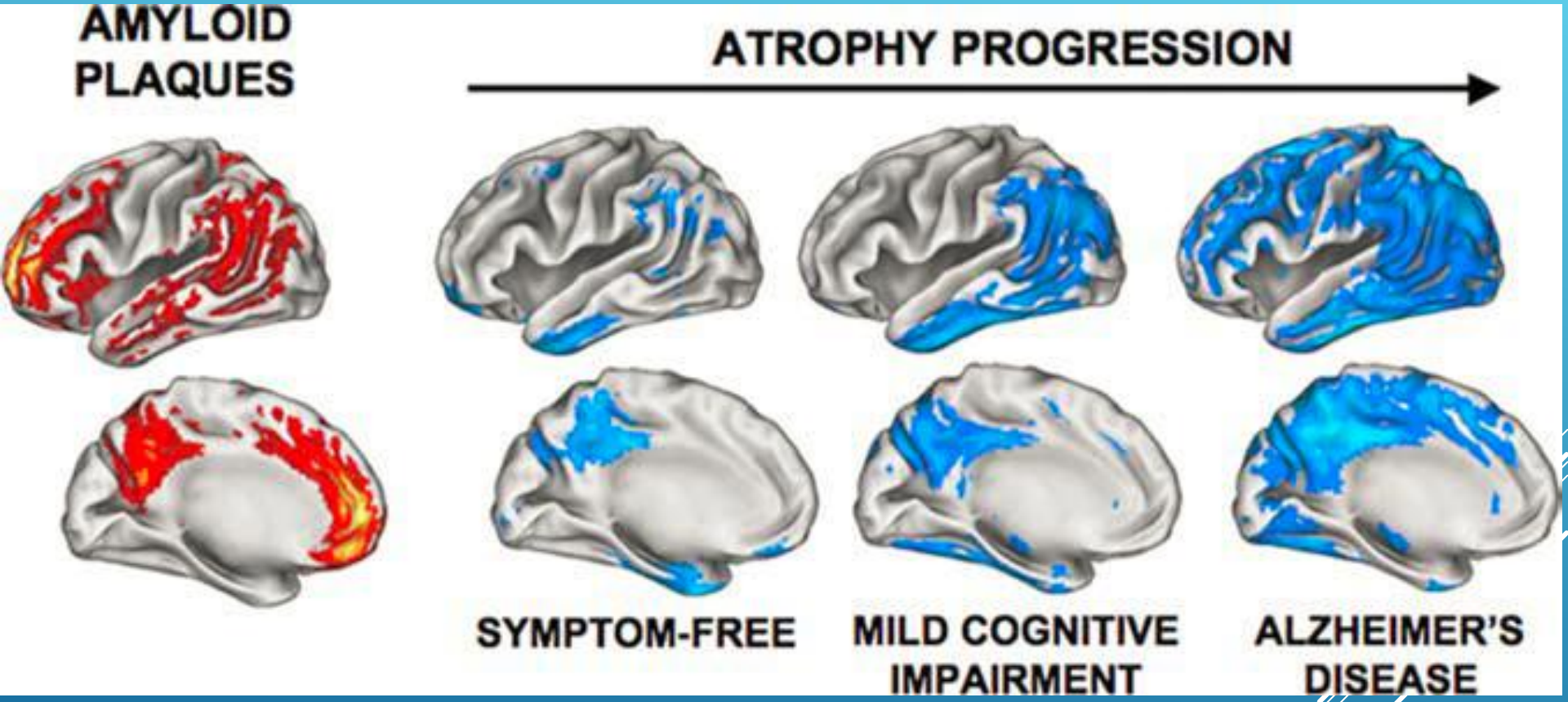

As the disease progresses the plaques move to other specific areas lower in the brain, as though they are following specific pathways. These cues suggest that the disease is moving by electrical activity through specific neuronal pathways, connecting one area to the next, driving new pathology.

Activity Dependent Degeneration (ADD)
de Haan W., 2012

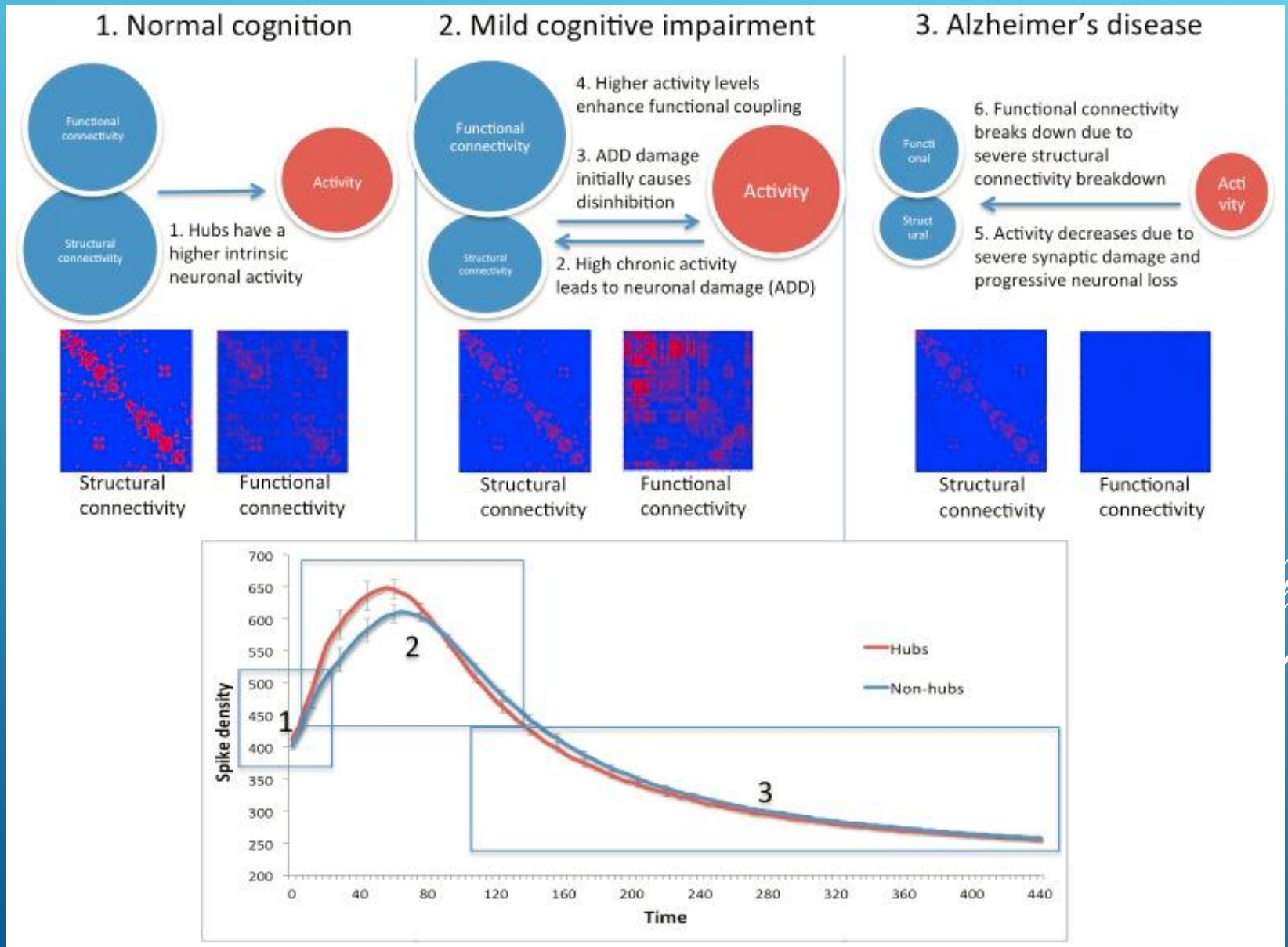

Figure 5. Effect of ADD on functional connectivity and network topology.

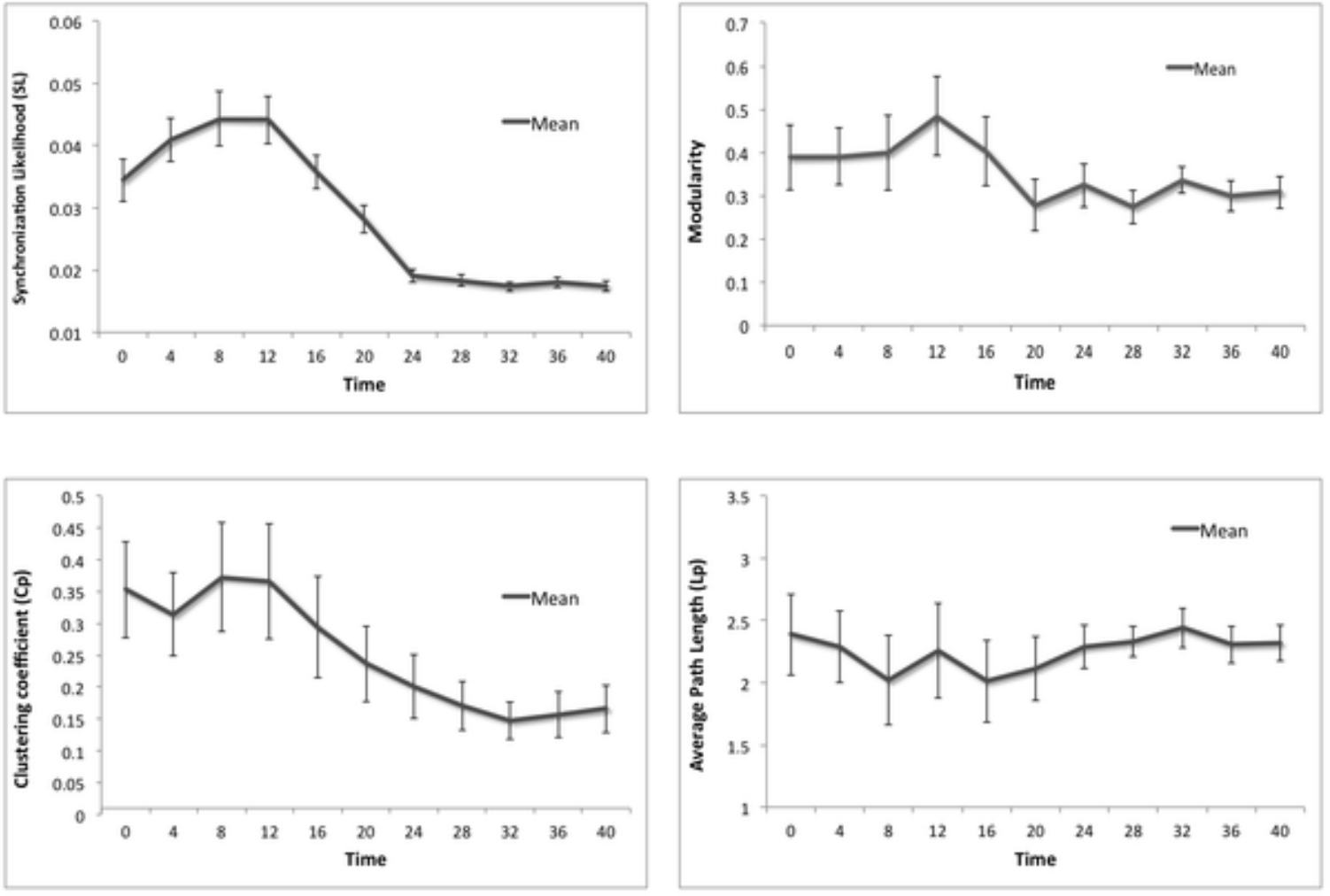

de Haan W, Mott K, van Straaten ECW, Scheltens P, Stam CJ (2012) Activity Dependent Degeneration Explains Hub Vulnerability in Alzheimer's Disease. PLoS Comput Biol 8(8): e1002582. doi:10.1371/journal.pcbi.1002582
http://127.0.0.1:8081/ploscompbiol/article?id=info:doi/10.1371/journal.pcbi.1002582

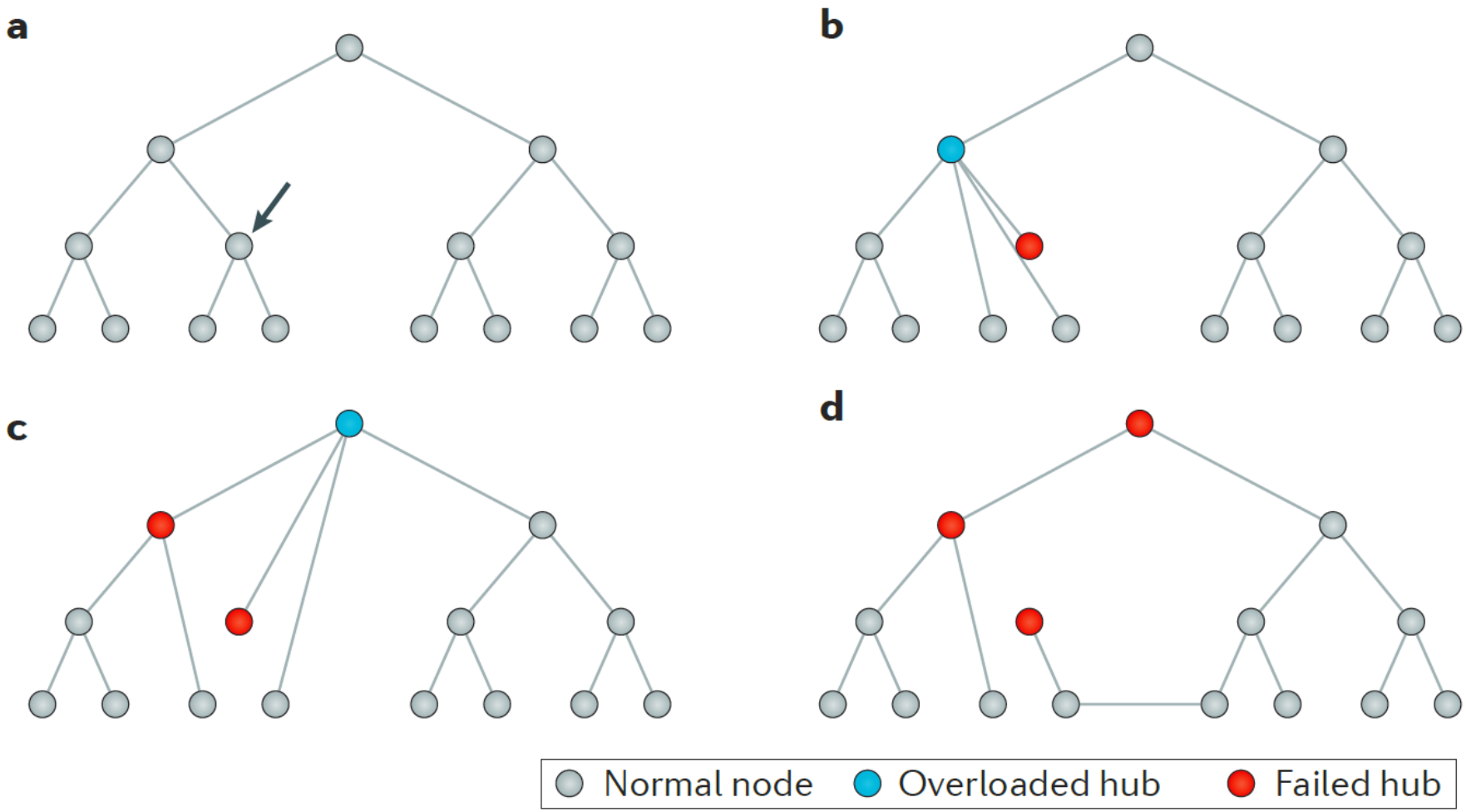
a
b
c
d
Normal node
Overloaded hub
Failed hub

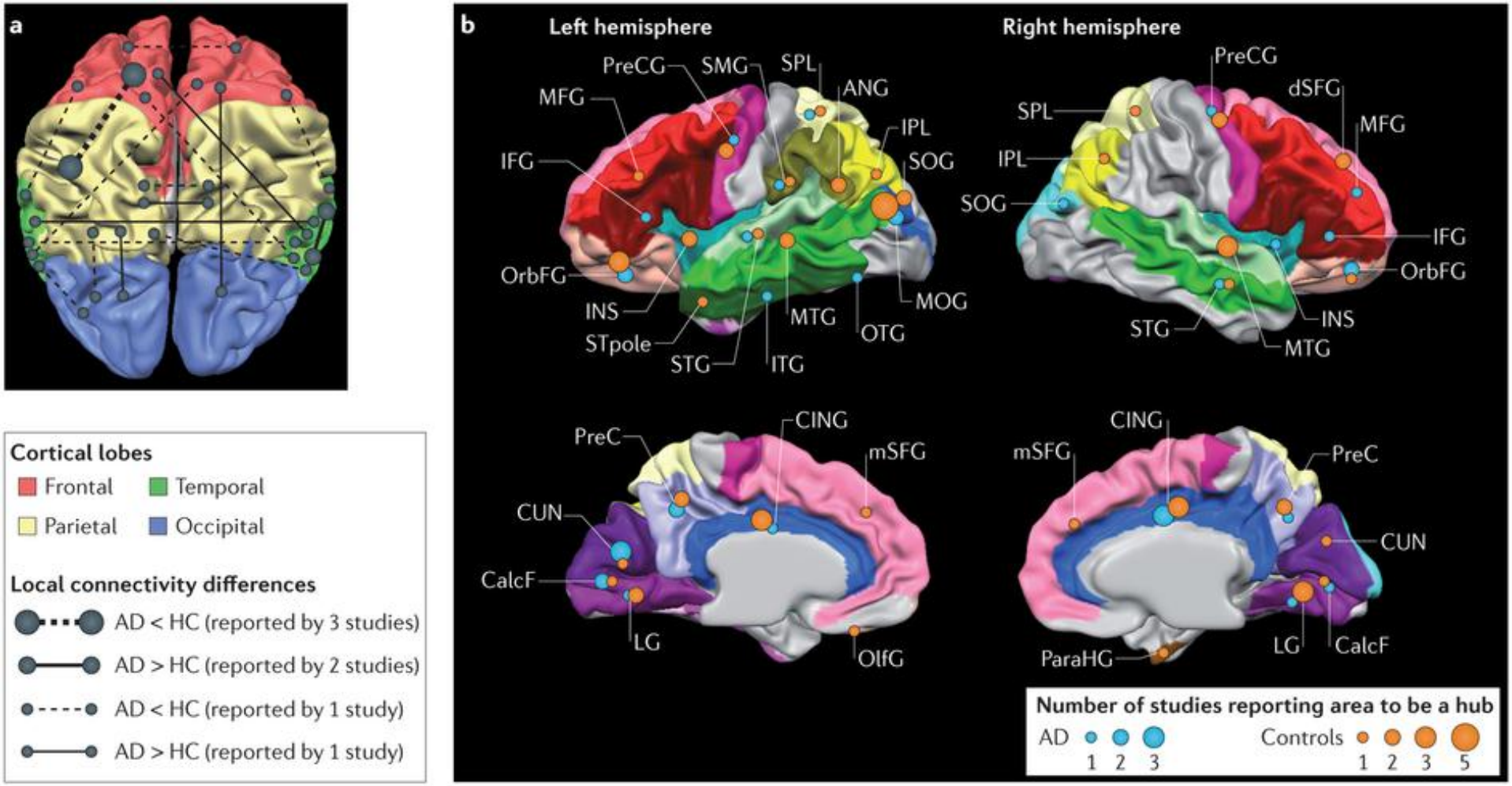

Nature Reviews | Neuroscience

STAM C.J., 2014 NETWORK CHANGES IN AD

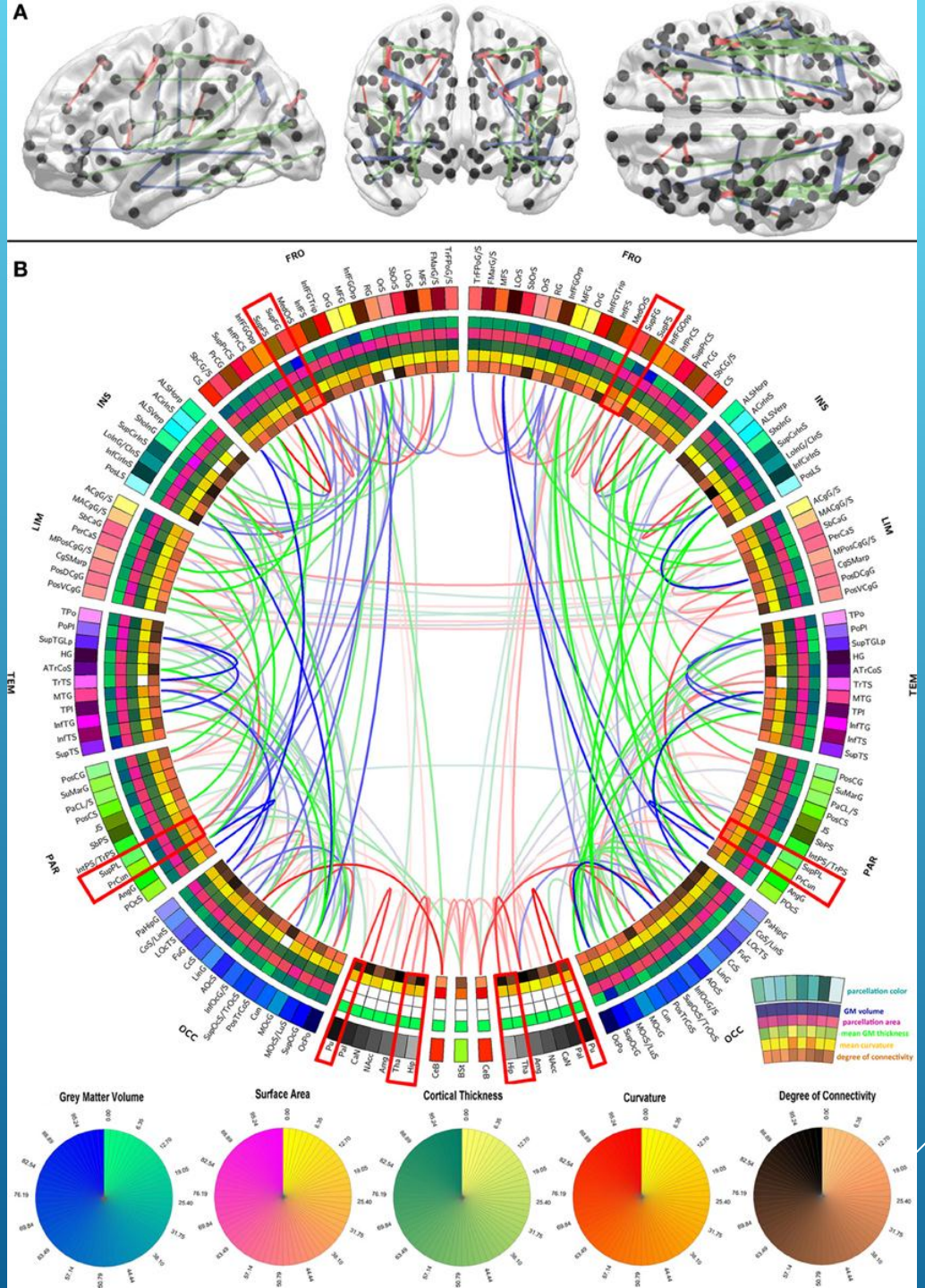
A
B
FRO
INS
LIM
TEM
PAR
OCC
parcellation color
GM volume
parcellation area
mean GM thickness
mean curvature
degree of connectivity
Grey Matter Volume
Surface Area
Cortical Thickness
Curvature
Degree of Connectivity

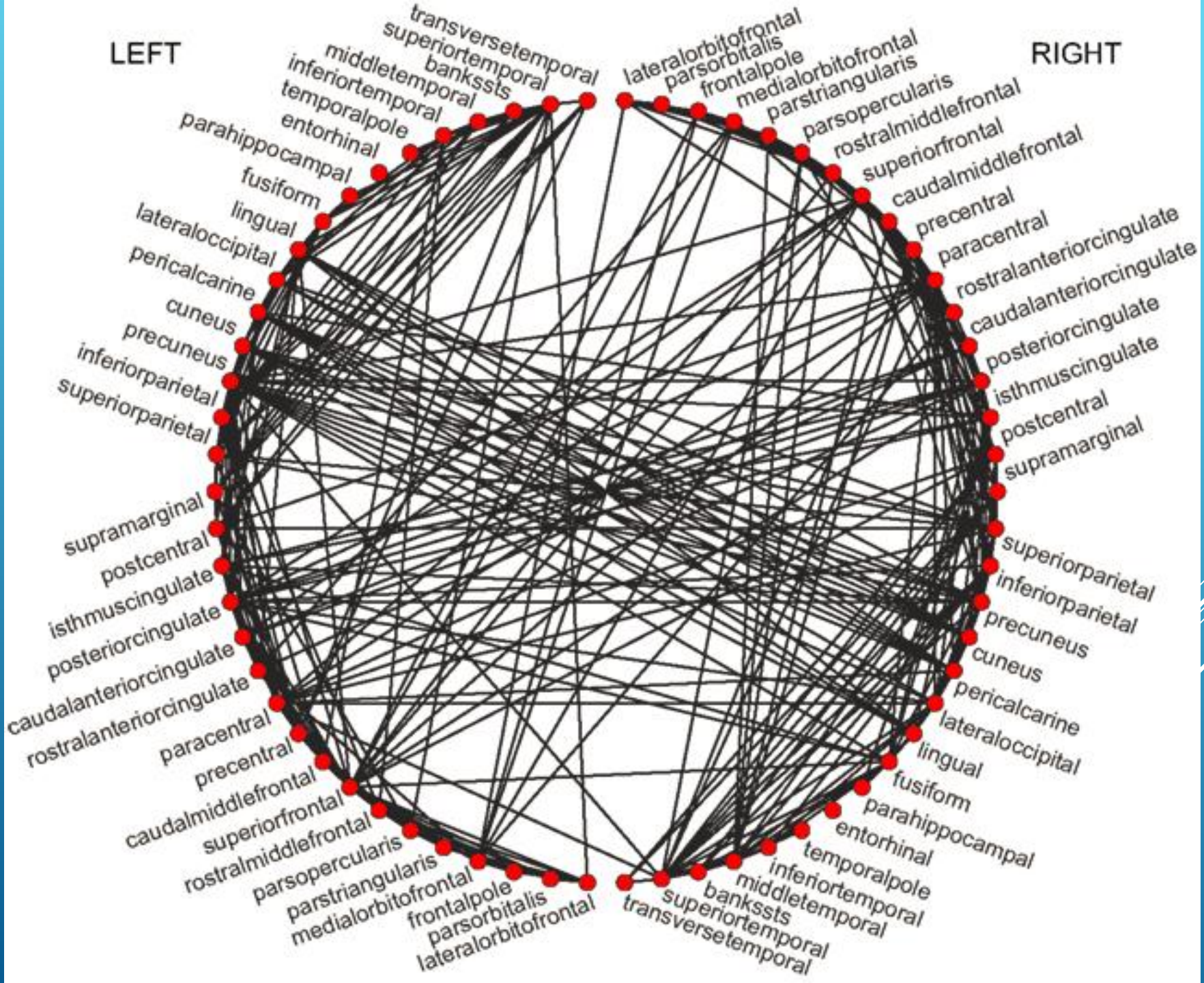
LEFT
RIGHT
transversetemporal
superiortemporal
bankssts
middletemporal
inferiortemporal
temporalpole
entorhinal
parahippocampal
fusiform
lingual
lateraloccipital
pericalcarine
cuneus
precuneus
inferiorparietal
superiorparietal
supramarginal
postcentral
isthmuscingulate
posteriorcingulate
caudalanteriorcingulate
rostralanteriorcingulate
paracentral
precentral
caudalmiddlefrontal
superiorfrontal
rostralmiddlefrontal
parsopercularis
parstriangularis
medialorbitofrontal
frontalpole
parsorbitalis
lateralorbitofrontal
lateralorbitofrontal
parsorbitalis
frontalpole
medialorbitofrontal
parstriangularis
parsopercularis
rostralmiddlefrontal
superiorfrontal
caudalmiddlefrontal
precentral
paracentral
rostralanteriorcingulate
caudalanteriorcingulate
posteriorcingulate
isthmuscingulate
postcentral
supramarginal
superiorparietal
inferiorparietal
precuneus
cuneus
pericalcarine
lateraloccipital
lingual
fusiform
parahippocampal
entorhinal
temporalpole
inferiortemporal
middletemporal
bankssts
superiortemporal
transversetemporal

RS-FMRI AND EEG WHOLE-BRAIN CONNECTOMES

Deligianni F., 2014

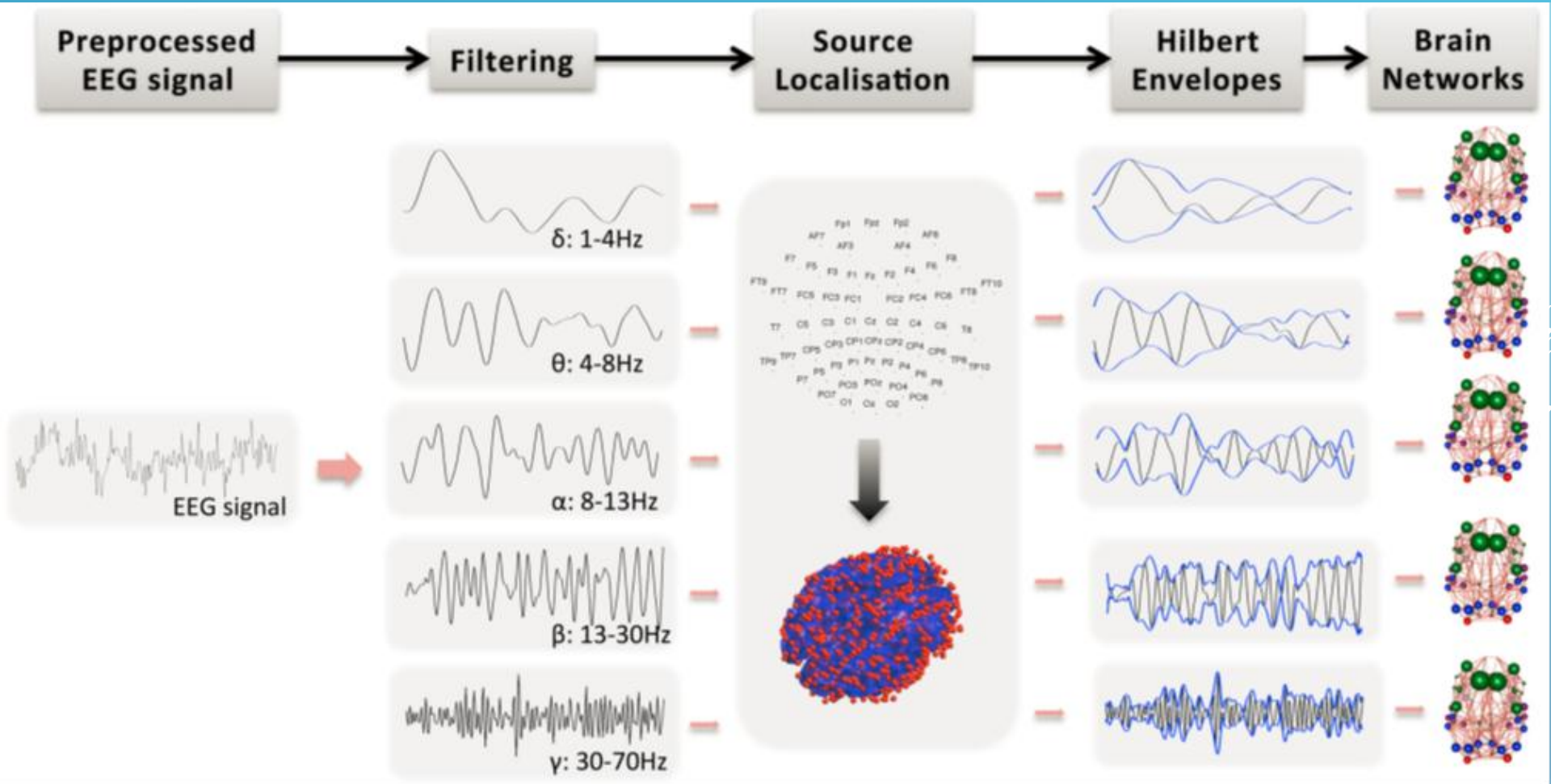

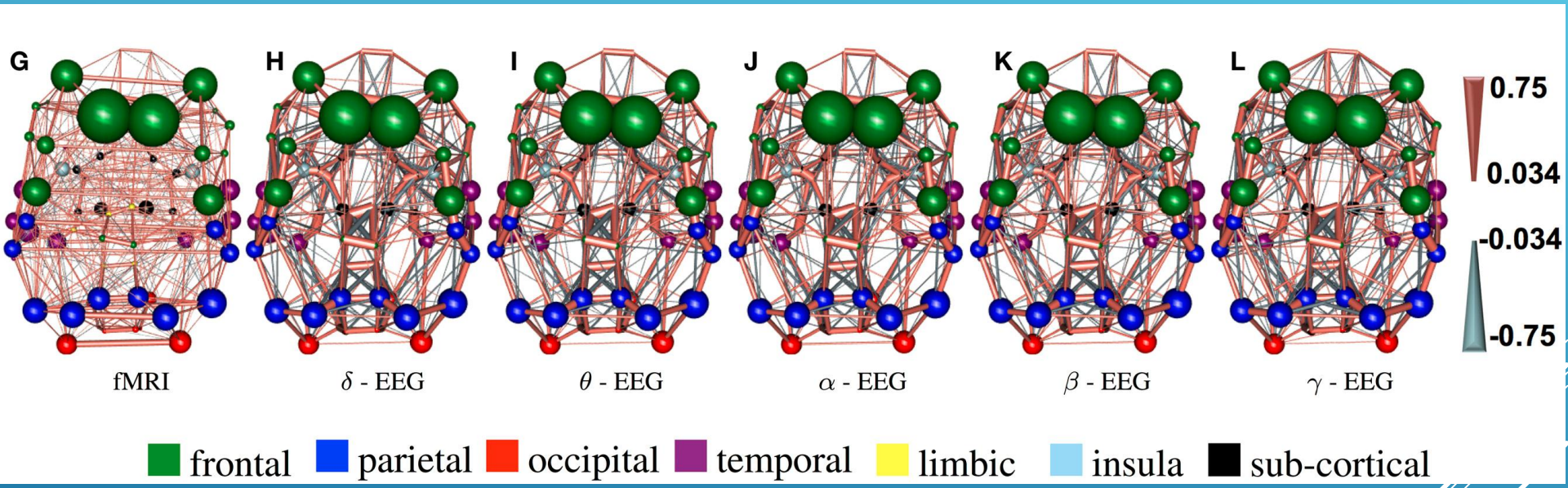
G
H
I
J
K
L
0.75
0.034
-0.034
-0.75
fMRI
δ - EEG
θ - EEG
α - EEG
β - EEG
γ - EEG
frontal
parietal
occipital
temporal
limbic
insula
sub-cortical

- The results indicate that in this spatial resolution (1-2 cm) the information carried in the EEG signal is richer than the averaged hemodynamic activity. In this context, the question of which EEG band represents best the fMRI is not important; any EEG band can provide similar connectivity information. This implies that scalp EEG can be used to provide similar information to resting state fMRI based connectomes at substantially reduced cost while providing much greater possibilities in dynamic information content.
- These findings are consistent with the concept of nested oscillations and cross spectral coupling often found within EEG.

eLORETA FC in schizophrenia-like psychosis of epilepsy: Increased beta2 (21-30 Hz) FC in R frontotemporal circuits Canuet L., 2011

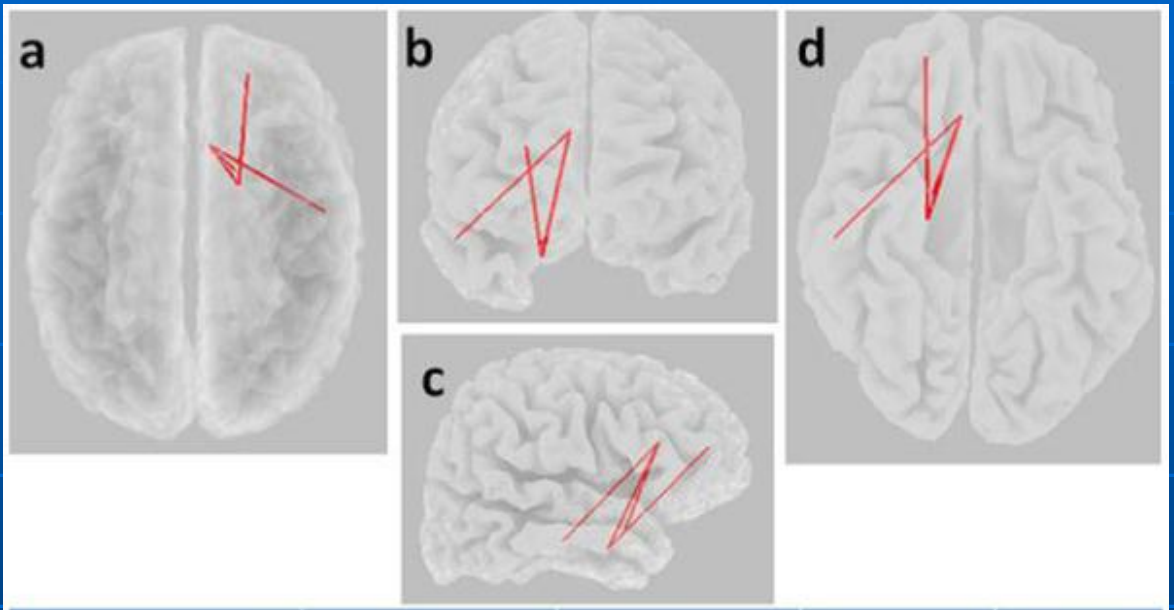

Interconnected Regions [a]	SLPE n = 21	nPE n = 21	t	p (corrected)
BA32 & BA34 (ACC/mPreF & medial-Temporal)	0.086 ± 0.034	0.037 ± 0.011	5.64	0.000
BA32 & BA28 (ACC/mPreF & medial-Temporal)	0.082 ± 0.032	0.037 ± 0.026	4.89	0.000
BA28 & BA9 (medial-Temporal & DLPFC)	0.077 ± 0.029	0.036 ± 0.019	5.30	0.000
BA32 & BA21 (ACC/mPreF & Middle Temporal)	0.081 ± 0.031	0.054 ± 0.058	1.95	0.056

FUNCTIONAL CONNECTIVITY (LORETA) IN PSYCHOSIS IN TLE

Canuet L., 2011

For functional connectivity analysis, a "whole-brain Brodmann areas (BAs)" approach is used, selecting all 42 BAs in each hemisphere as regions of interest (ROI). The anatomical definitions of BAs provided by eLORETA software package are based on the Talairach Atlas (http://www.talairach.org/).

For the analysis of connectivity between pairs of BAs, a method using a single voxel at the centroid of each BA was chosen. This procedure is justified because eLORETA has a low spatial resolution, which makes it unable to separate two closely spaced sources, and additionally, the single centroid voxel (the closest to the center of the BA mass) is an excellent representative of the corresponding BA.

Overall, 5166 tests were performed by eLORETA to compare all connections between 42 BAs (861 connections) for each of the six frequency bands (861×6 = 5166).

Transgenic mice

Goutagny R., 2013

We therefore assessed whether theta and gamma oscillations and their cross-frequency coupling, which are known to be essential for normal memory function, were altered precociously (before Aβ overproduction) in the hippocampus.

1-month-old TgCRND8 mice showed robust alterations of theta-gamma cross-frequency coupling in the principal output region of the hippocampus, the subiculum.

Compared to controls, these mice expressed negligible levels of Aβ. Finally, these network alterations were not due to genetic factors as 15-day-old animals did not exhibit theta-gamma coupling alterations.

Thus, initial alterations in hippocampal network activity arise before Aβ accumulation and may represent an early biomarker for AD.

Transgenic mice

Wulf P., 2008

We generated genetically modified mice (PV-Δγ2) in which synaptic inhibition was ablated in parvalbumin-positive (PV+) interneurons.

These data indicate that synaptic inhibition onto PV+ interneurons is indispensable for theta-activity and its coupling to gamma oscillations but not for rhythmic gamma-activity in the hippocampus.

Such cross-frequency coupling may aid the execution of cognitive functions such as working memory.

Fast synaptic inhibition shapes both theta and gamma oscillations and could also control cross-frequency coupling.

Cross-frequency coupling between distinct brain rhythms facilitates the transient coordination of cortical areas required for adaptive behavior in humans.

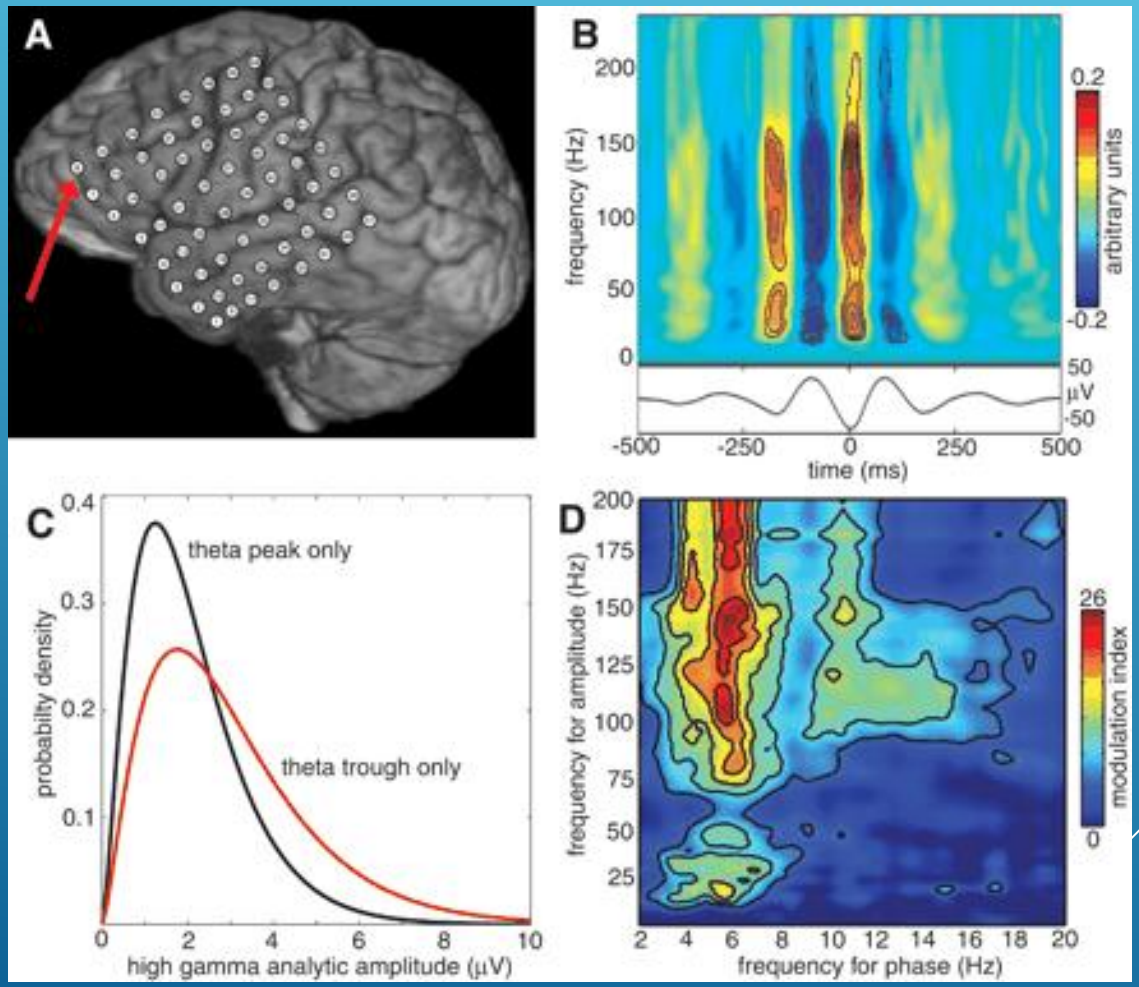

NEUROFEEDBACK
en toestandregulatie bij ADHD

Een therapie zonder medicatie

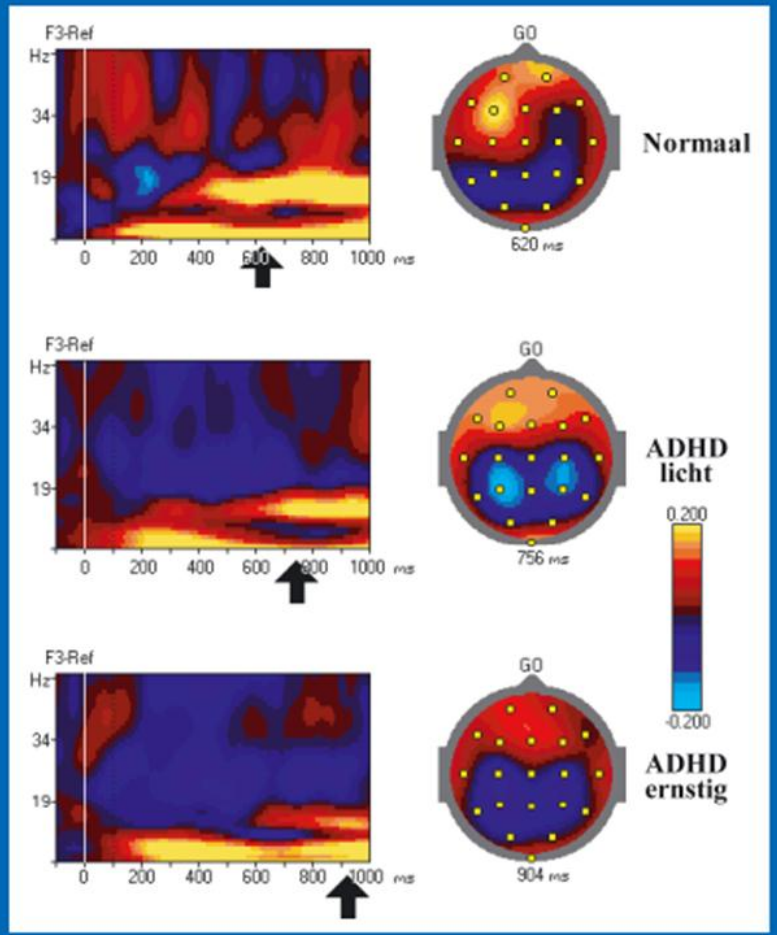

Werner Van den Bergh

Gainotti L.R.R., 2007

Differences between mild and moderate AD patients, and controls

Correlations between MMSE scores and LORETA current density in the two EEG frequency bands with significant correlations

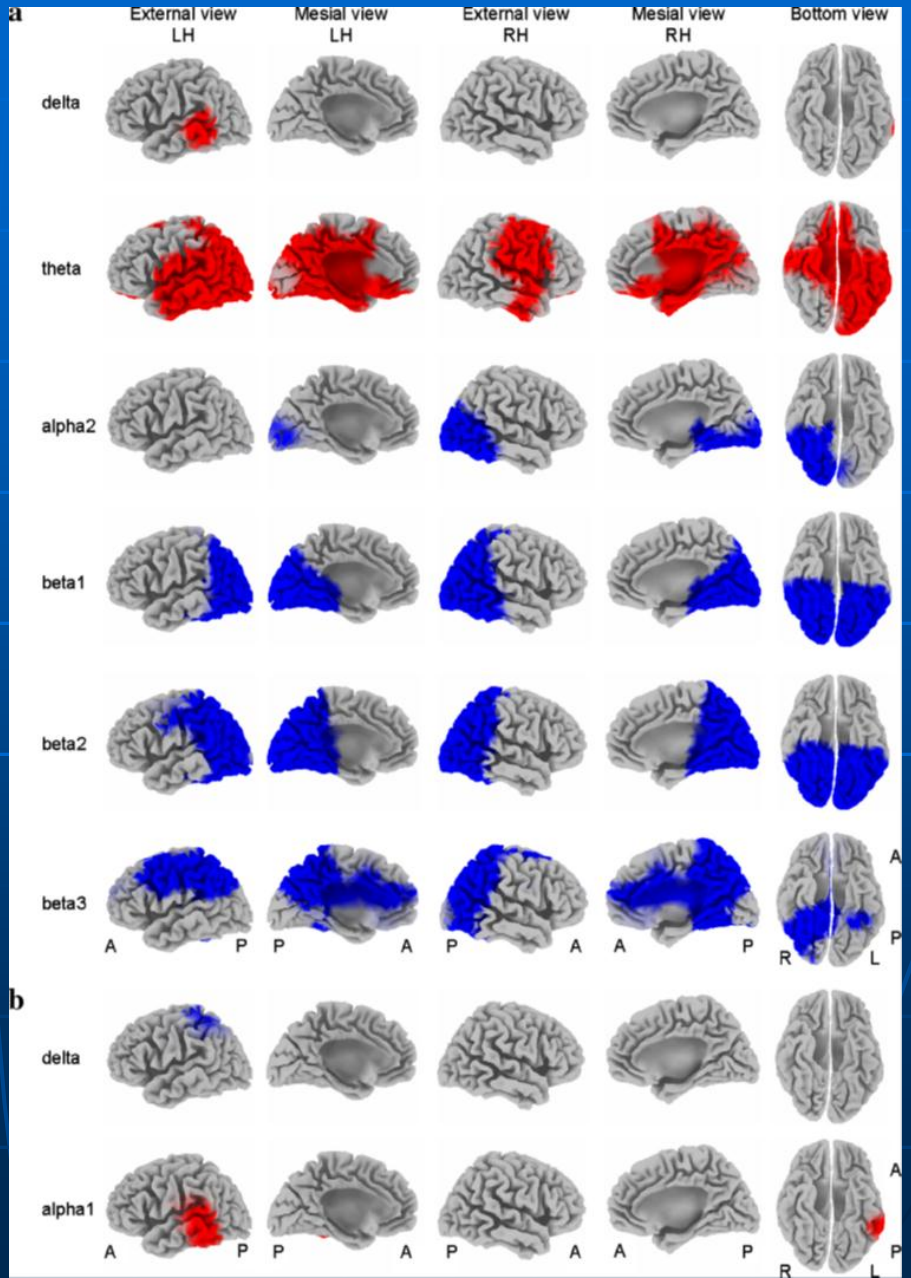

Rivastigimine 3 months
Gainotti L.R.R., 2008

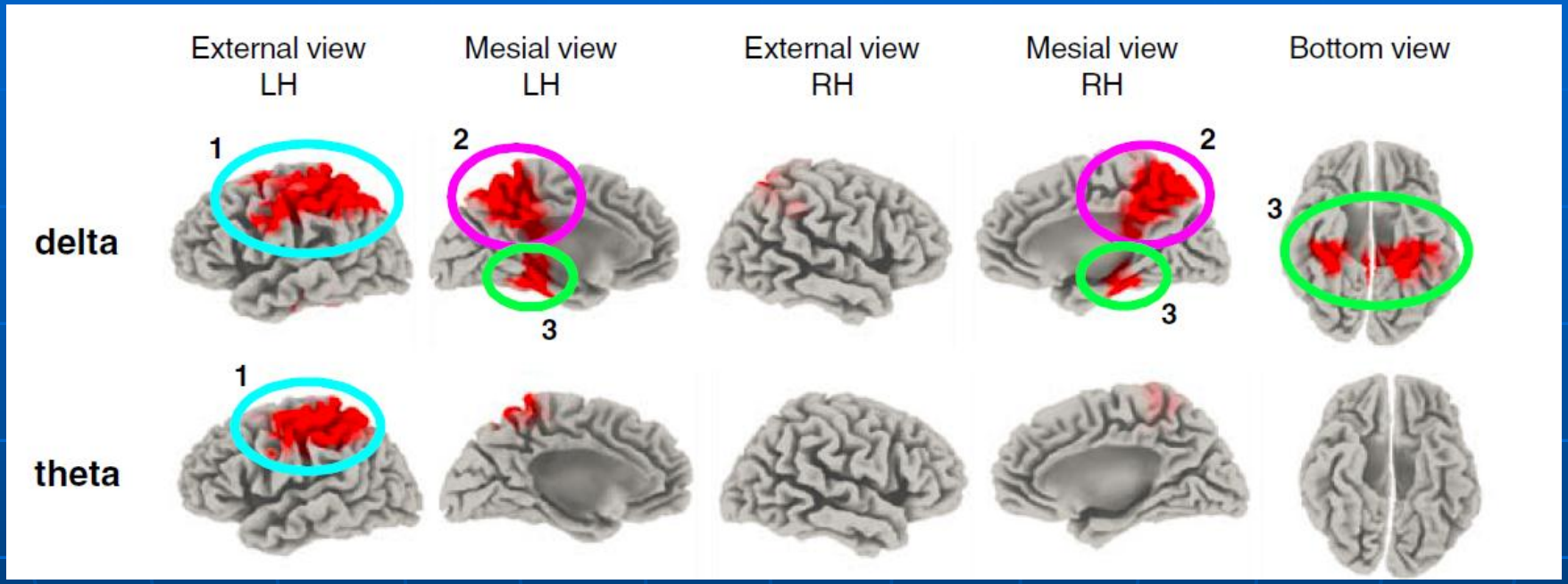

Left fronto-parietal regions, bilateral posterior cingulate cortex and precuneus , bilateral parahippocampal regions and hippocampus.

Rivastigimine 3 months
Gainotti L.R.R., 2008

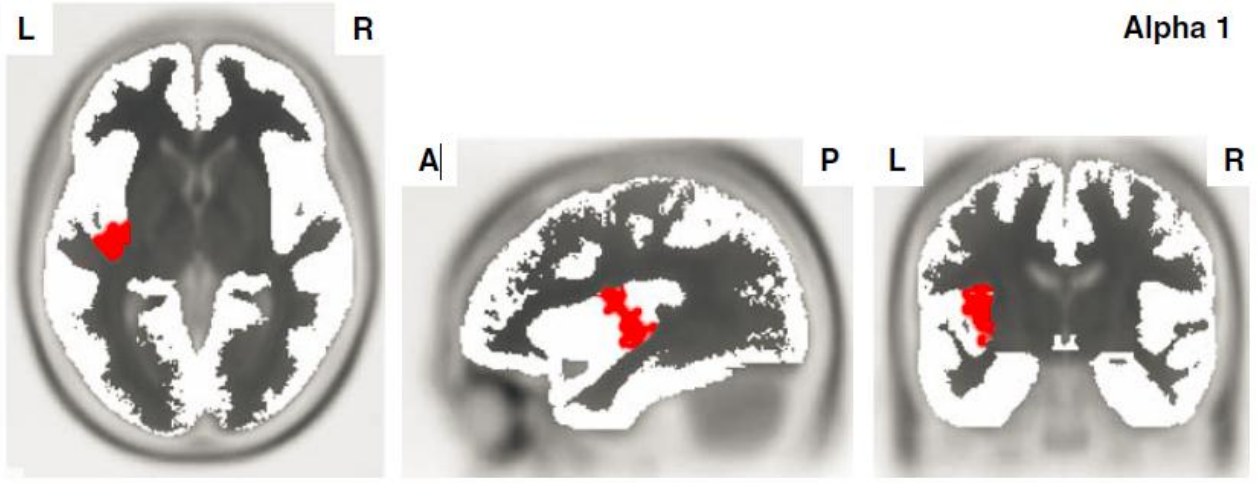

Fig. 4 Axial, sagittal, and vertical slices centered at the voxel of strongest correlation (X=−38, Y=−11, Z=1 in Talairach coordinates) showing in *red* results of voxelwise Pearsons' product-moment correlation (p< 0.05) between difference in current density (session t_1-t_0) in the alpha 1 band and difference in MMSE scores (session t_1-t_0)

Our data showed a significant correlation in the alpha1 band between the differences in the cognitive functions measured with MMSE during the two sessions and LORETA-computed intracortical activity in the left insula, indicating better cognitive performance with increased alpha1 current density. L Insula is part of circuit involved in verbal memory.

The most significant finding of this module study is the interrupted integration of insula module in AD group. Anatomically, the insula is a crucial hub in the human brain network; it is widely connected to the cortical, limbic, and paralimbic structures. Functionally, it is involved in high-order cognition, emotion, autonomic, and sensory process (Naqvi et al., 2007; Allen et al., 2008). The previous study has shown that the insula was affected in AD and its atrophy was significantly decreased from the normal population (Fan et al., 2008). The seed-based functional connectivity of the insular regions was discovered to be significantly decreased in the regions that functionally connected with insula. This disruption was associated with episodic-memory deficits in aMCI patients (Xie et al., 2012). Our results are not only consistent with these previous findings, they indicate a disruption between the insula and other brain regions. Also, we detected the breakdown of the insula module in the AD group, which is a possible neural underpinning of AD dementia.

Alpha1 rhythms (8–10 Hz): synchronization of diffuse neural networks regulating the fluctuation of subject's global awake and conscious states;

Alpha rhythms (10-12 Hz): synchronization of more selective neural networks specialized in the processing of modal specific or semantic information (Klimesch, 1999; Pfurtscheller and Lopes da Silva, 1999).

When the subject is engaged in sensorimotor or cognitive tasks, alpha and beta1 (12-20 Hz) rhythms reduce in power (i.e. “desynchronization or blocking”) and are replaced by fast EEG oscillations at beta2 (20-30 Hz) and gamma (>30 Hz) rhythms.

It can be speculated that in the resting state eyes-closed condition, the EEG source markers of MCI and of the disease progression along 1 year would reflect an abnormal tonic desynchronization of the alpha1 rhythms, suggesting an exaggerated and **unselective** activation of brain networks underlying cortical arousal. Effective cognitive processing is expected to stem upon the selectivity and flexibility of the excitation and inhibition across brain neural networks during both resting state condition and task demands.

In the MCI progression, this abnormality would be associated to an abnormal tonic desynchronization of the alpha2 rhythms indicating a worsening of the **selective** neural networks specialized in the processing of modal specific or semantic information.

It can be speculated that in the resting state eyes-closed condition, the EEG source markers of the AD state and disease progression would reflect an abnormal enhancement of the pathological EEG slow-frequency rhythms (i.e., delta and theta) in the temporal, parietal and occipital areas as a cortical “disconnection mode” impinging upon thalamo-cortical circuits.

Neuroscience. 2006 Dec;143(3):793-803. Epub 2006 Oct 13.

Conversion from mild cognitive impairment to Alzheimer's disease is predicted by sources and coherence of brain electroencephalography rhythms.

Rossini PM[1], Del Percio C, Pasqualetti P, Cassetta E, Binetti G, Dal Forno G, Ferreri F, Frisoni G, Chiovenda P, Miniussi C, Parisi L, Tombini M, Vecchio F, Babiloni C.

Author information

Abstract

Objective. Can quantitative electroencephalography (EEG) predict the conversion from mild cognitive impairment (MCI) to Alzheimer's disease (AD)? Methods. Sixty-nine subjects fulfilling criteria for MCI were enrolled; cortical connectivity (spectral coherence) and (low resolution brain electromagnetic tomography) sources of EEG rhythms (delta=2-4 Hz; theta=4-8 Hz; alpha 1=8-10.5 Hz; alpha 2=10.5-13 Hz: beta 1=13-20 Hz; beta 2=20-30 Hz; and gamma=30-40) were evaluated at baseline (time of MCI diagnosis) and follow up (about 14 months later). At follow-up, 45 subjects were still MCI (MCI Stable) and 24 subjects were converted to AD (MCI Converted). Results. At baseline, fronto-parietal midline coherence as well as delta (temporal), theta (parietal, occipital and temporal), and alpha 1 (central, parietal, occipital, temporal, limbic) sources were stronger in MCI Converted than stable subjects (P<0.05). Cox regression modeling showed low midline coherence and weak temporal source associated with 10% annual rate AD conversion, while this rate increased up to 40% and 60% when strong temporal delta source and high midline gamma coherence were observed respectively. Interpretation. Low-cost and diffuse computerized EEG techniques are able to statistically predict MCI to AD conversion.

Posterior sources of resting delta, theta, and alpha rhythms at baseline recording were unselectively higher in amplitude in MCI subjects who will progress to AD (MCI converted) than in MCI subjects who will remain stable (MCI stable) after 1 year

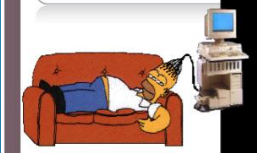

Resting EEG data:

45 MCI stable

24 MCI converted

50 Nold

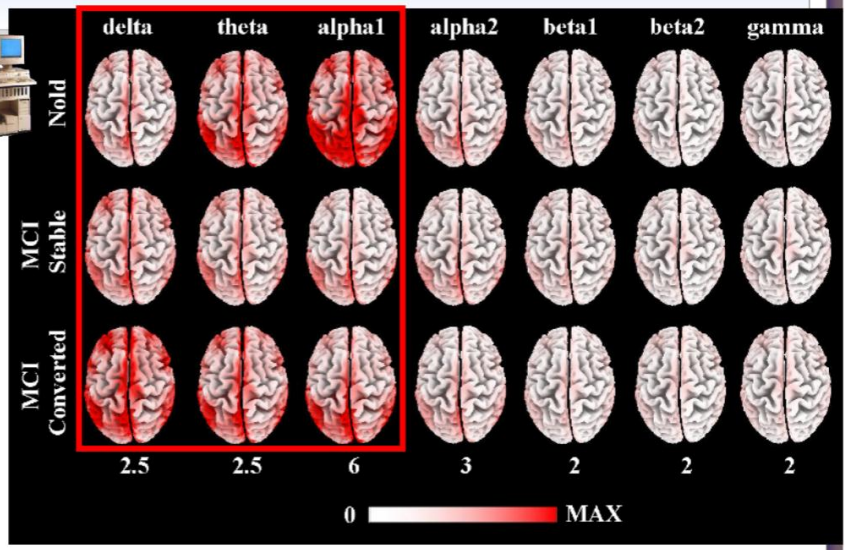

Resting EEG data:

126 Nold

155 MCI

193 mild AD

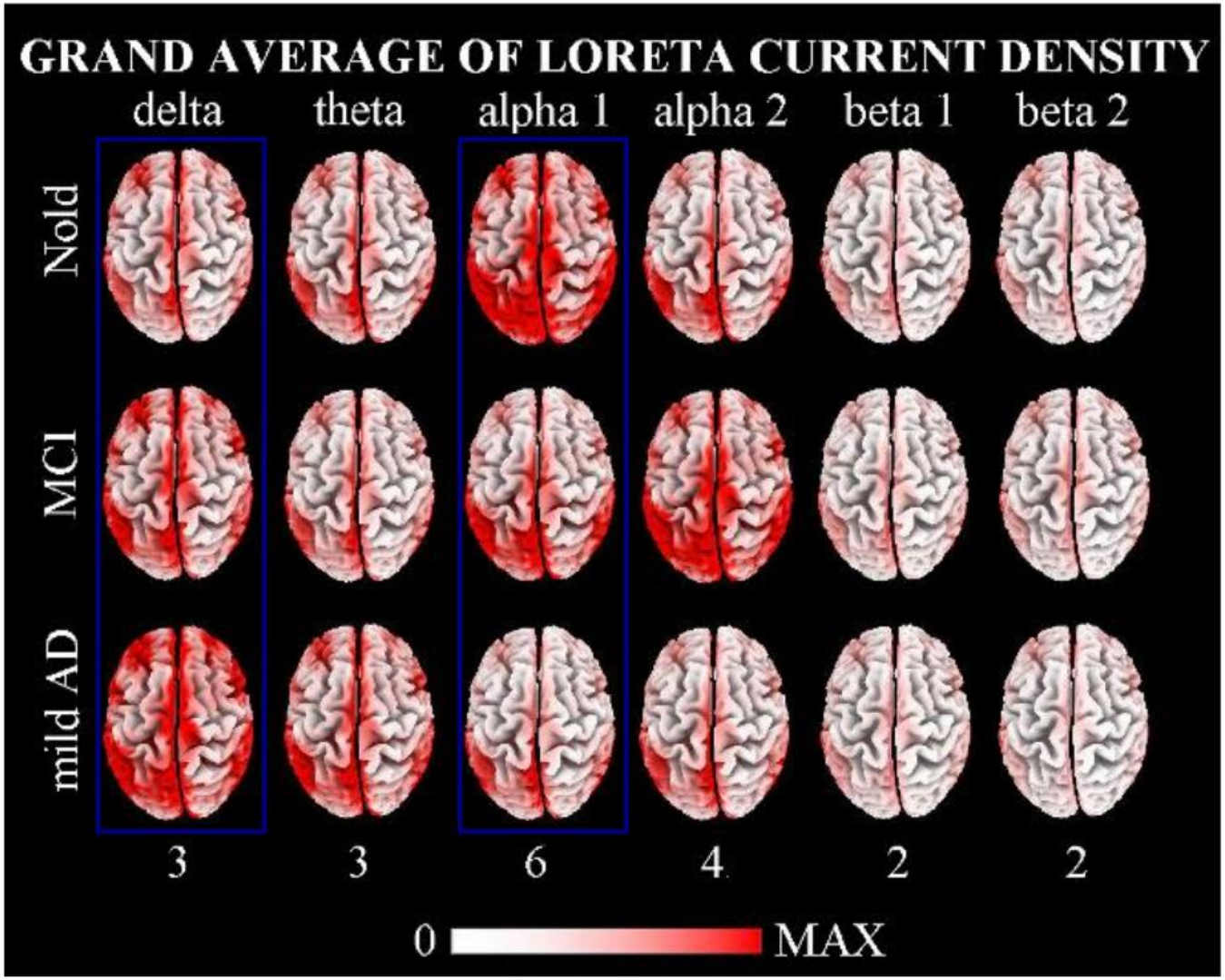

Babiloni C, Binetti G, Cassetta E, Dal Forno G, Del Percio C, Ferreri F, Ferri R, Frisoni G, Hirata K, Lanuzza B, Miniussi C, Moretti DV, Nobili F, Rodriguez G, Romani GL, Salinari S, and Rossini PM Sources of cortical rhythms in subjects with mild cognitive impairment: a multi-centric study Clinical Neurophysiology 2006

Babiloni C., 2013

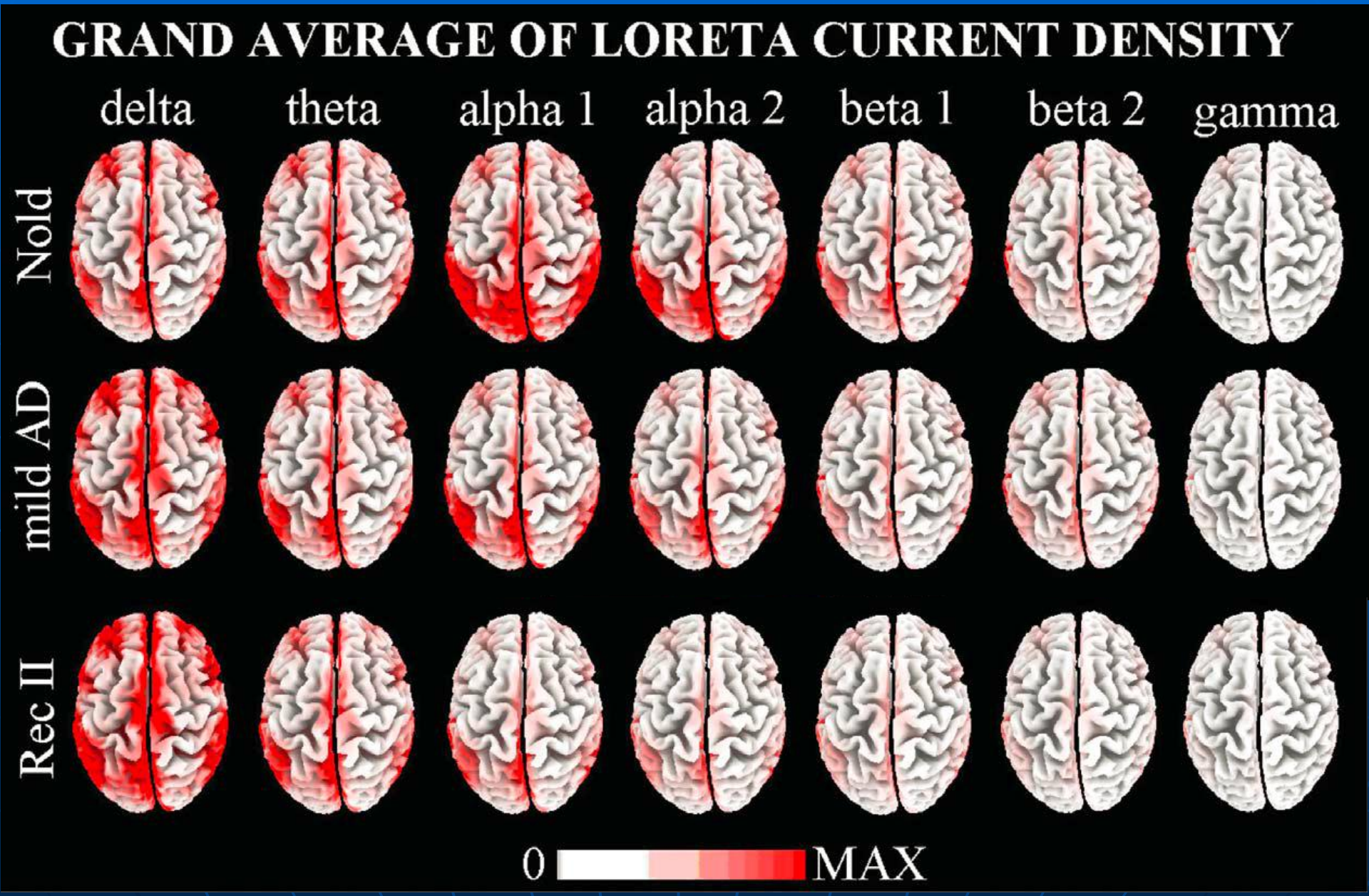

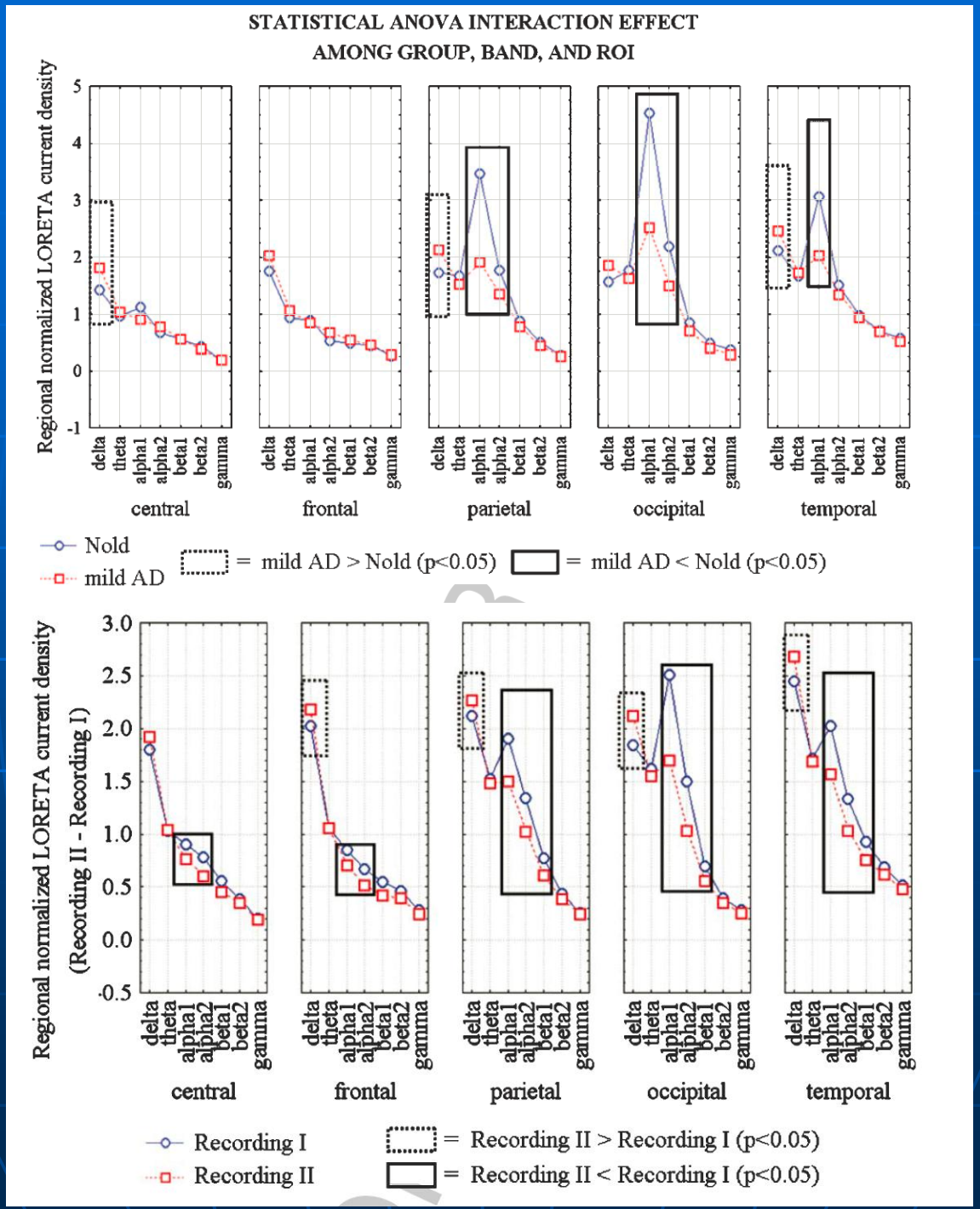
STATISTICAL ANOVA INTERACTION EFFECT
AMONG GROUP, BAND, AND ROI
Regional normalized LORETA current density
5
4
3
2
1
0
-1
delta
theta
alpha1
alpha2
beta1
beta2
gamma
central
frontal
parietal
occipital
temporal
Nold
mild AD
= mild AD > Nold (p<0.05)
= mild AD < Nold (p<0.05)
Regional normalized LORETA current density
(Recording II - Recording I)
3.0
2.5
2.0
1.5
1.0
0.5
0.0
-0.5
Recording I
Recording II
= Recording II > Recording I (p<0.05)
= Recording II < Recording I (p<0.05)

Sheer D.E., 1989

The Alzheimer patients were markedly lower on cognitive evoked gamma (35-45 Hz) activity, as compared with the normal geriatric, multi-infarct, and depression groups.
Predictive efficiency of individual cases, differentiating early Alzheimer patients from normal geriatrics, multi-infarct, and retarded depression patients, was 80 to 90 percent.

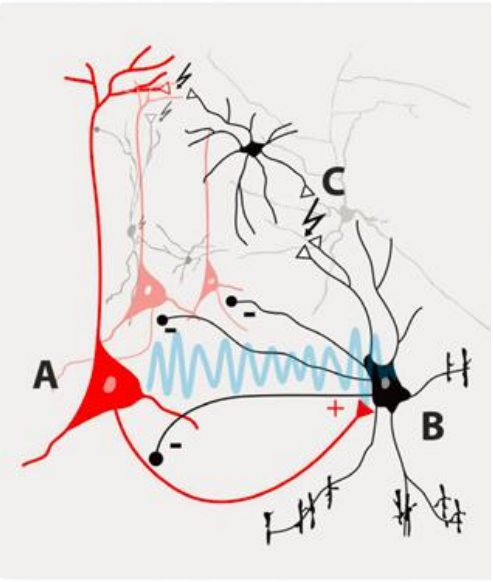

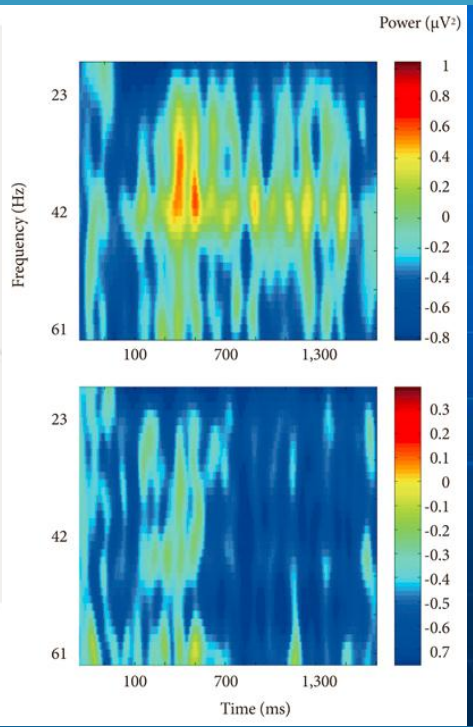

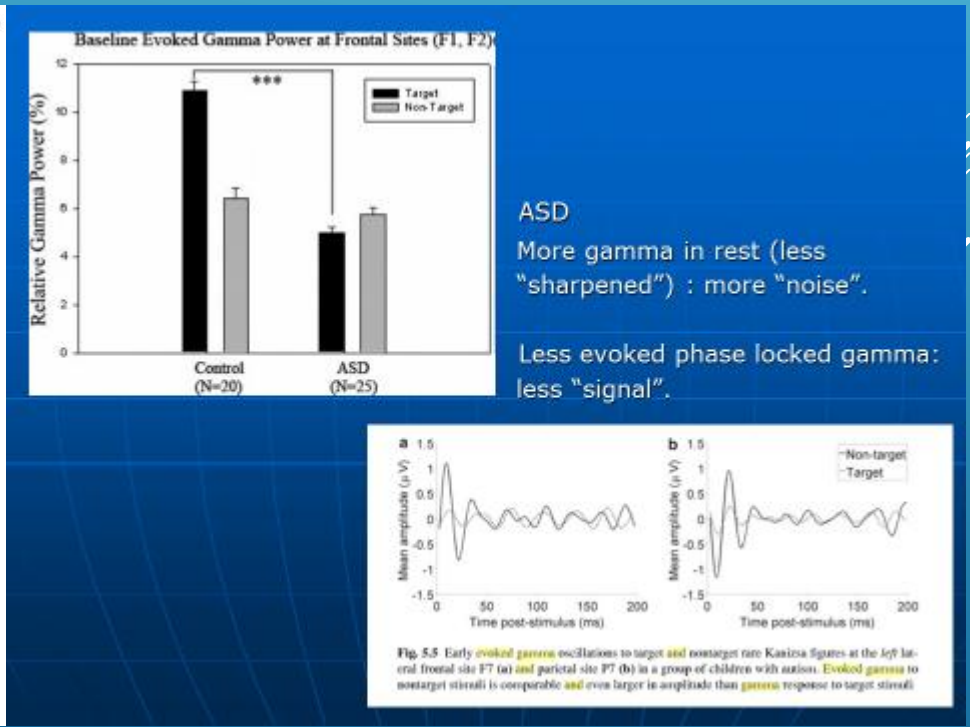

Hippocampal Oscillatory Activity in Alzheimer's Disease: Toward the Identification of Early Biomarkers?

Romain Goutagny[1,2] and Slavica Krantic[3*]

It is now well documented that AD patients and animal models of AD exhibit reorganization of hippocampal and cortical networks. This reorganization is initiated by an early imbalance between excitation and inhibition, leading to altered network activity. The mechanisms underlying these changes are unknown but recent evidence suggests that either soluble amyloid-beta (Aß) or fibrillar forms of Aß are central to various network alterations observed in AD. However, recent evidence also suggests that Aβ overproduction in animal models is not systematically linked to network overexcitation. We hypothesize here that early changes in the excitation-inhibition balance within the hippocampus occurs much earlier than currently believed and initially produces only slight changes in overall hippocampal activity. In this review, we introduce the concept according to which the subtle changes in theta and gamma rhythms might occur during the very first stages of AD and thus could be used as a possible predictor for the disease.

What are EEG and MEG Signals?

EEG measures the electric potential differences across scalp arising from current flow within the head & brain.

$$V = IR$$

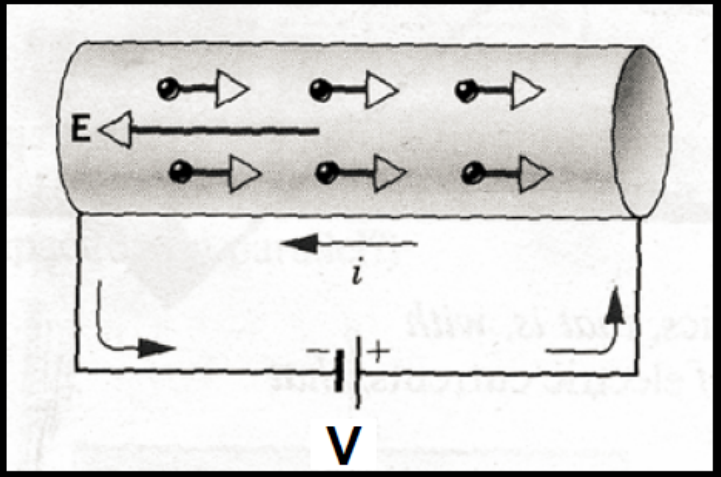

Figure from Halliday, Resnick, & Krane, 1992)

V = electric potential ("voltage") analogous to water pressure

I = electric current (analogous to rate of water flow)

R = resistance to flow of electricity (size of pipes)

$\sigma \sim 1/R$ = conductance of flow of electricity

Current I = Total Flow of Charge Per Time [A]

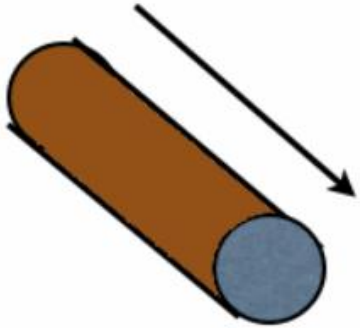

www.maxwells-equations.com

Current Density J = Total Flow of Charge Per Time [A] over a cross section of area [m^2]

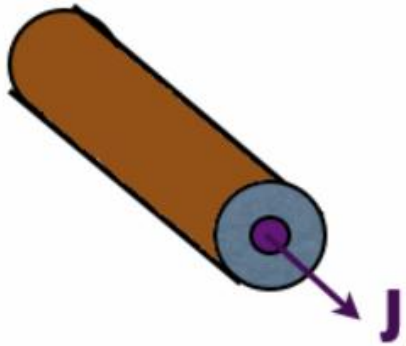

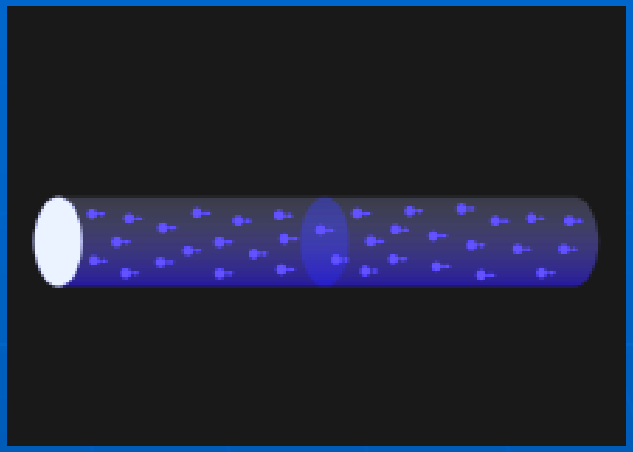

1st derivative
Ampère= flow of coulombs (charges) per seconde

Electrical Field
V = IR
(Ohm's Law)

Integration of multiple biomarkers using logistic regression predicts of Alzheimer's disease at the MCI stage. Simon-Shlomo P., 2013

A recent suggestion for a potential improvement of Alzheimer's disease symptoms is transcranial direct current stimulation (tDCS) (Hansen, 2012).

tDCS increased theta and alpha oscillations together with improved working memory performance. These effects may be caused by altered GABA concentration within the stimulated cortex, and potentially by an adjustment of the excitatory/inhibitory balance, which is disturbed in Alzheimer's disease. This balance may be directly linked to EEG biomarkers that have been shown sensitive to Alzheimer's disease.

Integration of multiple biomarkers using logistic regression predicts of Alzheimer's disease at the MCI stage.
Simon-Shlomo P., 2013

As in AD, GABAergic cortical inhibitory interneurons play a role in the disease's early stage, modulation of these inter-neurons by tDCS is a possible disease-modifying mechanism.

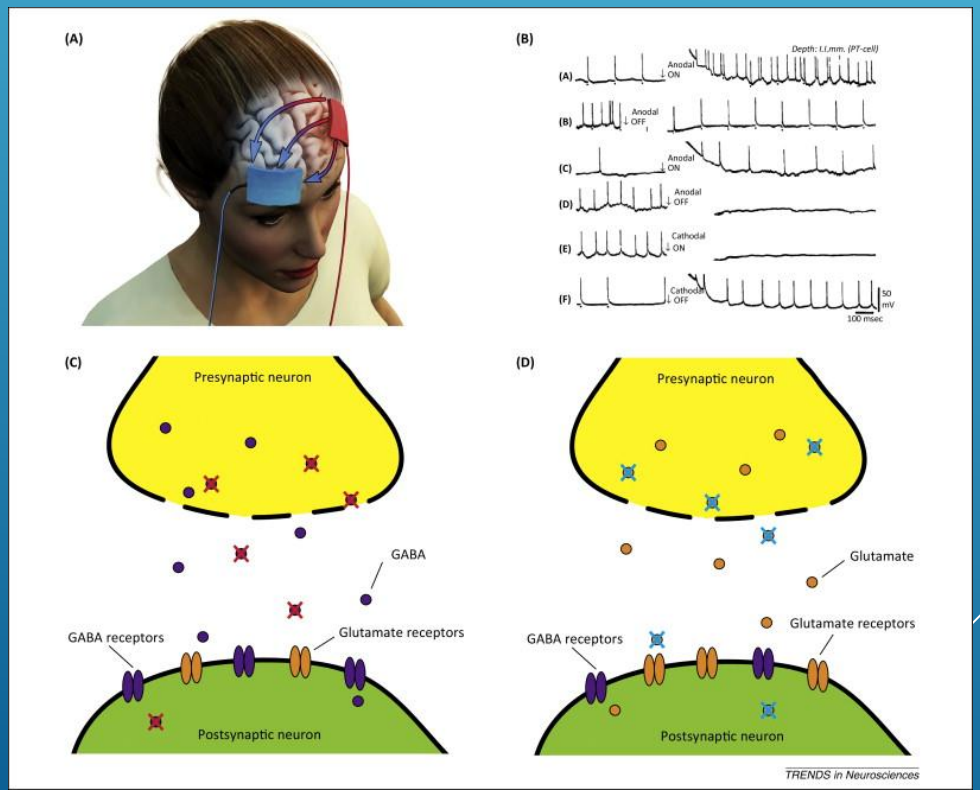

Repairing Rhythms in Alzheimer's Models

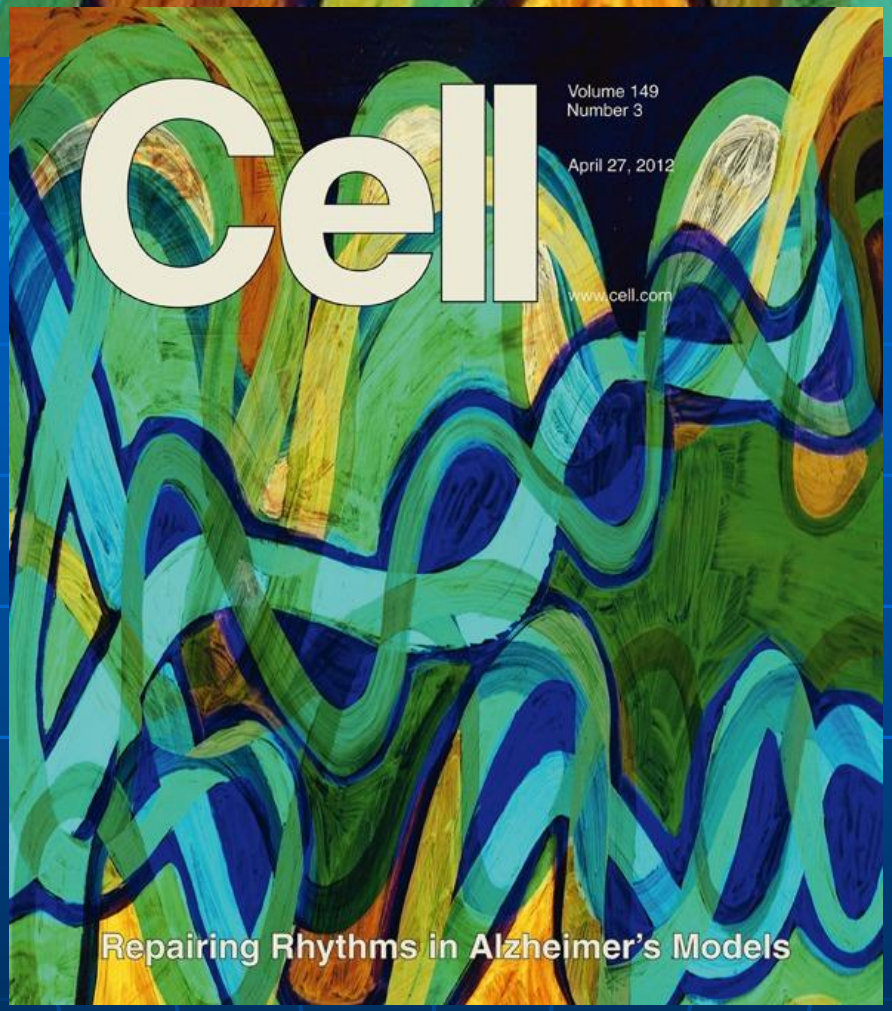

Reducing Nav1.1 (sodium channel subunit) levels specifically in inhibitory interneurons improves oscillatory rhythms, network synchrony and memory in AD mice, offering a new therapeutic approach for potentially treating cognitive disorders (Verret L. , 2012).